

**Aus der Klinik für Allgemeine, Unfall- und Wiederherstellungschirurgie,  
der Universität München,**

**Direktor: Prof. Dr. Wolfgang Böcker**

**Investigation of the molecular and biophysical mechanisms of  
prostate cancer cell interactions with  
bone marrow-derived proteins and stem cells**

**Dissertation  
zum Erwerb des Doktorgrades der Humanbiologie  
an der Medizinischen Fakultät  
der Universität zu München**

**vorgelegt von**

**Ediz SARIISIK  
aus Ankara**

**2016**

Mit Genehmigung der medizinischen Fakultät der Universität München

Berichterstatter: Priv.-Doz. Dr. rer. nat. Denitsa Docheva

Mitberichterstatter: Prof. Dr. rer. nat. Olivier Gires  
Priv.-Doz. Dr. rer. nat. Robert Kammerer

Mitbetreuung durch den  
promovierten Mitarbeiter: Dr. rer. nat. Martin Benoit,  
Prof. Dr. rer. nat. Hauke Clausen-Schaumann

Dekan: Prof. Dr. med. dent. Reinhard Hickel

Tag der mündlichen Prüfung: 09.06.2016

**Content table**

<b>1. Introduction.....</b>	<b>5</b>
1.1. Prostate cancer and bone metastasis.....	5
1.1.1. Local invasion and migration.....	6
1.1.2. Survival in the bone.....	9
1.2. Collagen type-I.....	13
1.3. Mesenchymal stem cells and their role in prostate cancer metastasis.....	15
1.4. Integrins.....	17
1.5. Cell adhesion and single cell force spectroscopy.....	20
<b>2. Aim and goals of the thesis.....</b>	<b>22</b>
<b>3. Materials and methods.....</b>	<b>24</b>
3.1. General cell culture conditions.....	24
3.1.1. Cell passaging and counting.....	24
3.1.2. Cryopreservation.....	25
3.1.3. Cell culture prior capture of cells for force spectroscopy.....	25
3.1.4. Application of integrin blocking antibody.....	26
3.1.5. Latrunculin-A treatment and fluorescent staining of actin cytoskeleton.....	26
3.2. Time-lapse microscopy and quantification of cell adhesion.....	27
3.3. Cell proliferation analysis.....	27
3.4. Cell shape analysis.....	28
3.5. Optical density adhesion assay on 96-well plates.....	28
3.6. Immunofluorescent staining of collagen type-I.....	28
3.7. Evaluation of integrin expression with RT-PCR.....	29
3.7.1. Semi-quantitative PCR.....	29
3.7.2. Quantitative PCR.....	30
3.8. Single cell force spectroscopy.....	31
3.8.1. Substrate preparations for AFM experiments.....	31
3.8.2. AFM setup and collection of the force spectroscopy data.....	31
3.8.3. Latrunculin-A treatment of a cell on the cantilever.....	33
3.8.4. Elasticity measurements of the prostate cancer cells.....	33
3.8.5. Force spectroscopy data evaluation.....	33
3.8.6. Density plots of tethers and jumps.....	34

---

3.9. Statistical analysis.....	35
3.10. Softwares used in the study.....	35
<b>4. Results.....</b>	<b>37</b>
4.1. PC3 and LNCaP adhesion, proliferation and spreading in co-culture with SCP1.....	37
4.2. Calculation of Young`s modulus of PC3 vs LNCaP cells.....	40
4.3. Quantification of the short-term adhesion of PC3 and LNCaP cells on Col-I coated surfaces and SCP1 monolayers.....	41
4.4. Integrin expression on PC3 and LNCaP cells.....	49
4.4.1. Semi quantitative PCR data.....	49
4.4.2. Quantitative PCR data.....	50
4.5. Col-I expression on SCP1 monolayers.....	51
4.6. Long-term adhesion of PC3 cells with $\beta$ 1 integrin antibody blocking and collagenase treatment on Col-I coated surfaces.....	52
4.7. Short-term adhesion of PC3 and LNCaP cells on Col-I and SCP1 surfaces with $\beta$ 1 integrin antibody blocking and collagenase treatment.....	54
4.8. Membrane and cytoskeleton anchoring of cell surface receptors.....	61
<b>5. Discussion.....</b>	<b>68</b>
<b>6. Conclusions and outlook.....</b>	<b>77</b>
<b>7. Summary.....</b>	<b>80</b>
<b>8. Zusammenfassung.....</b>	<b>82</b>
<b>9. Literature.....</b>	<b>84</b>
<b>10. List of abbreviations.....</b>	<b>95</b>
<b>11. Curriculum vitae (CV).....</b>	<b>97</b>
<b>12. Acknowledgements.....</b>	<b>100</b>

## **1. Introduction**

Adenocarcinoma of the prostate is one of the most frequently diagnosed carcinoma in males. It begins when normal semen-secreting prostate gland cells mutate into cancer cells. The region of the prostate gland where the adenocarcinomas are most common is the peripheral zone [1]. Over time, these cancer cells begin to multiply and spread to the surrounding prostate tissue (the stroma) forming a tumor. Eventually, the tumor may grow large enough to invade nearby organs such as the seminal vesicles or the rectum, or the tumor cells may develop the ability to enter in the bloodstream and lymphatic system. Prostate cancer (PC) is considered a malignant tumor because it is a mass of cells that can invade other parts of the body. Prostate cancer most commonly metastasizes to the bones and lymph nodes [2,3].

### **1.1. Prostate cancer and bone metastasis**

At the early stages of cancer, surgical and hormonal therapies can be applied and be useful. After some point cancer cells form hormone-independent cells, which can also convert into highly invasive cell types. The tendency of the PC cells to metastasis originates from specific molecular mechanisms and interactions that together lead to local infiltration of tumor cells into the adjacent tissue, transendothelial migration of cancer cells into vessels known as intravasation, survival in the circulatory system, followed by endothelial attachment, extravasation and site-specific establishment of metastases at secondary sites [4–6]. Development of the PC into a metastatic state causes patients to end up with complications that may not be curable. In most of the cases, which involve the skeleton as a metastatic site for PC, events occur in a similar way, with lesions tending to appear first in the axial skeleton and subsequently in the appendicular skeleton [7]. Skeletal metastasis causes significant complications including bone pain, impaired mobility, pathological fracture and spinal cord compression [8].

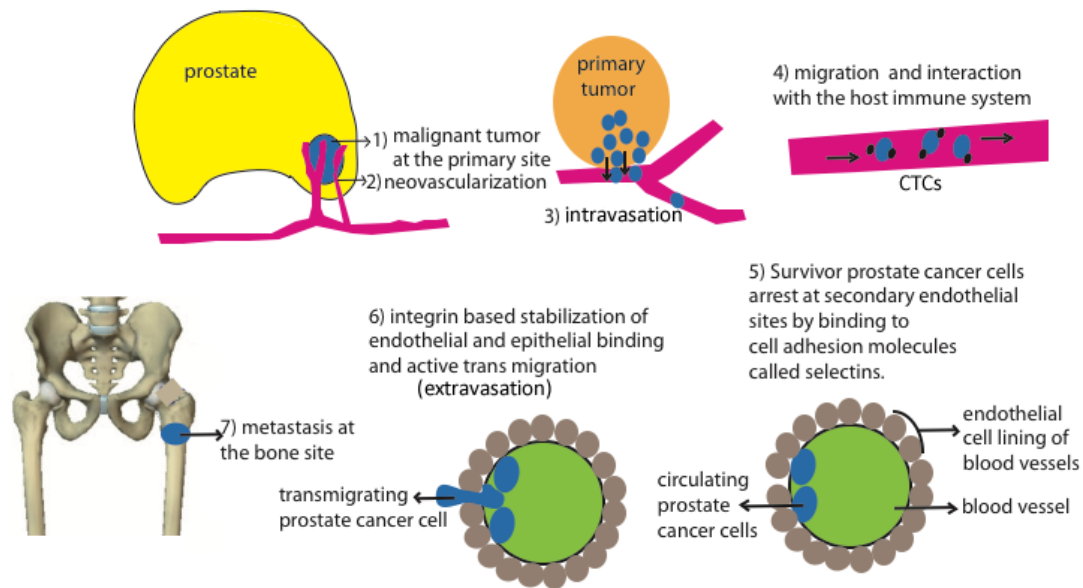


**Figure 1:** Formation of metastasis at the distant bone sites. Metastasis is characterized by proliferation at the primary site, neovascularization and intravasation into the circulation. In the circulation, circulating tumor cells (CTCs) interact with the host immune system, typically resulting in cancer cell destruction or apoptosis. Surviving cells arrest at secondary endothelial sites by a process of lectin binding consolidated by integrin-based stabilization of the epithelial–endothelial binding. The cells then undergo active transmigration and extravasate into the secondary site. Once the cells reach the bone marrow stroma, they may remain dormant for an undefined period or may proliferate and hence form a metastatic colony (based on [4]).

### 1.1.1 Local invasion and migration

Tumor growth depends on angiogenesis and lymphangiogenesis triggered by chemical signals from tumor cells in a phase of rapid growth. Without vascular support, tumors may become necrotic or even apoptotic [10]. Cancer cells also need to develop altered affinity for their extracellular matrix (ECM). The phenotypic change is initially mediated by alterations in the expression of cell-surface molecules known as integrins, release of proteases that remodel the ECM and deposition of new ECM molecules. Various signal transduction pathways are activated resulting in regulation of gene expression, cytoskeletal organization, cell adhesion and cell survival. As a result, cancer cells become more invasive, migratory and are able to survive in different microenvironments [11].

Local invasion is one of the fundamental early steps in metastasis formation, as without it tumor spread cannot occur. To develop invasive potential, the malignant cell must downregulate its cell–cell and cell–matrix adhesive characteristics, become motile and must acquire the ability to break down the ECM by using degradative enzymes [12]. Normally, the cells forming the epithelial sheets are strong enough and tightly bound to each other, to neighbouring cells or basement membranes by adherens junctions, tight junctions, desmosomes and hemi-desmosomes. These connection sites keep normal epithelial cells, as well as benign carcinomas inside the boundaries. However, as a tumor progresses, some of the carcinoma cells inside this tumor detach themselves from these limiting constraints and begin to move out on their own, first by dissolving underlying basement membranes and then invading adjacent stromal compartments. This acquired invasiveness seems to allow carcinoma cells to both intravasate and subsequently extravasate [13]. Within individual tumors, the populations of neoplastic cells are not homogeneous. Inside carcinomas, the subpopulations of cancer stem cells (CSCs) seem to be responsible for many of the biological traits of high grade malignancy [14]. Invasiveness, motility and self-renewal, which are principal traits for malignancy, may be the reflection of the CSC subpopulations.

In early embryonic morphogenesis, cell-biological program called epithelial-to-mesenchymal transition (EMT) enables cells of epithelial phenotype in the ectoderm to migrate, generate mesenchymal derivatives, invade and insert themselves between ectoderm and endoderm layers. This transdifferentiation program is driven by EMT-inducing transcription factors (EMT-TFs) [15].

A variety of cell types are recruited to the surrounding stroma of advanced primary tumors. These recruited cells, including fibroblasts, granulocytes, macrophages, mesenchymal stem cells, and lymphocytes create a “reactive” stroma, and form an inflammatory microenvironment that appears to result in the release of EMT-inducing signals. Expression of certain EMT-TFs are activated in carcinoma cells that govern EMT programs inside the cells [16]. Recent studies have reported that the EMT can induce non-CSCs to enter into a CSC like state [17]. Essentially, the set of traits that would allow epithelial cells to disseminate from primary tumors and seed metastases are

results of EMT. Thus, EMT is an attractive way to understand the mechanisms of dissemination. Moreover, the acquired resistance to apoptosis that is central to cells generated by an EMT is surely critical for the ability of carcinoma cells to survive the difficult journey from primary tumors to secondary metastatic sites [18].

E-cadherin is a transmembrane glycoprotein and it is used normally for critical functions during embryogenesis and organogenesis through intercellular adhesion and signaling [19]. The cadherin–catenin complex is essential for cell-to-cell adhesion. The locus coding for E-cadherin is well characterized and considered to be a tumour-suppressor gene as loss of E-cadherin function enables cell detachment and induces an invasive phenotype [20]. Actually, down-regulation of E-Cadherin is a critical component in the general process of EMT. Decreased E-cadherin expression has been associated with increased tumor stage, and with bone metastasis in PC [21]. Cell polarity and cell-to-cell binding are lost during this transition of epithelial cancer advancement and metastasis. These cells transform to a mesenchymal phenotype, which gives them the capacity to invade the ECM and move to distant sites [5].

Once the malignant cell has reached the stroma, it must enter the vascular or lymphatic circulation by permeating through the endothelial barriers. Tumor cells that are identified in transit within the blood stream are referred to as circulating tumor cells (CTCs) [22]. Tumor cells arrest on endothelial surfaces within the circulatory system and subsequently undergo transendothelial migration; this is another key event in cancer metastasis (**Fig. 1**). After that point, the cell binds to the endothelium, extravasates and transmigrates through the endothelial layer, where it proliferates and/or coalesces with other metastasized cells to form a micro-metastasis [5]. Interactions of tumor cells with the endothelium involve multiple adhesive connections (docking and locking) at the molecular level [23]. The initial binding step begins with selectins, followed by stabilization through integrin binding [24]. The surface proteins integrin  $\alpha$ L, integrin  $\beta$ 2, intercellular adhesion molecule (ICAM-1) and platelet endothelial cell adhesion molecule (PECAM-1) have been also shown to take part in the binding process [25]. Once the PC cells reach the bone marrow, the survival ones there establish a tumor microenvironment and build

a reactive stroma by interacting with other cells in the bone marrow [26].

### 1.1.2 Survival in the bone

The metastasis formation in particular organs is favored, because it may be influenced by differences in the structures of capillaries in various tissues. For example, the sinusoid capillaries in the bone marrow are thin structures and are formed from single layers of endothelial cells without any supporting cell lining, to facilitate the normal in and out trafficking of hemopoetic cells [27]. Because of this feature of bone marrow vessels, they may also be an easy destination for carcinoma cells and favorable site for metastasis for certain types of cancers (e.g., prostate, breast and lung) [28].

Cellular invasion and migration depend on the dynamic interaction between cells and the ECM. For instance, during invasion, cells release proteases that degrade and redesign the ECM, promoting cell passage through the stroma and entrance into new tissue [29]. During migration, cells extend lamellipodia and filopodia that attach to the ECM, and simultaneously break existing ECM contacts at their trailing edge. This permits the cell to move itself forward [30]. Most cancer cells that successfully translocate from the primary tumor to a secondary site undergo apoptosis within 24 hours of extravasation [31]. Colonization is an extremely inefficient process, and most of the cancer cells are wasted when they localize to a potential metastatic site.

Favorable colonization is assumed to involve the ability to gain mitogenic stimulation from growth factors and cytokines that are naturally accessible in the alien microenvironment [32]. Micrometastases are made out of actively multiplying cells. Active cell division is crucial for the generation of genetic and epigenetic changes that are needed to create opportunities for cancer cells to develop complex colonization programs. Once the resulting derivatives appear in these micrometastases, their novel phenotypes can be evaluated for an ability to confer selective benefit in the presence of very challenging microenvironments.

The spreaded mesenchymal tumor cells must go through the reverse transition to EMT, namely Mesenchymal – Epithelial Transition (MET) [33]. At the site of metastasis, cancer cells reproduce the pathology of their

corresponding primary tumors. The rate-limiting step in metastasis is the initiation of tumor growth at the secondary site. This suggests that cellular plasticity, the ability to undergo EMT and subsequently MET in the favorable microenvironments, is a crucial feature of a successful metastatic cell [34].

Numerous complex signaling systems are required for the induction of EMT and are also closely linked with MET. For instance, the FGFR2 gene encodes for FGFR2b and FGFR2c isoforms due to alternative splicing. FGF10 and FGF7 are the binding partners of FGFR2b and FGFR2b is the isoform of choice in epithelial cells, whereas FGFR2c is expressed in cells of mesenchymal origin and binds FGF2. During the progression process of prostate cancer, a class switch from FGFR2b to FGFR2c occurs and EMT accompanies this switch with increased potential for invasion and metastasis [35]. In a research conducted by Matsubara et al. [36], prostate cancer cells with decreased FGFR2b expression were transfected with FGFR2b expression construct and the proliferation and tumorigenicity of the prostate cancer cells were shown to be significantly suppressed, suggesting that EMT might be reversed. Epidermal growth factor receptor (EGFR) is a member of the receptor tyrosine kinase family and plays a major role in normal development. They are constantly overexpressed in malignant tumors and are thought to contribute to tumor progression. Yates et al. [37] reported that in vitro inhibition of autocrine EGFR signaling increased E-cadherin expression and cell-cell heterotypic adhesion. E-cadherin and catenins are also present in human prostate cancer metastases to liver, but without an activated EGFR, supporting the idea that the inverse relationship between E-cadherin expression and EGFR also exists in human tumors. This suggests that MET processes take place in the cancer cells [38].

When the cells enter the bone, they begin to interact with their environment and adapt themselves to the new conditions. The balance between the activities of osteoblasts (bone-forming cells) and osteoclasts (bone-lysing cells) in general determines the phenotype of metastatic bone lesions, and both type of cells have been implicated in bone metastasis [3]. Bone metastases with a bone-forming (osteoblastic) phenotype are the result of stimulation of osteoblasts or inhibition of osteoclasts (or both) by the cancer cells, whereas metastases with a bone-lysing (osteolytic) phenotype reflect

inhibition of osteoblasts or stimulation of osteoclast function (or both) by the cancer cells. Metastases from PC, most of which are adenocarcinomas, nearly always form osteoblastic lesions in bone; by contrast, bone metastases from kidney, lung or breast cancers more often are osteolytic. However, metastases from the relatively uncommon neuroendocrine tumours of the prostate also produce osteolytic lesions [7]. On the other hand researchers also observed that both osteoblastic and osteoclastic activities could be seen in the development of bone metastasis. Bones are remodeled in a way that osteoblastic activity causes increased mineralized bone formation on the sites of previous osteoclastic resorption. This process also takes place in normal bone development in a balanced way but metastatic state causes an increase in bone production [3,39].

PC cells have ability to alter bone environment by secreting factors that either directly affect osteoblast functions or influence bone formation indirectly, by modifying the bone matrix or microenvironment (**Fig. 2**). These factors take part normally in bone development and remodeling. For example, expression of several bone morphogenic proteins (BMP) has been detected in bone metastases from prostate carcinomas [40].

Concerning PC metastasis in bone, ET-1 production is a major factor in osteoblast overstimulation. ET-1 stimulates mitogenesis in osteoblasts. Tumor-produced ET-1 stimulates new bone formation via ET<sub>A</sub> receptor on osteoblasts. Incorporating growth factors produced by the osteoblasts into this new bone also enrich the local microenvironment. ET-1 induces PC proliferation by enhancing the mitogenic effects of insulin-like growth factor (IGF) and epidermal growth factor (EGF) as well [41]. Although ET-1 is an important factor, it is not the only osteoblast stimulator in PC metastasis.

PC cells produce many factors, including Wnts that are implicated in tumor-induced osteoblastic activity. Wnts are cysteine-rich glycoproteins that mediate bone development in the embryo and promote bone production in the adult. Wnts have been shown to have autocrine tumor effects, such as enhancing proliferation and protecting against apoptosis [42]. Some of the factors that are involved in the up-regulation of Wnt pathway, have also osteoblast regulatory roles, for example; bone morphogenic protein (BMP),

transforming growth factor- $\beta$  (TGF- $\beta$ ), IGF, vascular endothelial growth factor (VEGF) and platelet-derived growth factor (PDGF) [43–46].

Increment in osteoblast activity is in charge of the quantifiable enlargement in bone volume in PC bone metastases as well as for the accelerated bone mineralization rate [47,48]. The bone generated by prostate tumor stimulation is formed as abnormal ‘woven’ bone, characteristic of the bone produced in high-turnover states. This is the reason, why 90 % of the patients with metastatic PC have sclerotic lesions [47,49].

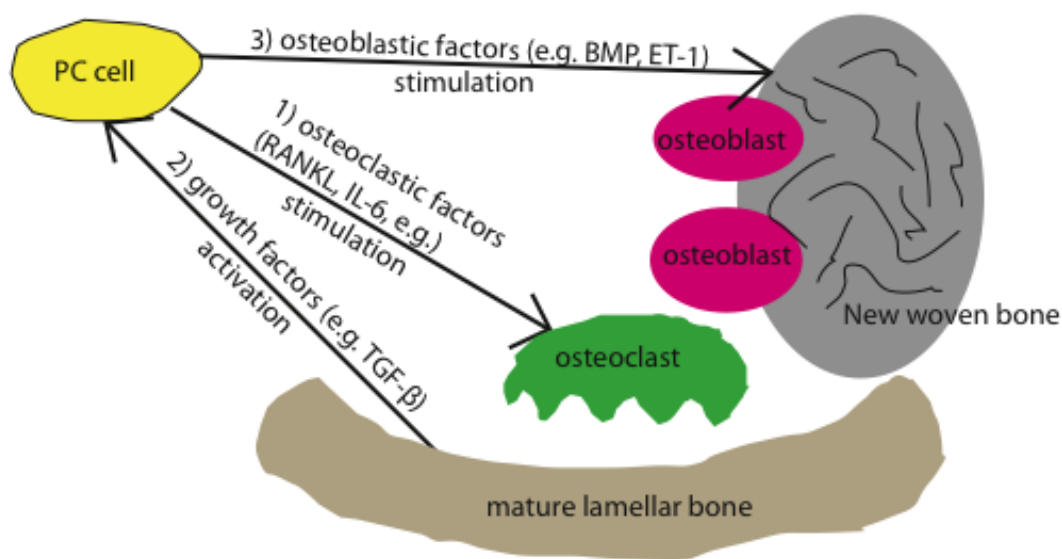


**Figure 2:** Putative mechanism of PC cell involvement in the bone. 1) PC cells secrete osteoclastic factors, which induce osteoclasts to resorb mature lamellar bone. 2) As the bone matrix is destroyed, it releases growth factors (e.g. TGF- $\beta$ ), which stimulates PC cells to grow and gain an osteoblast-like phenotype. 3) PC cells secrete osteoblastic factors (e.g. BMP, ET-1), which activate osteoblasts to form new woven bone (based on [3]).

Genetic alterations in PC cells alone are not enough to confer metastatic status without a supporting tumor microenvironment. Effective therapeutic targeting requires a more comprehension of the interactions between tumor and stroma [50]. Metastasis is a complex process, which involves the coordination of several signal-transduction pathways that allow cancer cells to adhere, proliferate, remodel their surrounding environment, to invade and migrate through new tissues, and to differentiate. Blocking the adhesive,

migratory and invasive capacity of tumor cells may be challenging but would be a useful way to treat the patients with malignant disease.

## 1.2. Collagen type-I

Collagen is an abundant structural protein in all animals. In humans, collagen comprises one third of the total protein, accounts for three-quarters of the dry weight of skin, and is the most widespread component of the extracellular matrix (ECM). In vertebrates, 46 distinct polypeptide chains form at least 28 different types of collagens [51].

The extracellular matrix of bone is mainly composed of type I collagen (Col-I), which is involved in bone mineralization process. For example, the mineralites of bone are stored almost solely within the collagen fibrils [52,53].

The defining feature of Col-I is an elegant structural motif in which three parallel left handed polypeptide strands staggered to form a right-handed triple helix. The crucial importance of Col-I as a scaffold for the body demands multiple essential features. These features include thermal stability, mechanical strength, and the ability to enroll in specific interactions with other biomolecules [51].

The most common motifs in the amino acid sequence of Col-I are glycine-proline-X and glycine-X-hydroxyproline, where X is any amino acid other than glycine, proline or hydroxyproline. Col-I has a hierarchical structure (**Fig. 3**). First, a three-dimensional stranded structure is assembled, with the amino acids glycine and proline as its principal components. This is not yet collagen but its precursor, procollagen. Procollagen is then modified by the addition of hydroxyl groups to the amino acids proline and lysine. This step is important for later glycosylation and the formation of the triple helix structure of Col-I. In addition N- and C- terminal ends are cleaved to form tropocollagen. Hydrogen bonds that form within the triple helix provides mainly its structural strength and stability. Individual tropocollagen monomers self-assemble into macromolecular fibers that are essential components of tissues and bones.

Col-I is a well-packed molecule; the rigid triple helical structure is responsible for the characteristic tensile strength. Col-I forms distinctive banded fibrils. These fibrils have a periodicity of 67 nm and a diameter of 50-200 nm. The

molecules in fibrils of Col-I are packed in a hexagonal array [54]. In bone collagen is synthesized intracellularly in osteoblasts as large precursor, called procollagen. It is then secreted into the ECM. After enzymatic modification, the mature Col-I monomers aggregate and become cross-linked to form Col-I fibrils.

PC cells can effectively attach and proliferate on Col-I [55]. Furthermore PC cells, which possess Col-I binding affinity, develop a significant number of bone tumors in contrast to cancer cells which do not attach to Col-I [56]. The PC cell line PC3 (bone metastatic cell) can spread and grow efficiently better on Col-I surfaces than on fibronectin surface [57]. The same integrins are also used by skin fibroblasts in the mechanism of modifying their Col-I containing ECM [58]. During invasion of bone tissue, prostate cancer cells need to establish connections to ECM proteins and grow on them. In addition, PC cells also need to degrade these ECM proteins to migrate through the bone tissue. In the research conducted by Nabha et al. [59], it is found that the combination of human prostate cancer PC3 and BMS (bone marrow stromal) cells stimulates the invasive ability of cancer cells through Col-I. The use of inhibitors for each of the major protease families indicated that matrix metalloproteinase-12 (MMP-12) was responsible for the BMS-induced invasion of PC cells. Downregulation of MMP-12 expression in PC3 cells by siRNA inhibited the enhanced invasion induced by PC3/BMS cell interaction. Hence, it was concluded that BMS cells induce MMP-12 expression in prostate cancer cells, which results in invasive cells capable of degradation of Col-I [59].

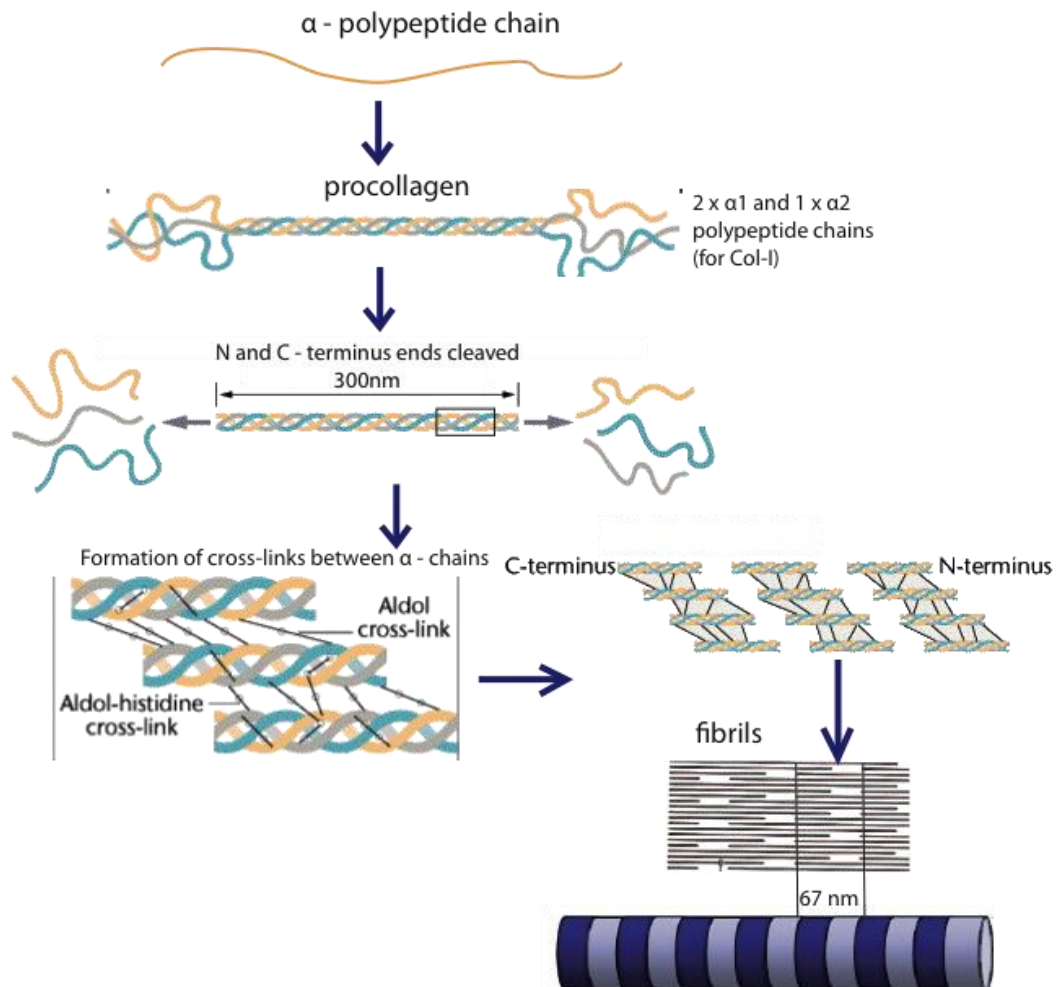


**Figure 3:** Biosynthesis of Col-I. Procollagen  $\alpha$ -chains are synthesized. Propeptides are associated to form trimers. N- and C-terminal propeptides are removed and trimers assemble into fibrils that are covalently crosslinked. The 67 nm staggering of the trimers gives the fibrils a banded appearance (Based on [60]).

### 1.3. Mesenchymal stem cells and their role in prostate cancer metastasis

Mesenchymal stem cells (MSCs) have the capacity of differentiating into a variety of mesodermal lineages, including fibroblasts, chondrocytes, osteoblasts, and adipocytes under proper culture conditions. They are plastic adherent cells that can be isolated from bone marrow, as well as some other tissues like adipose tissue, skeletal muscle, dermis etc [61]. Homing of adult bone marrow-derived MSCs to the sites of tumor growth is a well known phenomena [62]. In a recent study, researchers showed that PC cells can

induce MSCs to differentiate into osteoblasts [63]. Available data in this area of research suggest that conditioned medium from metastatic PC cell line favors commitment of MSCs toward osteoblasts, while a nonmetastatic PC cell line fails to induce osteoblast differentiation in the same culture conditions [63]. In agreement with this observation, it has been shown that intratibially injected MSCs stimulate new bone formation only when coinjected with the PC cell line PC3 [64].

Tumor cells are able to affect normal bone turnover by altering the bone marrow microenvironment, which has a reciprocal effect in promoting tumor growth. In the normal adult skeleton, bone is constantly being replaced in an interactive process controlled by osteoclasts, which are monocytic in origin and resorb existing bone [65]. This normal bone turnover may be disrupted by tumor cells at a number of levels. Uncoupling of normal bone turnover in favour of osteoclast activity induces osteolytic disease, typical of multiple myeloma and breast cancer-induced metastatic bone disease, whereas increased osteoblast activity induces osteosclerotic disease, characteristic of prostate cancer [66]. Tumor cells may directly induce osteolytic tumors in bone by activation or recruitment of osteoclasts via RANKL expression, a model proposed in multiple myeloma. Alternatively, tumour cells may alter osteoblast activation, either increasing osteoblast activity, resulting in osteosclerotic disease, or inhibiting osteoblast activation, resulting in osteolytic disease [65].

It has been suggested that the interaction between prostate cancer cells and another cell type, namely bone marrow stromal cells (BMSCs) is also critical for survival and proliferation of metastatic cancer cells in the bone microenvironment. BMSC-derived factors may be important for initial colonization and survival of prostate cancer cells in bone. Study using the osteoprotegerin, which is a factor produced by BMSCs and have inhibitory effect on TRAIL-induced apoptosis, have demonstrated that BMSCs protect PC cells from apoptosis [67]. Moreover, physical contact of metastatic PC cell with the BMSCs causes change in the expression of several genes. They include genes that function as growth factors, growth factor receptors, ECM proteins, cell adhesion molecules, proteases, and signal transduction molecules. Some of the genes that were regulated only by the physical

contact include collagen III  $\alpha 1$ , collagen IV  $\alpha 2$ , integrin  $\alpha 1$  and  $\alpha 2$ , MMP-2 and -9, osteopontin, raf-1, biglycan and uPA. They differed from genes regulated by soluble factors, implying that a separate mechanism is activated by physical contact [68].

#### 1.4. Integrins

Integrins are a diverse family of heterodimeric transmembrane receptors that bind different ECM molecules (**Fig. 4**). The family consists of at least 25 distinct pairings of 18  $\alpha$ -subunits and 8  $\beta$ -subunits, with each pairing being specific for a unique set of ECM ligands. Extracellular domains of the integrins are formed by an elongated trunk and a globular ligand-binding head region. There are also short cytoplasmic tails connected to the actin cytoskeleton. Integrins can bind different ECM such as collagens, laminins and fibronectin. Depend on which ECM protein they bind, integrins can be divided into different subfamilies. Common short RGD peptide domains are present on fibronectin, vitronectin and fibrinogen, while laminin and collagens possess different binding domains. Specifically, six-residue GFOGER sequence was found to be the recognition site on Col-I triple helices for  $\alpha 2\beta 1$  integrin [69]. Moreover, integrins expressed on the hematopoietic cells bind to counter receptors such as VCAM-1 or ICAM-1 on other cells [70].

Integrins are enzymatically inactive receptors, which connect to intracellular molecules that can trigger signal transduction. Integrin activation results from the ability to assume various affinity states that can be regulated bidirectionally. "Inside-out signaling" refers to the intracellular events involving the cytoplasmic domains of  $\alpha$  and  $\beta$  integrin subunits, which are coupled to extracellular conformational changes induced by extracellular factors. Integrins may increase signals generated by growth factor receptors by bringing kinases and substrates in close proximity [71]. Thus, integrins can move from an inactive state, in which they do not bind ligands, to an active state, in which they behave as high affinity receptors. Integrin activation is mainly regulated by talin, a large major actin-binding protein that associate to the cytoplasmic domain of  $\beta$  subunits. Talin binding to integrins disrupts an intracellular salt bridge between the  $\alpha$  and the  $\beta$  subunit, leading to increased

integrin affinity, which strengthens the interaction with the ECM. In addition, the kindlin family of proteins synergises with talin in integrin activation, behaving as an essential co-activator of integrin signaling [72].

The term “outside-in signaling” refers to the activation of integrins upon ECM binding and transmission of the signals inside the cells. This is needed for polymerization of actin cytoskeleton during cell adhesion and regulation of cell migration, proliferation, survival and differentiation [73]. In focal adhesions, ECM binding leads to formation of clustered integrins in the plane of the cell membrane and these are connected to the actin cytoskeleton. Integrin associated structural cytoplasmic proteins such as talin, kindlin, vinculin and  $\alpha$ -actinin are connected to F-actin at these focal adhesion sites, thus mobilizing actin filaments to integrin clusters [74]. Moreover, protein-protein interactions held by these integrin-associated molecules lead to multi-functional scaffolding, which brings kinases, phosphatases and their substrates together, hence regulating the dynamics of integrin-cytoskeleton joints [75]. The integrin clusters come in various forms, for example, focal adhesions, focal complexes, fibrillar adhesions, or podosomes, which are defined according to their size, shape, subcellular localization, molecular constituents, and organization [76]. The differences in size and composition of adhesion sites presumably reflect variances in the link to the cytoskeleton and integrin downstream signaling [77].

Induction of cytosolic kinases, stimulation of the phosphoinositides metabolism, activation of Ras/MAPK and PKC pathways and regulation of Rho GTPases could be regarded as integrin-mediated signaling events [78,79]. Signals from integrins, growth factor receptors or cytokines are well coordinated in a manner that the degree and duration of each signal differ depending on whether the growth factor receptors or the integrins are occupied by the ligand [70]. Integrin stimulation primarily results in tyrosine phosphorylation of proteins and this is a preferential way to transduce signals throughout the cell. For instance, the src family kinases (SFKs), focal adhesion kinase (Fak) and the adaptor molecule p130Cas are counted among the kinases that are activated and tyrosine phosphorylated upon ECM binding. In addition, these proteins play a distinctive role in integrin signaling [80,81].

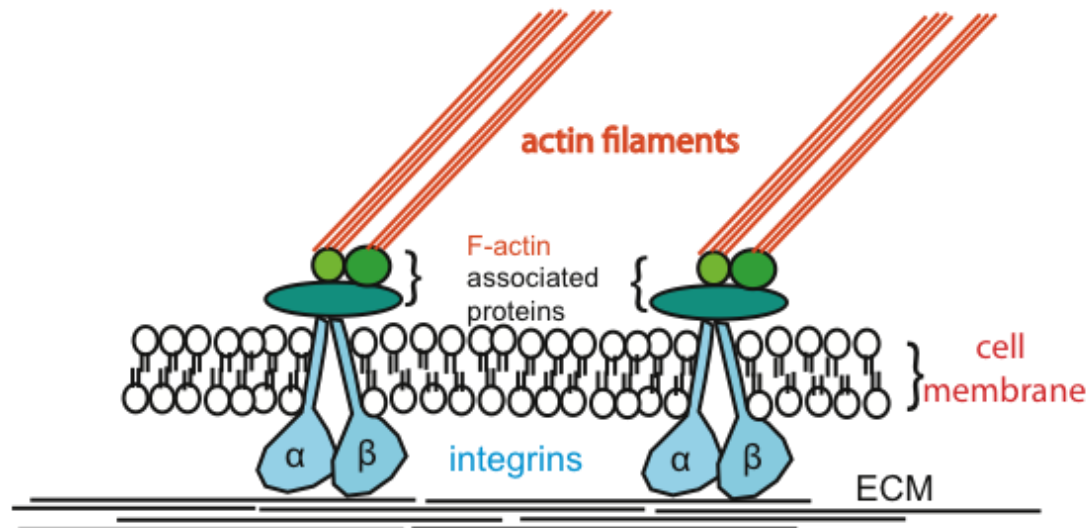


**Figure 4:** Schematic representation of a cell–matrix adhesion in which integrins connect the ECM to the actin cytoskeleton [based on 45].

Integrin expression varies between tumors and overexpression of some integrins have been associated with increased invasion [83–85]. In addition to change in protease activity, invasive cells also undergo dramatic alterations in levels of integrin expression and integrin affinity for ECM substrates. Numerous studies have documented marked differences in surface expression and distribution of integrins in malignant tumors compared with pre-neoplastic tumors of the same type [86]. For example, the integrin  $\alpha v \beta 3$  is strongly expressed at the invasive front of malignant melanoma cells and angiogenic blood vessels [87], but weakly expressed on pre-neoplastic melanomas and quiescent blood vessels. Furthermore, inducing expression of the  $\alpha v$  [88] or  $\beta 3$  [89] integrin subunit in a melanoma cell line increases metastatic potential. Similarly, the laminin-binding integrin,  $\alpha 6 \beta 4$ , is not expressed in normal thyroid cells, but induction of its expression correlates with the progression to invasive thyroid carcinoma [90].

PC cells preferentially adhere to bone marrow endothelium cells when compared to other endothelium tissue with the help of  $\beta 1$  integrins [91]. The ligand/receptor interactions are the elements, which are mostly responsible for the mechanical properties of cell adhesive attachments. However, formation, strength, and survival of a cell adhesive attachment also depend on how cytoskeleton-anchored molecular connections below the membrane, respond

to force [77].

### 1.5. Cell adhesion and single cell force spectroscopy

Cell connections involve multiple ligands and cell adhesion molecules (CAMs). Cell adhesion is commonly defined as the binding of a cell to a substrate, which can be another cell, a surface or an organic matrix. One way to study biophysical aspects of cell adhesion is to apply single cell force spectroscopy (SCFC). The method of SCFS is the combination of atomic force microscopy (AFM) and optical microscopy. Optical microscopy is used to position the cells to assess cellular interactions at a given location on a functionalized surface, tissue or on another cell [92]. An AFM that is fitted with a fluid chamber allows measurements to be made in aqueous environments under controlled temperatures. Suspended cells are added to the fluid chamber and allowed to settle. Thereafter, a single cell is captured by gently pressing a functionalized AFM cantilever onto it [93]. This converts the living cell into a probe (**Fig. 5A**), which is brought into contact with functionalized surfaces or other cells at a set force and for a specific adhesion time. Subsequently, the cantilever is withdrawn at a constant speed, detaching the cell from its binding place. During this separation process, the cantilever deflection, which is proportional to the vertical force that exists between the cell and substrate, is recorded in a force-distance curve (**Fig. 5B**). This curve provides the biomechanical signature of the cell adhesion. Analyzing this curve may be challenging because adhesion signals, which are observed on this curve, could be specific adhesions or unspecific adhesions, which can occur at the same time.

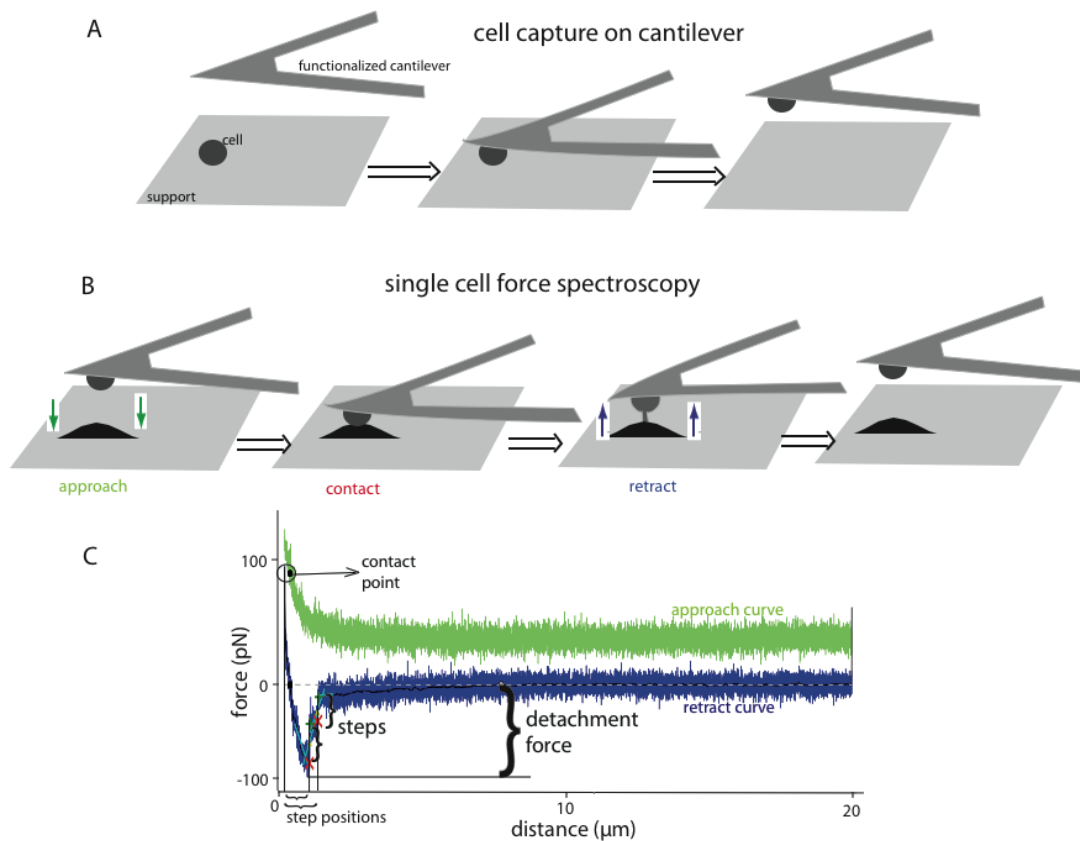


**Figure 5:** Force spectroscopic measurement of the interaction between a cell attached on AFM cantilever and a cell immobilized on given surface. **(A)** Cell capture on Poly-D-Lysine (PDL) functionalized AFM cantilever **(B)** The attached cell on the AFM cantilever approaches the immobilized cell on specific surface, make a contact for a defined period of time and then retracts to a certain level where the two cells are completely separated. **(C)** De-adhesion steps can be read on the recorded force-distance curves.

## 2. Aim and goals of the thesis

Prostate cancer (PC) is a malignant tumor, which commonly metastasizes into bone tissue. However, the exact mechanisms of how PC cells select this tissue as a metastatic site are still unknown and therefore, it is needed to investigate them in detail. Bone is a complex environment with several important cellular and matrix components building up the tissue. Collagen type-I (Col-I) is the most abundant cell matrix protein found in the bone environment and it has been already shown that an interaction of metastatic cells with this protein network is crucially important. On the other hand, mesenchymal stem cells (MSCs) residing in the bone marrow are precursors of the bone forming cells osteoblasts. Moreover, these MSCs have ability to secrete Col-I protein to make up their own extracellular matrix [94]. PC cells have several effects on these stem cells to form tumor microenvironment [68]. To investigate the mechanism of how PC cells invade bone marrow, several important questions should be addressed. Firstly, we should know whether these cells interact with the MSCs in the bone marrow; secondly, how strong they can adhere to Col-I and MSCs; and thirdly, what kind of forces are generated while these interactions are going on.

Thus, the **main aims** of this study were to find out the biophysical characteristics of the interactions of PC cells with bone marrow-derived MSCs and the ECM protein Col-I and to identify the responsible cell adhesion molecules.

We have defined the following **goals** to reach the above aims, which are:

1. Comparison of two different prostate cancer cell lines, which are namely PC3 (derived from bone marrow metastasis) and LNCaP (derived from lymph node metastasis) in terms of their abilities to adhere on bone marrow-derived components.
2. Estimating the affinity of these prostate cancer cells, during co-culturing, towards MSCs in terms of adhesion, spreading and proliferation.
3. Investigation of the involvement of the cell adhesion molecules (CAMs), specifically  $\beta 1$  integrins. Those may have important roles in the binding process between prostate cancer cells and Col-I or MSCs.

- 3.1. Analyzing integrin expression profile in the prostate cancer cell lines.
- 3.2. Investigation of single molecule forces generated by CAMs using single cell force spectroscopy.
4. Determination of the changes in the adhesion forces after blocking  $\beta 1$  integrins and degradation of the Col-I.
5. Detection of the participation of actin cytoskeleton in the adhesion of PC cells by inhibiting F-actin via Latrunculin-A treatment.
6. Evaluation of the force spectroscopy data to decipher the anchorage of cell membrane receptors and their connection to the cytoskeleton.

### 3. Materials and methods

#### 3.1. General cell culture conditions

PC3 and LNCaP cells were obtained from ATCC (Wesel, Germany). PC3 cells were maintained in RPMI-1640 cell culture media (PAA, Cölbe, Germany) and 10% FBS (Sigma-Aldrich, Munich, Germany). The SCP1 cell line is an immortalized human MSC line fully described in Böcker et al [95]. LNCaP and SCP1 cells were cultured in Alpha-MEM GlutaMAX culture media (Life Technologies, Karlsruhe, Germany) supplemented with 10% FBS. During routine cell culture, the three cell types were grown up to 80% confluence in T-25 or T-75 culture flasks and maintained at 37°C in humidified 5% CO<sub>2</sub>. The culture medium was changed three times per week and for cell passaging, cells were detached by treatment with 1x trypsin/EDTA solution (PAA).

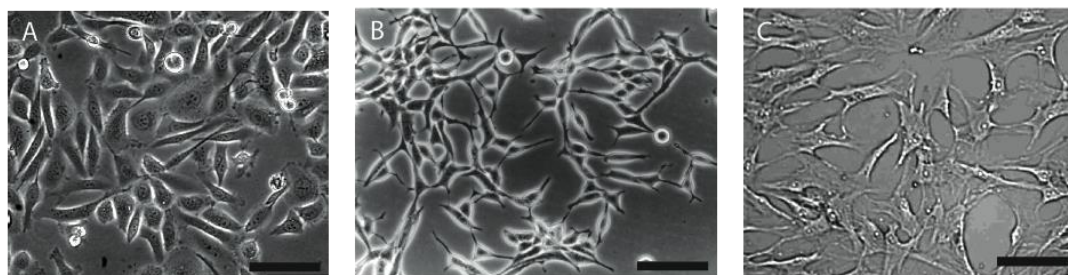


**Figure 6:** Phase contrast images of the cells grown in culture plates. PC cell lines PC3 and LNCaP are shown in (A) and (B) respectively. And MSC cell line SCP1 is shown in (C). Bars = 100µm

##### 3.1.1. Cell passaging and counting

Cell passaging was performed by washing the cell monolayer with PBS (PAA) and trypsinizing it with 1x Trypsin/EDTA (PAA) at 37 °C and 5 % CO<sub>2</sub> for 5 min. Detached cells were suspended in culture medium. A 10 µl of the cell suspension was used for cell counting. Cells were counted microscopically in a Neubauer chamber (brand, Grafrath, Germany). The total number of cells was determined by the following formula:

$$\text{cells/ml} = \frac{\text{cell number (counted in chamber A+B+C+D)}}{4} \times 10^4$$

### **3.1.2. Cryopreservation**

A freezing medium was prepared prior cryopreservation. Freezing medium contained 70 % normal culture medium, 20 % FBS and 10 % dimethylsulfoxid (DMSO) (Merck, Darmstadt, Germany). After trypsinization and counting, cells were pelleted by centrifugation at 500 g for 5 min. The supernatant was completely aspirated and the cell pellet was resuspended in pre-cooled at 4 °C freezing medium. Afterwards, the cell suspension was aliquoted in cryovials which were then stored -80 °C or in liquid nitrogen.

### **3.1.3. Cell culture prior capture of cells for force spectroscopy**

Cells (LNCaP or PC3) grown to 80% confluency were incubated in trypsin/EDTA solution (0.02%) for 5 min to 10 min until released from the substrate after washing with PBS lacking calcium and magnesium. This procedure should remove any matrix proteins possibly covering the cell surfaces without affecting the integrin receptors [96,97]. Then the cells were transferred with additional MEM-Alpha medium into a centrifuge tube. The cells were then spun down (1000 rpm, 3 min) before resuspending the pellet with fresh MEM-Alpha medium. The cells were left in an incubator at 37°C for 15 min., in order to adapt them to the measurement temperature of 37°C in the AFM. Either PC3 or LNCaP cells (approx. 2 ml containing 100 to 300 cells) were then gently injected onto the non-adhesive BSA-coated cover slip in order to subsequently capture one of them with the adhesive PDL-coated cantilever: The adhesive cantilever was positioned over one of the obviously healthy cells (medium size, round shaped at normal contrast, no blebs, no other abnormal indications in shape) on the BSA-coated cover slip, and lowered in a stepwise manner until it was close to the surface of this cell. Then, the cantilever was gently in held contact with the cell for a few seconds before the cantilever-bound cell was lifted vertically by approximately 100 nm [92]. The cell was allowed to establish firm adhesion on the cantilever for a couple of minutes. Some cells (approx. 10%) refused to adhere firmly to the lever rather hanging loosely as determined by gently shaking the microscope and watching the cell move with the induced agitation. In this case the cell

was washed off the cantilever by lifting it out of the liquid and back again in order to capture a new cell. In the case of firm adhesion, the cell was used for adhesion experiments and monitored by the experimenter via the light microscope image during the entire period of measurements.

#### **3.1.4. Application of integrin blocking antibody**

After detachment of PC3 cells, the released cells were collected and washed with PBS (lacking calcium and magnesium). Prior to force spectroscopy and cell adhesion assay measurements, PC3 cells were suspended with fresh serum-free Alpha-MEM medium (Life Technologies) supplemented with 15 mM HEPES (Sigma-Aldrich). Integrin  $\beta$ 1 blocking antibody (Acris antibodies, San Diego, USA) in a concentration of 4.8  $\mu$ g/ml was added into 0.5 ml cell suspension containing  $2 \times 10^5$  cells and incubated for 30 minutes at 37°C.

#### **3.1.5. Latrunculin-A treatment and fluorescent staining of actin cytoskeleton**

$3 \times 10^4$  PC3 cells were plated on two Col-I coated (100  $\mu$ g/ml) glass slides. Cells were incubated overnight at 37 °C. One of the slides were treated with 0.2  $\mu$ M latrunculin-A (Sigma-Aldrich) diluted in culture medium containing 0.2% FBS for 20 min at 37°C. After cells were washed with PBS, they were fixed %4 Paraformaldehyde/PBS for 15 min at room temperature. After fixation PC3 cells were used for staining of the actin cytoskeleton. Cells were rehydrated in PBS (3x5 min) and permeabilized with %0.2 Triton X-100 in PBS (Sigma-Aldrich) for 2 min. After applying Image-iT FX enhancer (Molecular Probes, Invitrogen) for 30 min, the actin filaments were stained with dye Alexa Fluor 546 labelled phalloidin (Invitrogen). Phalloidin was diluted 1:50 in 1% BSA/PBS and it was applied on cells in darkness for 20 min. Finally, slides were rinsed in PBS (3x5 min) and mounted with anti-fading medium (6 g glycerol, 2.4 g Mowiol, 12 ml 0.2 M Tris HCl pH 8.5, 0.024 g DABCO and 6 ml dH<sub>2</sub>O). Fluorescent images were taken with the AxioCam MRm camera on Axiovert S 100 inverted microscope (Carl Zeiss) [98].

### 3.2. Time-lapse microscopy and quantification of cell adhesion

SCP1 cells ( $10^6$  cells) were grown in 6-well dishes to full confluence. PC3 and LNCaP cells were labelled with the 10 mM green fluorescent CFDA dye (carboxyfluorescein diacetate, acetoxymethyl ester, Invitrogen) and then plated on the formed SCP1 monolayers ( $5 \times 10^5$  cancer cells/well). Directly after, microscopy images were collected with 25 minutes intervals for at least 12 hours. Microscope stage was moving automatically to place the plates on the objective. Because of plate shake off effect non-adherent cells were kept out of focus and excluded in the imaging. During time-lapse the cells were kept in a bio-chamber, providing stable 37 °C and 5% humidified CO<sub>2</sub> atmosphere (Pecon, Erbach, Germany), mounted on an inverted optical microscope (Axiovert 100, Carl Zeiss Hallbergmoos, Germany). The images were taken with an AxioCam MRm CCD camera (Carl Zeiss) and by using manually the cell counter tool of Image J version 1.40 software (National Institute of Health, USA) the number of adherent cells was estimated and shown as percentage to the initial cell input at 4 and 12 hours.

### 3.3. Cell proliferation analysis

SCP1 monolayers were formed as described above and  $2 \times 10^5$  PC3 and LNCaP cells were added and left to expand onto SPC1 cells for a period of 8 days. In addition, several culture wells were retained only with SCP1 cells (SCP1<sub>mono</sub>) in order to be used as controls for the quantification analysis. The co-cultures (PC3<sub>+SCP1</sub>, LNCaP<sub>+SCP1</sub>) were monitored microscopically and photographed with the AxioCam MRm camera (Zeiss). At day 1, 5 and 8 the cocultures were trypsinized and by using Neubauer cell counting chamber, the total cell number was estimated. The proliferation of PC3 and LNCaP cells on SCP1 monolayer (PC3<sub>on mono</sub>, LNCaP<sub>on mono</sub>) was calculated as follows:

$$PC3_{on\ mono} = PC3_{+SCP1} - SCP1_{mono}$$

$$LNCaP_{on\ mono} = LNCaP_{+SCP1} - SCP1_{mono}$$

### 3.4. Cell shape analysis

Cell shape analysis PC3 and LNCaP cells ( $4 \times 10^4$  cells/slide) were grown on Col-I (10  $\mu\text{g/ml}$  protein) glass slides for 48 h. Then, the cells were fixed with 4% PFA for 20 min at room temperature and maintained in PBS during the AFM scanning. From the AFM image data, using JPK Image Processing 3.1.1.5 software (JPK Instruments), the following three parameters were estimated: h – height, A – area and V – volume. Using these parameters, the flatness shape factor  $f = \sqrt{\pi/(4A)}$  was calculated [23].

### 3.5. Optical density adhesion assay on 96-well plates

Cell adhesion assays were performed according to Docheva et al [99]. Prior to the adhesion assays, 96-well plates were coated with 10  $\mu\text{g/ml}$  Col-I at 4°C overnight and then blocked with 5% skim milk powder (Merck, Darmstadt, Germany) in PBS for 1 hour at 37°C. The wells were washed with PBS and a fraction of these wells was treated for 1 hour at 37°C with 200  $\mu\text{g/ml}$  collagenase type-2 (in PBS 7,4 PH). PC3 cells ( $3 \times 10^5$ ) were plated and incubated for three distinct time periods at 37°C in humidified 5% CO<sub>2</sub>. Non-adherent cells were removed by washing with PBS. The adherent cells were lysed and stained overnight at 37°C with a substrate buffer consisting of 7.5 mM NPAG, 0.1 M sodium citrate, pH5.0 and 0.5% Triton X-100. Prior to the measurements, a stopping buffer (50mM glycine, pH10.4 and 5mM EDTA) was added to the wells and then the optical density was measured at 405 nm on a micro-titre-plate reader (Multiscan FC, Thermo Fisher scientific, Waltham, USA). The amount of adherent cells was finally calculated as a percentage of the absorption of  $3 \times 10^5$  cells, which were directly lysed with the substrate buffer.

### 3.6. Immunofluorescent staining of collagen type-I

Prior to protein coating, glass slides were cleaned with 70% ethanol and then autoclaved. In order to verify the collagen type I (Col-I) -coating of the glass

slides and the Col-I expression on SCP1, slides and SCP1 monolayers were prepared as follows. SCP1 cells were grown on glass slides for two days in order to form confluent cell monolayers, while Col-I - coated glass slides were prepared by adding 1mg/ml Col-I solution at 4°C overnight. Next, SCP1 monolayers and the Col-I-coated slides were fixed with pure acetone for 20 min at -20°C, rinsed with PBS. Image-iT FX Signal Enhancer (an Invitrogen product for background reduction and signal intensification of Alexa Flour secondary antibodies) was applied for 30 min and blocked with 10% BSA for 1 hour. The primary mouse monoclonal anti-collagen-I antibody (Sigma) was applied overnight at 4°C. This step was followed by incubation with the secondary anti-mouse antibody conjugated to Alexa Flour 488 for 1 hour and the nuclear stain DAPI for 5 minutes. In parallel, negative controls were carried out by omitting the primary antibody. Photomicrographs were taken with an Axiocam MRm camera on an Axioskope 2 microscope (Carl Zeiss) using 40x objective. Additional SCP1 monolayer slides and Col-I coated slides were prepared to make analysis using confocal microscopy.

### **3.7. Evaluation of integrin expressions with RT-PCR**

#### **3.7.1. Semi-quantitative PCR**

The semi-quantitative PCR was performed as described in Popov et al, 2011 [100]. Briefly, total RNA was extracted from PC3 and LNCaP cells with RNeasy Mini Kit (Qiagen, Hilden, Germany) and 1 µg RNA was used for cDNA synthesis with AMV First-Strand cDNA Synthesis Kit (Invitrogen). 1:10 diluted cDNA was used for PCRs. PCR for integrin  $\alpha$ 1,  $\alpha$ 2,  $\beta$ 1 and GAPDH (used for normalizing the cDNA input) was performed with Taq DNA Polymerase (Invitrogen) in a MGRsearch instrument (BioRad, Munich, Germany). Primer sequences and PCR conditions are available on table 1 [100]. All PCR results have been reproduced three times independently.

Primer pairs	Product size (bp)	Annealing temperature (°C)
Integrin genes		
$\alpha$ 1 F: 5'-ACATCAGCCAAGTCAATGTTTCG-3' R: 5'-AGCATTAAACAGCAACAATCCGG-3'	241	51
$\alpha$ 2 F: 5'-GCTGCTGTGCATTAGATATTAG-3' R: 5'-CTGTAACCTTCTGGTGAAATCCT-3'	217	48
$\alpha$ 11 F: 5'-TGGGCGCACCCATGTACTTC-3' R: 5'-ATGGCTCCTGCGTGGTTGTC-3'	223	55
$\beta$ 1 F: 5'-ATGAATGAAATGAGGAGGATTACTTCG-3' R: 5'-AAAACACCAGCAGCCGTGTAAC-3'	322	52
House-keeping gene		
GAPDH F: 5'-CAACTACATGGTTTACATGTTC-3' R: 5'-GCCGTGGCTCCACGAC-3'	181	50

**Table 1:** Primer sequences for RT quantitative and semi-quantitative PCRs. Abbreviations: F– forward; R – reverse; bp – base pairs (taken from Popov et al, 2011 [100])

### 3.7.2. Quantitative-PCR

The quantitative RT-PCR was performed as described in Popov et al [100]. Briefly, total RNA was extracted from PC3 and LNCaP cells with RNeasy Mini Kit (Qiagen, Hilden, Germany). For cDNA synthesis, 1  $\mu$ g total RNA and AMV First-Strand cDNA Synthesis Kit (Life technologies) were used. LightCycler Fast Start DNA Master SYBR Green kit (Roche, Munich, Germany) and primer kits for  $\alpha$ 1,  $\alpha$ 2,  $\alpha$ 11,  $\beta$ 1 and glyceraldehyde 3-phosphate dehydrogenase (GAPDH) (all Search-LC, Heidelberg, Germany) were applied. The PCR was performed in LightCycler 1.5 instrument (Roche) equipped with LightCycler 3.5.3 software. Crossing points for each sample were determined by the second derivative maximum method and relative

quantification was performed using the comparative  $\Delta\Delta\text{Ct}$  method according to the manufacturer's protocol. The relative gene expression was calculated as a ratio to GAPDH.

### **3.8. Single cell force spectroscopy**

#### **3.8.1. Substrate preparations for AFM experiments**

We have used collagen type-I (Col-I)-coated glass cover slips and SCP1 monolayers as substrates for the AFM force spectroscopy experiments within the same culture dish lid. To form SCP1 monolayers, SCP1 cells were grown on untreated culture dish lids (petri dish 35 X 10mm, nunc A/S, Roskilde, Denmark) for two days at 37 °C, 5% CO<sub>2</sub>. Prior to use, they were washed with and covered by 1.5ml fresh serum-free MEM-Alpha medium (Invitrogen, Karlsruhe, Germany) supplemented with 15mM HEPES (Sigma-Aldrich, Germany) resulting in a CO<sub>2</sub> independent measurement medium. For cell to Col-I measurements glass cover slips (Ø 15mm washed in 70% ethanol and distilled water) were coated with Col-I (100µg/ml) at 4°C overnight. Prior to the cell adhesion measurements, the Col-I-coated cover slips were placed on top of the SCP1 monolayer in the culture dish lids (as depicted in **Fig. 12**). An additional glass cover slip coated with BSA (0.5%w/v) at 4°C overnight was placed on top of another section of the SCP1 monolayer and it was used for cell capture. The culture dish lid, containing all three types of substrates (BSA, Col-I and SCP-1 monolayer) was then mounted on a temperature-controlled stage in the AFM and it was left to equilibrate for 10 min in ambient air at 37°C.

#### **3.8.2. AFM setup and collection of the force spectroscopy data**

As shown in **Fig. 12** and **25**, we used Col-I-coated glass cover slides, SCP1 monolayers and BSA-coated glass cover slides (control) as substrates for AFM force spectroscopy experiments. Fresh serum-free Alpha-MEM medium supplemented with 15 mM HEPES (Sigma-Aldrich) was used as measurement media throughout all force spectroscopy experiments. The culture dish lid, containing BSA and Col-I coated substrate as well as the SCP1 monolayer

was mounted on a temperature-controlled stage in the AFM and was left to equilibrate for 10 min at 37°C. Force Spectroscopy experiments were conducted using a NanoWizard II together with a CellHesion module (JPK Instruments, Berlin, Germany), mounted on a Zeiss Axiovert 200 M (Carl Zeiss, Goettingen, Germany) with a custom made temperature unit for 37°C. The force sensors used for force spectroscopy were tipless silicon nitride cantilevers with a nominal spring constant of 0.01 N/m (Tipless, MLCT-O10, Veeco, USA). Prior to cell adhesion experiments, the force sensors were coated overnight with 100 mg/ml Poly D-Lysine (PDL, Millipore, USA). The spring constants of the force sensors were determined individually by the thermal noise method.

Either a PC3 or a LNCaP cell resting on the BSA coated coverslide was allowed to firmly adhere to the PDL coated tipless force sensor (**Fig. 7**) [101]. Force-distance curves were recorded while the piezo traveled in a closed loop up to 20  $\mu\text{m}$  at an approach velocity of 7  $\mu\text{m/s}$  until a trigger force of 100 pN was reached. Subsequently at a retraction velocity of 3  $\mu\text{m/s}$ , the adhesion force signature was recorded (**Fig. 5B**).

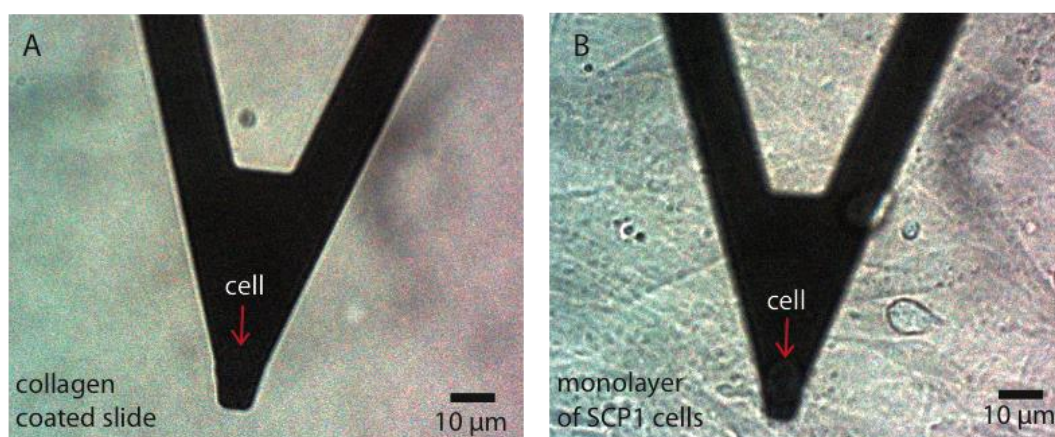


**Figure 7:** PC3 cell is attached on AFM tipless cantilevers used as a probe for single cell force spectroscopy experiments on substrates (A) Col-I-coated slide (B) SCP1 cell monolayer

### 3.8.3. Latrunculin-A treatment of a cell on the cantilever

PC3 cells were prepared as described above for force spectroscopy experiments. One of the cells was captured from the BSA surface and attached to the PDL coated cantilever. Initially 60 force curves were collected on Col-I substrate with this cell, to check for normal adhesion properties (data not shown). (Subsequently Latrunculin-A (Sigma-Aldrich, USA) was added into the measurement medium until a final concentration of 0.2  $\mu\text{M}$  was reached. After a period of 15 minutes for allowing Lat-A to disrupt the actin cytoskeleton, 60 additional curves were recorded with the same cell. In total 4 different cells were treated and measured in this way.

### 3.8.4. Elasticity measurements of the prostate cancer cells

From AFM adhesion force spectroscopy curves, we determined the Young's modulus from both LNCaP and PC3 cell types to estimate the contact area at a given contact force. We have analyzed 800 force curves of 9 cells from each cell type to determine the Young's modulus of the cells (**Fig. 11**). The Young's modulus of the cells were determined using Hertz model assuming the indenter is in a spherical geometry. The radius of the spheric cell was assumed to be approximately 10  $\mu\text{m}$ .

### 3.8.5. Force spectroscopy data evaluation

For data analysis only the retraction parts of the approach-retract cycles were evaluated. In order to obtain characteristic quantitative information from the force-distance curves, a custom-designed data evaluation and step detection software [102] was used to denoise the signal (black lines in **Fig. 5B**), find the baseline (dashed lines in **Fig. 5B**), correct for hydrodynamic drag and possible drift. Furthermore we extracted the following parameters from the force spectroscopy curves [101]:

**a) step height [pN]** describing the difference in force measured before and after an individual detachment event, visible as a force step. The algorithm

identifies such a step by maxima in the derivative of the denoised signal that surmount a certain threshold and marks it by a small red cross (Fig. 5C). The last step in a force curve is the most reliable one since in contrast to all other (intermediate) steps no other connection between cell and substrate persists.

**b) adhesion rate [%]** describing the fraction of curves with at least one detected force step.

**c) number of steps** describing the average number of steps detected per curve (only counting curves with at least one detected force step).

**d) step position [mm]** describing the distance between the contact point (black circle at the intersection of baseline and retrace curve) and a force step.

**e) work of detachment [aJ]** describing the energy dissipated during that force experiment by integrating the area between baseline (zero force) and retract curve. (Note: this has no trivial relation to the adhesion energy. In fact, velocity dependent viscous and plastic deformation of the cell and the cell membrane itself strongly contribute to the work of detachment far from the thermodynamic equilibrium).

**f) detachment force [pN]** describing the highest measured adhesion (global maximum) per curve.

**g) plateau steps**, for this set of data appear after a force plateau of at least 500 nm length at loading rates of less than 27 pN/s (see step in Fig. 30B). At loading rates between 27 and 40 pN/s the criterion was not clear enough to avoid false positive or negative step discrimination.

**h) steep (jump) steps** consequently occur after an increase in force of at least 40 pN/s (See steps in Fig. 30A).

### 3.8.6. Density plots of tethers and jumps

We also analyzed force-loading rates (slope of the force trace) prior to each step. Due to a constant velocity of 3  $\mu\text{m/s}$  the loading rate was directly derived from the force-distance trace. Steps were defined as plateau steps (tethers) with loading rates less than 24 pN/s ( $\sim$ slope of 8 pN/ $\mu\text{m}$ ) and as steeper steps (jumps) with loading rates higher than 36 pN/s ( $\sim$ slope of 12 pN/ $\mu\text{m}$ ). We have normalized the data relative to the total number of steps in each group and

plotted slope versus positions (in logarithmic scale for a better visualization) and created 2D maps of the data and finally smoothed it using a computer algorithm with the bin intervals of x and y axes:

Sigma x = 0.1

Sigma y = 5

### **3.9. Statistical analysis**

An unpaired t-test assuming unequal variances was used to analyze the adhesion rate, the average number of steps, percentage of F- & T-steps (in SCFC) by comparing the means collected from individual cell types with or without treatment of antibody on different substrates. The means were indicated as columns and error bars represent the standard error of the mean. Same t-test was used to compare the numbers of cell attachments on SCP1 monolayers (in time lapse microscopy).

A nonparametric Mann-Whitney test without assumptions was applied to compare Young`s modulus, detachment forces, step heights, works from all force curves between individual cells with or without treatment of antibody on different substrates. Medians are indicated as the middle line inside the box-plot and boxes represents the quartiles of +/- 25% of the data from the median values. Error bars covers the whole data in which a few extreme values were excluded.

### **3.10. Softwares and websites used in the study**

For the evaluation of the force spectroscopy curves we have used a custom designed step detection algorithm [102]. Analyses of the collected data have been done with the Microsoft, Excel (2008) program. And statistical calculations were done with the StatPlus extension of the Microsoft, Excel program. 2D heat plots of the membrane anchoring data were done with the Mathematica software version number 9.0.1.0. The figures of the thesis were created with Adobe Illustrator and Microsoft PowerPoint.

For the analysis of the images taken from time-laps, fluorescent and confocal microscopy data we have used ImageJ program, can be downloaded from the

---

website <http://imagej.nih.gov/ij/>. The literature searches were done with the websites Pubmed (<http://www.ncbi.nlm.nih.gov/pubmed>) and Web of Science (<http://apps.webofknowledge.com/>).

## 4. Results

### 4.1. PC3 and LNCaP adhesion, proliferation and spreading in co-culture with SCP1

First, cell adhesion was analysed by using time-lapse imaging for up to 12 h. CFDA (Carboxyfluorescein diacetate) pre-labelled PC3 and LNCaP cells were plated on previously formed SCP1 monolayer. The added PC3 and LNCaP cells were monitored on the SCP1 monolayer and after 4 hours, most of the PC3 cells appeared spread on the SCP1 monolayer whereas the LNCaP cells appeared small and round (**Fig. 8A**). Microscope stage was moving automatically to place the plates on the objective. Because of plate shake off effect during imaging non-adherent cells were kept out of focus and excluded. Despite that the morphologies of the two cell types were different, only the adherent cells were included in all countings. Our quantitative analysis showed that approx. 90% of the PC3 cells were able to adhere to the SCP1 monolayer already after 4 h and that their adhesion also remained close to 90% after 12 h (**Fig. 8B**). In contrast, LNCaP cells had lower adhesion to SCP1 (approx. 25%), which did not increase significantly after longer cultivation time.

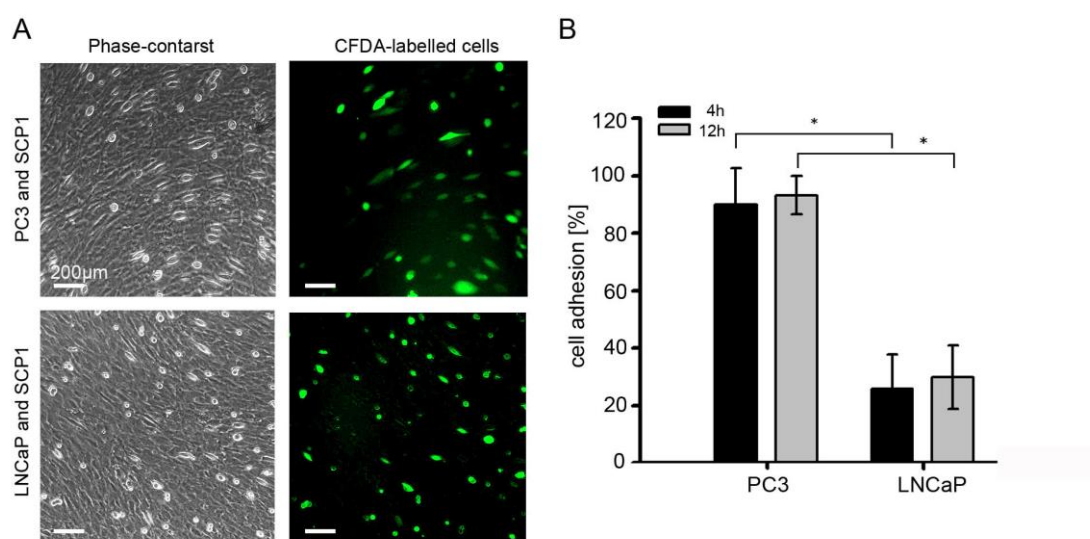


**Figure 8:** Cell adhesion of PC3 and LNCaP cells on SCP1 monolayers analysed by time lapse imaging. **(A)** Phase-contrast and fluorescent microscopy of CFDA-labelled PC3 and LNCaP cells plated on SCP1 monolayers in 6-well dishes. Images are taken after 4 h. **(B)** Quantification of adherent PC3 and LNCaP cells after 4 and 12 h cultivation on SCP1

monolayers. The percentage of adherent cells was quantified first, by manual counting of the CFDA-labelled cells with the cell counter tool in Image J software and second, by comparing to the initial number of plated cells (approx..  $50 \times 10^3$  cells/well). In the images also a slight background of CFDA dye particles is visible (more apparent in the LNCaP image). The graph bars show mean  $\pm$  SD of four independent experiments ( $p < 0.0001$ , unpaired t-test).

In order to investigate PC3 and LNCaP cell proliferation on SCP1 monolayers, we performed co-culture experiments for up to 8 days. Phase-contrast microscopy at day 1 and 8 demonstrated the formation and propagation of PC3 colonies on top of the SCP1 cells, whereas LNCaP cells formed small cell clusters, which did not expand but rather regressed during this period (**Fig. 9A**). Next, the co-cultured cells were counted at three different time points and the growth of PC3 and LNCaP was calculated by subtracting the cell number of SCP1 monolayers cultivated in parallel as controls. Our quantitative analysis confirmed the microscopy observation that PC3 cells, but not LNCaP cells, were able to divide and further expand on SCP1 cells (**Fig. 9B**).

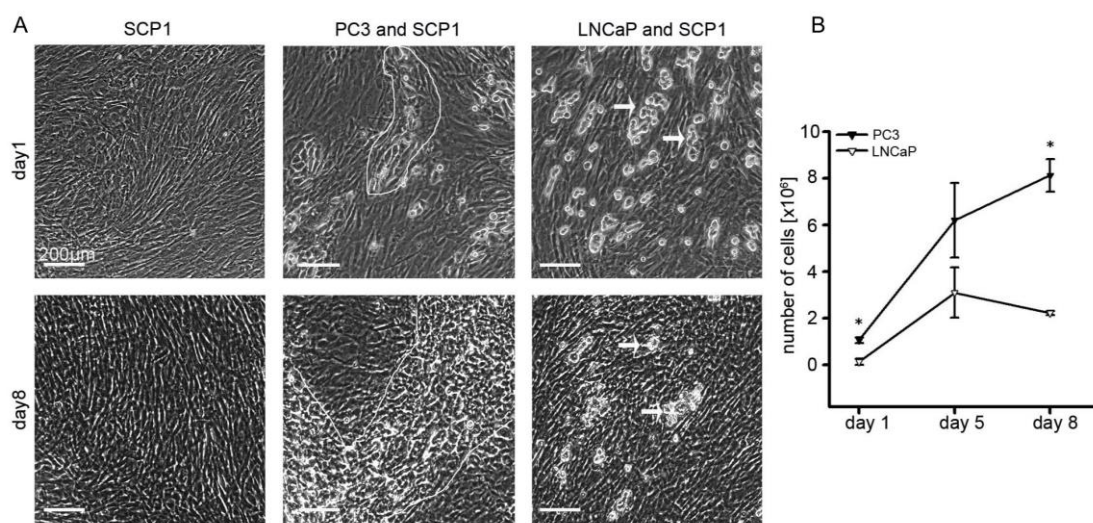


**Figure 9:** Expansion of PC3 and LNCaP cells on SCP1 monolayers (**A**) PC3 and LNCaP cells (approx..  $20 \times 10^3$  cells/well) were grown on SCP1 monolayers in 6-well dishes for up to 8 days. Phase-contrast images demonstrated the formation and propagation of PC3 colonies (outlined) on the top of SCP1 cells between day 1 and 8. In contrast, LNCaP cells formed small cell clusters (arrows) that did not expand but rather regressed by day 8. (**B**) Quantification of PC and LNCaP cell numbers after 1, 5 and 8 days of cultivation on SCP1 monolayers. The proliferation of PC3 and LNCaP cells was calculated by subtracting the SCP1 control monolayers from the total cell count of the co-culture. The graph shows mean  $\pm$  SD of three independent experiments for each time point ( $p < 0.0001$ , unpaired t-test).

To find out how much cells could spread when they cultured on the surfaces, Shape analysis of the cells PC3 and LNCaPs were carried out by calculating their flatness shape factor. As shown in **Fig. 10A**, PC3 cells grown on glass or Col-I-coated glass have a lower flatness shape factor compared to LNCaP cells, indicating a higher capacity to spread. However, shape analysis of both cell types cultivated on SCP1 monolayers were not carried out due to the risk of inaccurate measurements of area, diameter and volume due to the underlying cell bodies of the SCP1 cells. In contrast to the data given in **Fig. 9B**, when cultivated on polystyrene (without SCP1 cells), PC3 and LNCaP cells, have comparable proliferative capacity (**Fig. 10B**). Hence, we concluded that PC3 cells have a strong affinity towards SCP1 cells in terms of cell adhesion and proliferation.

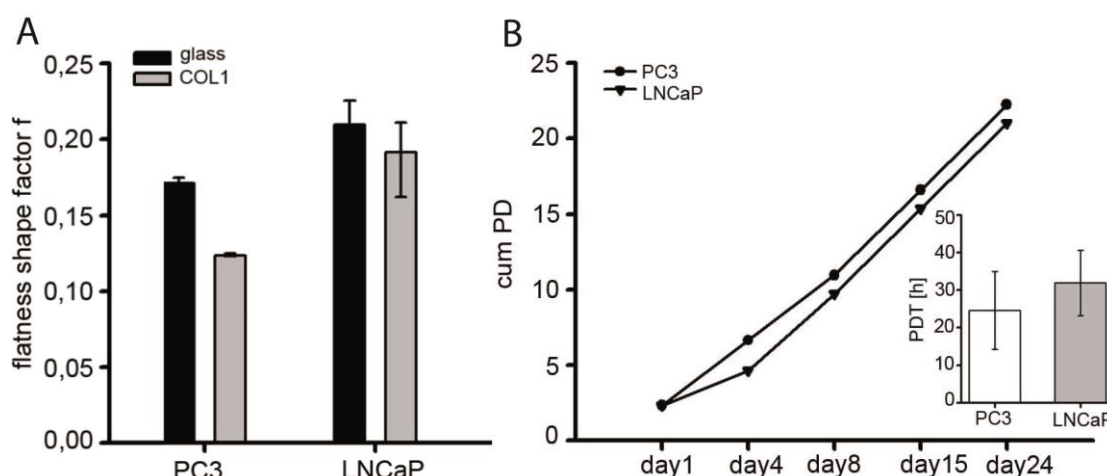


**Figure 10:** (A) Flatness shape factor of PC3 and LNCaP cells, cultivated on glass or Col-I coated glass slides, was calculated as described in Docheva et al [57]. The results revealed that PC3 cells are flatter on both surfaces compared to LNCaP cells. Graph bars represent mean  $\pm$  SD of at least three independent AFM scans for both cell type on each surface. (B) Analysis of PC3 and LNCaP proliferation on polystyrene. Both cell types were cultivated in T-75 flasks and during passaging over a period of 24 days their number was recorded. Cumulative population doubling (cum PD) and population doubling time (PDT) were calculated as described in Huang GT et al 2006 [103]. The obtained results demonstrate that in a non co-culture condition both cell types have comparable proliferative capacity. In the calculation of PDT, graph bars represent mean  $\pm$  SD of the different passages for each cell type.

#### 4.2. Calculation of Young`s modulus of PC3 vs LNCaP cells

Cells, which are attached on the tipless AFM cantilevers, were used as a probe to elucidate their adhesion behaviors toward different substrates specifically SCP1 monolayer and Col-I. The contact area of a cell has an important impact on its adhesion to a given substrate when a contact force is applied on them. Elasticities of the PC3 and LNCaP cells were calculated in order to shed light on the contact area of the cells to the surface when they were used as a probe on AFM cantilever. In principle higher contact area predicts more adhesion. When a force is applied on a cell during contact to the substrate, as expected contact area of the softer cells will be higher than the stiffer ones. But it does not mean that when they have higher contact area, LNCaP cells has a higher adhesion than PC3 cells, because adhesion is primarily related with the number of adhesion molecules present on the cell membrane that contact to the substrate. We have measured the Young`s modulus of the cells when they were used as a probe on an AFM cantilever. In accordance with earlier measurements [57], PC3 cells appeared significantly stiffer than LNCaP cells (**Fig. 11**). This result showed that LNCaP cells probed a larger contact surface than the stiffer PC3 cells with contact forces of 100 pN for all cells. Consequently, a larger contact surface will contribute higher to LNCaP cells adhesion to the probed substrates when compared with PC3 cells.

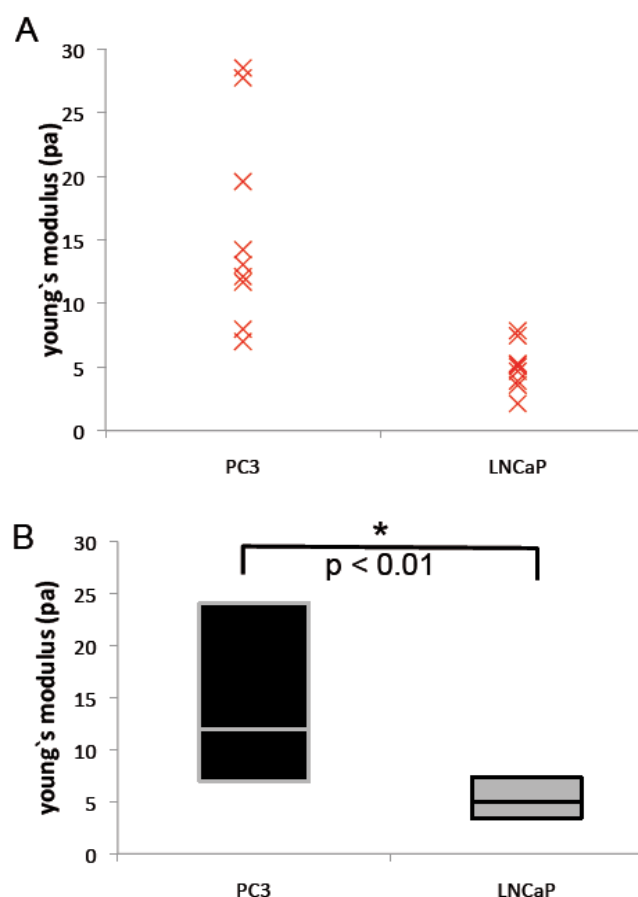


**Figure 11:** Young's modulus of PC3 and LNCaP cells attached on AFM cantilevers. (A) Red crosses represent the median values of the young's modulus of measured 18 cells. (B) Middle line on Box-plots shows the median value of the corresponding Young's modulus values for 800 force distance curves. Whole box range covers the +/- 25% of the data from the median value. A significant p-value from a nonparametric Mann Whitney test of the "PC3" versus "LNCaP" versus is marked by \* ( $p < 0.01$ )

#### 4.3. Quantification of the short-term adhesion of PC3 and LNCaP cells on Col-I coated surfaces and SCP1 monolayers

Cell to cell and cell to matrix adhesion experiments were performed in cell culture dishes with PC3 or LNCaP cells. In our experimental set up one of these cells was immobilized on the AFM cantilever (**Fig. 12**), while SCP1 and Col-I were used as substrates in the cell culture dishes. The prostate cancer cell on the AFM cantilever was then brought into contact with Col-I or the SCP1 monolayer for a predefined contact time (0.3 s) and with a predefined contact force (100 pN). Afterwards, the force necessary to withdraw the prostate cancer cell from each of the substrates was recorded. The resulting force-distance curves (**Fig. 13**) contain detailed information about the cellular interaction forces on the molecular level [96,97,104].

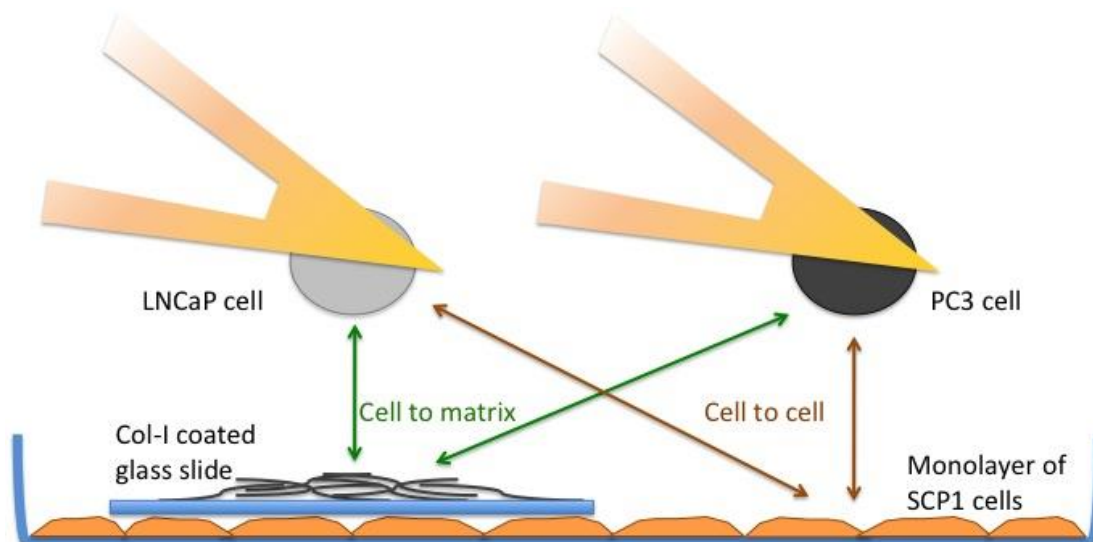


**Figure 12:** Schematic representation of the experimental setup. Single cells from two different prostate cancer cell lines (PC3 and LNCaP) were immobilized to a tipless AFM cantilever (force sensor) in order to study their interaction forces with the apical surface of a SCP-1 monolayer (representing mesenchymal stem cells) or with Col-I (representing bone matrix) [101].

**Fig.13** shows representative force traces indicating typical multiple de-adhesion events for PC3 cells and single de-adhesion events for LNCaP cells on Col-I and SCP1 substrates. The evaluation of these force curves confirms that PC3 cells exhibit a greater affinity than LNCaP cells to SCP1 cells and Col-I. In order to evaluate these rather complex force-distance curves a step detection algorithm [102] was applied to locate de-adhesion events and to quantify the corresponding forces despite the varying levels of noise.

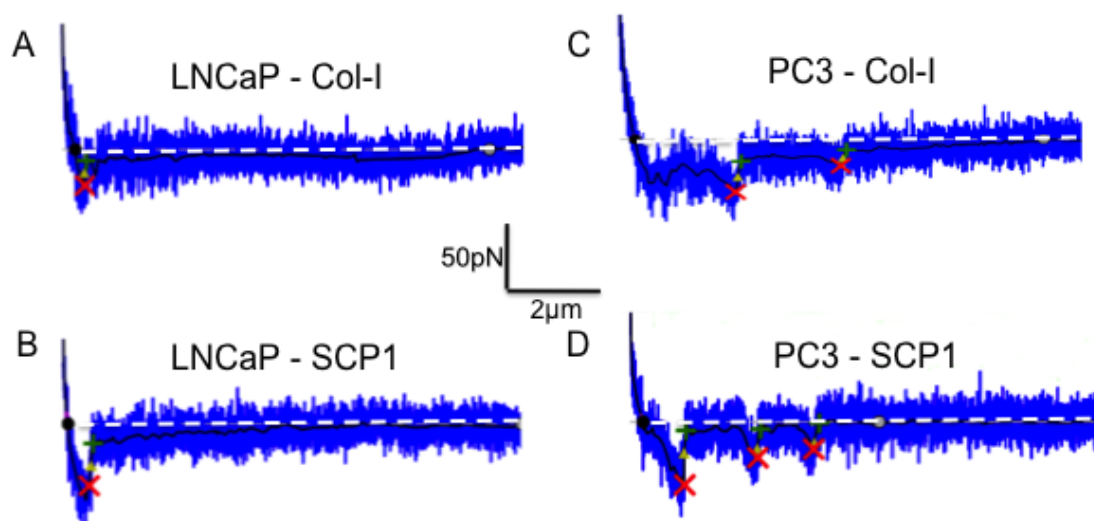


**Figure 13:** Characteristic force curves from each of the four different types of experiments are represented. (A) LNCaP on Col-I, (B) LNCaP on SCP1 monolayer, (C) PC3 on Col-I and (D) PC3 on SCP1 monolayer [101].

We have calculated the adhesion rates for the corresponding interactions and number of steps in each force curve to see how often PC3 and LNCaP cells can form adhesion events to their substrates. The force measurements of PC3 on Col-I showed an overall adhesion rate of more than 50%, whereas the adhesion rate of LNCaP on Col-I was around 30% (**Fig. 14A**). A similar behavior in adhesion rates was found on SCP1 surfaces, where PC3 had an adhesion rate of more than 45% while the adhesion rate of LNCaP was less than 30% (**Fig. 15A**). Also, the average number of de-adhesion force steps from force curves, containing at least one de-adhesion event, is significantly higher for PC3 than for LNCaP, both on Col-I and SCP1 monolayer substrates (**Fig. 14B** and **Fig. 15B**). This means firstly, that PC3 cells can form higher numbers of binding events than LNCaP cells and secondly, affinities for Col-I and SCP1 substrates are higher for PC3 cells than LNCaP cells.

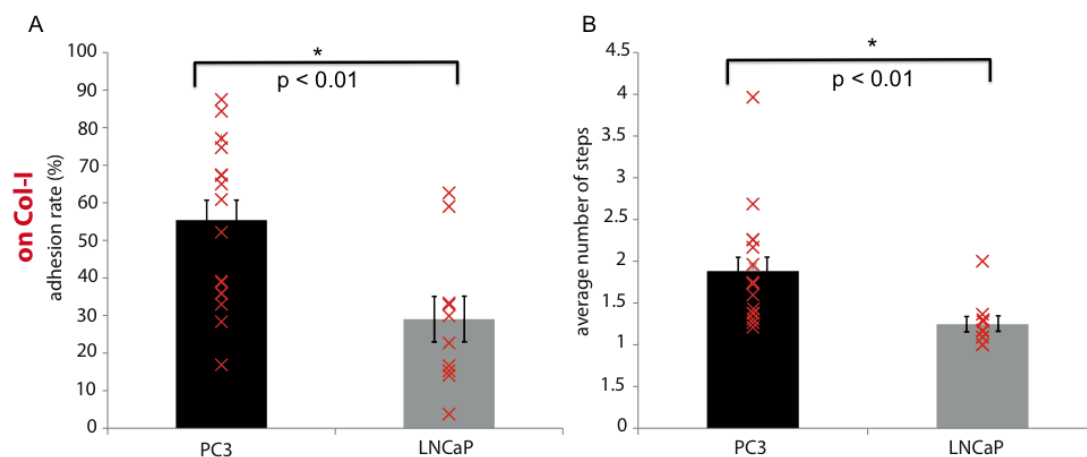


**Figure 14:** Adhesion rates (percentage of the force curves which have at least one de-adhesion event) and average number of steps in these force curves (which have at least one de-adhesion event) of PC3 and LNCaP cells on Col-I monolayer substrates. Mean values of at least 10 cells for **A)** adhesion rates and **B)** average numbers of steps of PC3 and LNCaP cells are indicated with red crosses and mean values of the measured total number of cells given as columns. Double-error bars show the standard error of the means. P-values from an unpaired t-test of the “PC3” data versus “LNCaP” are marked by \*( $p < 0.05$ )

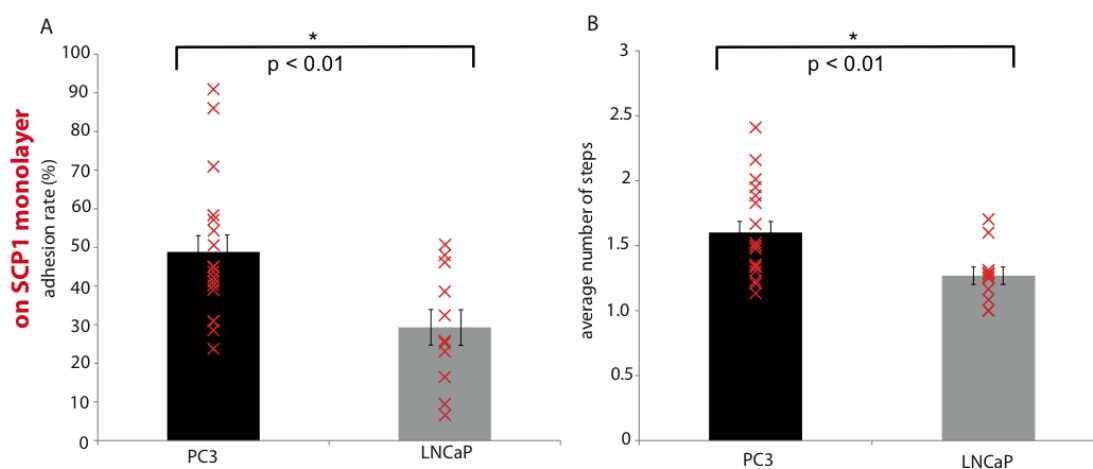


**Figure 15:** Adhesion rates and average number of steps in these force curves of PC3 and LNCaP cells on SCP1 monolayer substrates. Mean values of at least 10 cell for **A)** adhesion rates and **B)** average numbers of steps of PC3 and LNCaP cells are indicated with red crosses and mean values of the measured total number of cells given as columns. Double-error bars show the standard error of the means. P-values from an unpaired t-test of the “PC3” data versus “LNCaP” are marked by \*( $p < 0.05$ )

We have measured the heights of the individual de-adhesion steps in each force curve and the positions of these steps. The heights and positions of the steps could vary depending on what kind of bonds were used by the cells during their interactions with their substrates. The forces of the individual de-adhesion steps appeared slightly higher for PC3 cells on both Col-I substrate and SCP1 monolayer, when compared to LNCaP cells (**Fig. 16A** and **Fig. 17A**). Because the step force values of the last adhesive event in a force curve did not significantly differ from the values of intermediate steps, all adhesive events were included into the evaluation. Since the force distribution did not follow a Gaussian distribution, **Fig. 16** and **Fig. 17** depict medians and quartiles. For PC3 cells the median was at 17.4 pN on SCP1 monolayers and 17.0 pN on Col-I. The step height medians of LNCaP cells, on the other hand, were 14.9 pN on SCP1 monolayers and 14.8 pN on Col-I. Control measurements of PC3 cells on bare glass surfaces incubated with BSA resulted in step forces below 13 pN (not shown).

Significant differences between the two prostate cancer cell lines were also observed for step positions, i.e. the distance between PC cell and substrate, at which the bond rupture was detected (**Fig. 16B** and **Fig. 17B**). The adhesive bonds of PC3 cells break for both Col-I substrates and for SCP1 monolayers roughly twice as far as the bonds of LNCaP cells. On Col-I substrate for PC3 cells, they finally break at a median distance of 0.7  $\mu\text{m}$  (**Fig. 16B**). On SCP1 monolayers this distance was even further at 1.1  $\mu\text{m}$  (**Fig. 17B**). The fact that these bonds rupture up to several micrometers away from the observed contact point between the two cell types or between cell and Col-I can be explained by either: a) extremely compliant cells; b) by membrane tethers, which are pulled out of the cell membrane by the external force; or c) by filopodia or other micro-extensions which are actively formed by the cells [101].

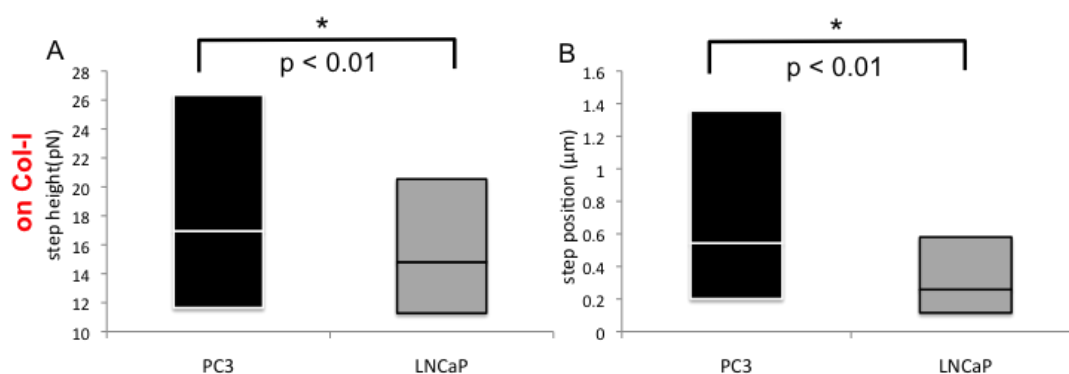


**Figure 16:** Heights and positions of the individual de-adhesion steps for PC3 and LNCaP cells on Col-I substrates. Medians are indicated in the middle lines of Box-plots for **A**) heights of de-adhesion steps and **B**) step positions. Whole box range covers the quartile values (+/- 25% of data from the median). Significant p-values from a nonparametric Mann Whitney test of the “PC3” and “LNCaP” versus the others are marked by \*(p<0.01).

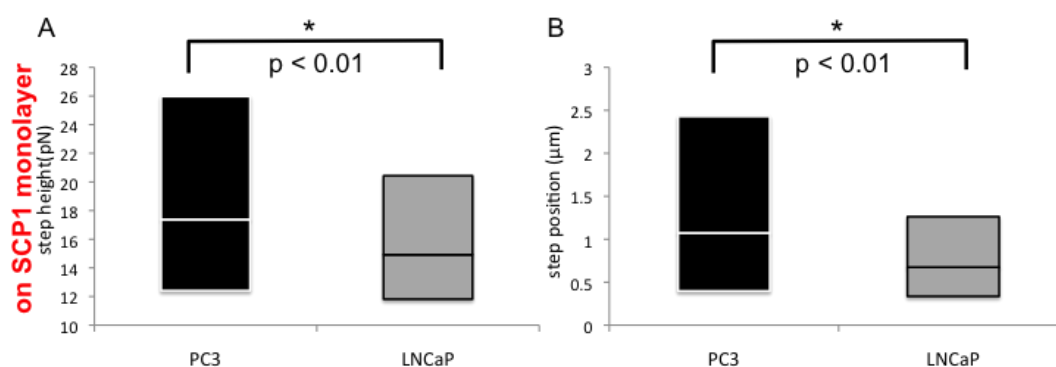


**Figure 17:** Heights and positions of the individual de-adhesion steps for PC3 and LNCaP cells on SCP1 monolayers. Medians are indicated in the middle lines of Box-plots for **A**) heights of de-adhesion steps and **B**) step positions. Whole box range covers the quartile values (+/- 25% of data from the median). Significant p-values from a nonparametric Mann Whitney test of the “PC3” and “LNCaP” versus the others are marked by \*(p<0.01).

In each force curve detachment forces and work of detachments were also calculated. The quantity of these parameters shows the total force and energy needed to separate the cell from their substrates. This can tell us how strong these cells can bind to their substrates and give an idea about the involvement of the CAMs. Stronger detachment forces and higher energy were needed to separate the PC3 cells from both of the Col-I and SCP1 substrates. PC3 adhesion to SCP1 was the strongest of the four measured interactions and the LNCaP cells were the weaker binders to both Col-I and SCP1 (**Fig. 18** and **Fig. 19**). Control measurements on bare glass surfaces

incubated with BSA revealed the weakest interactions for all adhesion parameters (data not shown).

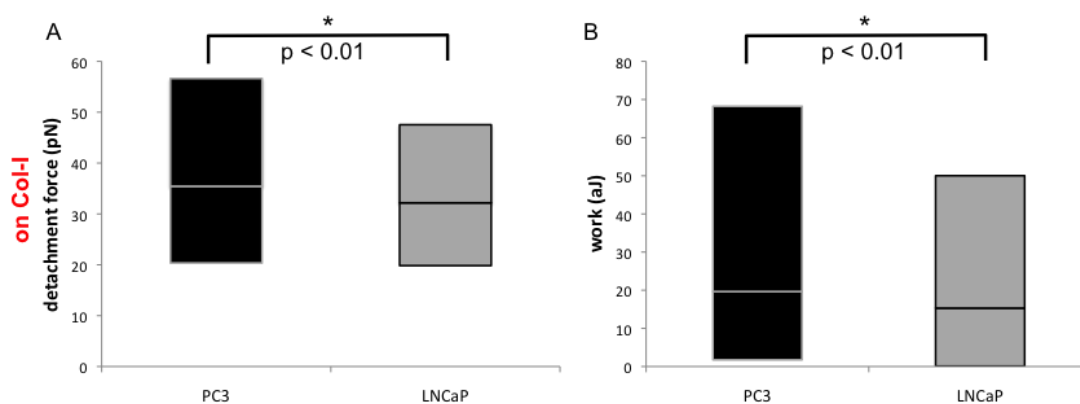


**Figure 18:** Detachment forces and work done on force curves calculated for PC3 and LNCaP cells. Medians are indicated in the middle lines of Box-plots for (A) detachment forces and (B) work on Col-I substrate. Whole box range covers the quartile values (+/- 25% of data from the median). Significant p-values from a nonparametric Mann Whitney test of the “PC3” and “LNCaP” versus the others are marked by \*( $p < 0.01$ ).

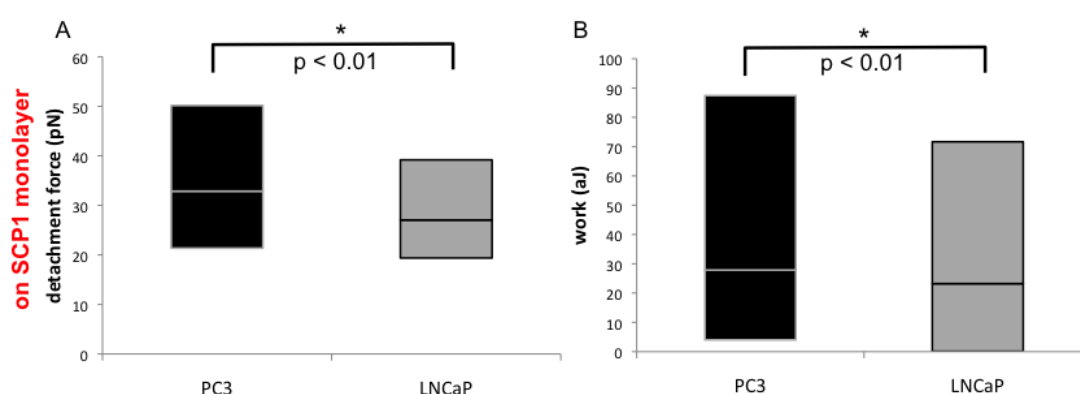


**Figure 19:** Detachment forces and work done on force curves calculated for PC3 and LNCaP cells. Medians are indicated in the middle lines of Box-plots for (A) detachment forces and (B) work on SCP1 substrate. Whole box range covers the quartile values (+/- 25% of data from the median). Significant p-values from a nonparametric Mann Whitney test of the “PC3” and “LNCaP” versus the others are marked by \*( $p < 0.01$ ).

Tethers are viscous membrane tubes [105], which are pulled out of the cell membrane at a constant force and therefore exhibit a characteristic force plateau [106] (see **section 4.8**. Membrane and cytoskeleton anchoring of cell surface receptors). Filopodia, on the other hand, are not generated by the pulling force. They contain protruding actin fibers and already exist before the

cells are brought into contact with their substrate. Consequently, filopodia are expected to exhibit an initial force-free unbending phase, followed by a sudden increase in force when loaded at a distance from the contact point that corresponds to their initial length (steps as shown in **Fig. 13D**). Therefore, in contrast to tethers they lack a force plateau. The de-adhesion steps may be displayed as tether-like (t-like) and filopodia-like (f-like) jump steps in force curves as explained above. We have defined the steps first and then classified them as t-like (tether) or f-like (jump). And finally, the fractions of these t- and f-like steps were calculated. In the case of PC3 cells, more than 50% of all detected steps exhibit these characteristic signatures of filopodia and less than 40% exhibit the typical signature of tethers. For LNCaP cells, on the other hand, less than 40% of the steps appear as filopodia like steps and about 45% as tether-like steps (**Fig. 20**). Furthermore, the step position of the filopodia-like steps of PC3 cells increased over time within the experiments at an average rate of 0.6 nm/s, while no significant change in step position was observed in LNCaP cells.

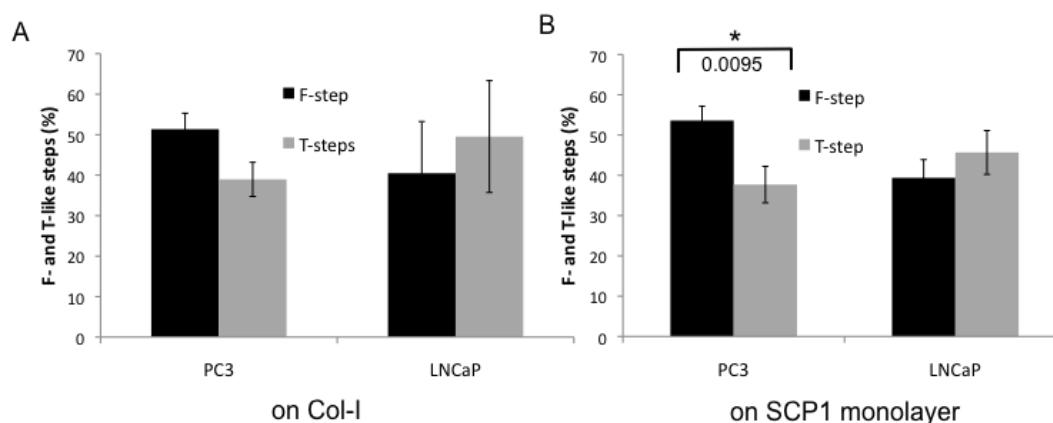


**Figure 20:** Analysis of filopodia-like steps versus tether-like steps in both cancer cell types to (A) Col-I and to (B) SCP1 monolayer. Means of the percentage of individual de-adhesion steps representing the typical force pattern of filopodia-like steps (solid) and tether-like steps (striped) for the two cell lines PC3 and LNCaP. Error bars correspond to standard error of the mean. A significant p-value from a t-test between the different steps within a prostate carcinoma cell line is indicated by \*(p,0.05). Due to the discrimination criterion, steps at positions shorter than 1  $\mu\text{m}$  were not counted and therefore the ensemble size for LNCaP and on Col-I in particular was small. The number of uncounted steps, because the slope did not allow for a clear distinction between tether and filopodia (loading rates between 27 and 40 pN/s) was less than 7%.

Consequently, PC3 cells showed specific binding to both bone related substrates. They have higher adhesion rates and adhesion forces than LNCaP cells. And also they have exhibited longer step positions, with specific signatures of filopodia-like steps. These results confirmed that the PC3 cells have a higher adhesive capacity on bone tissue, which may support them to stabilize in the metastatic site and subsequently to propagate.

#### 4.4. Integrin expression on PC cells

##### 4.4.1. Semi-quantitative PCR data

To find out which receptors are possibly responsible for the increased affinity of PC3 cells to Col-I substrate and SCP1 cells, we investigated the expression of two major integrin receptors which have binding affinity to collagen type I, namely  $\alpha1\beta1$  and  $\alpha2\beta1$  in PC3 and LNCaP cells by using semi-quantitative PCR. Our results demonstrated that both receptor types are strongly expressed in PC3 cells, in contrast to LNCaP cells (**Fig. 21**).

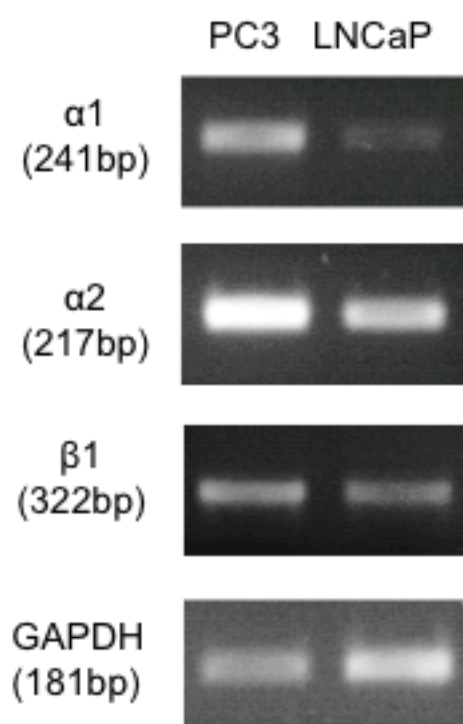


**Figure 21:** Investigation of integrin expression. Semi-quantitative PCR for  $\alpha1\beta1$  and  $\alpha2\beta1$  integrins was performed with cDNA from PC3 and LNCaP cells and revealed a strong expression of both receptors in PC3 cells in comparison to LNCaP cells. The PCR results were reproduced independently three times (consider that the PCR experiments were done with 1:10 diluted cDNAs).

#### 4.4.2. Quantitative PCR data

Expression levels of integrins  $\alpha 1$ ,  $\alpha 2$ ,  $\alpha 11$ , and  $\beta 1$ , which constitute the Col-I binding cell surface receptors  $\alpha 1\beta 1$ ,  $\alpha 2\beta 1$  and  $\alpha 11\beta 1$ , were assessed also by quantitative real time PCR. The results (**Fig. 22**) show that along with  $\beta 1$ , which is a constituent of all three Col-I binding receptors,  $\alpha 2$  was strongly expressed by PC3 cells, followed by  $\alpha 1$ , while  $\alpha 11$  expression was not detectable in PC3 cells. In comparison, the lymph node-derived LNCaP cells expressed eight-fold lower levels of integrin  $\beta 1$  and none of the three  $\alpha$ -integrin subunits were detected. This data confirmed our findings in **Fig. 21** and furthermore, demonstrated that among the Col-I integrins the major receptor in PC3 is  $\alpha 2\beta 1$ .

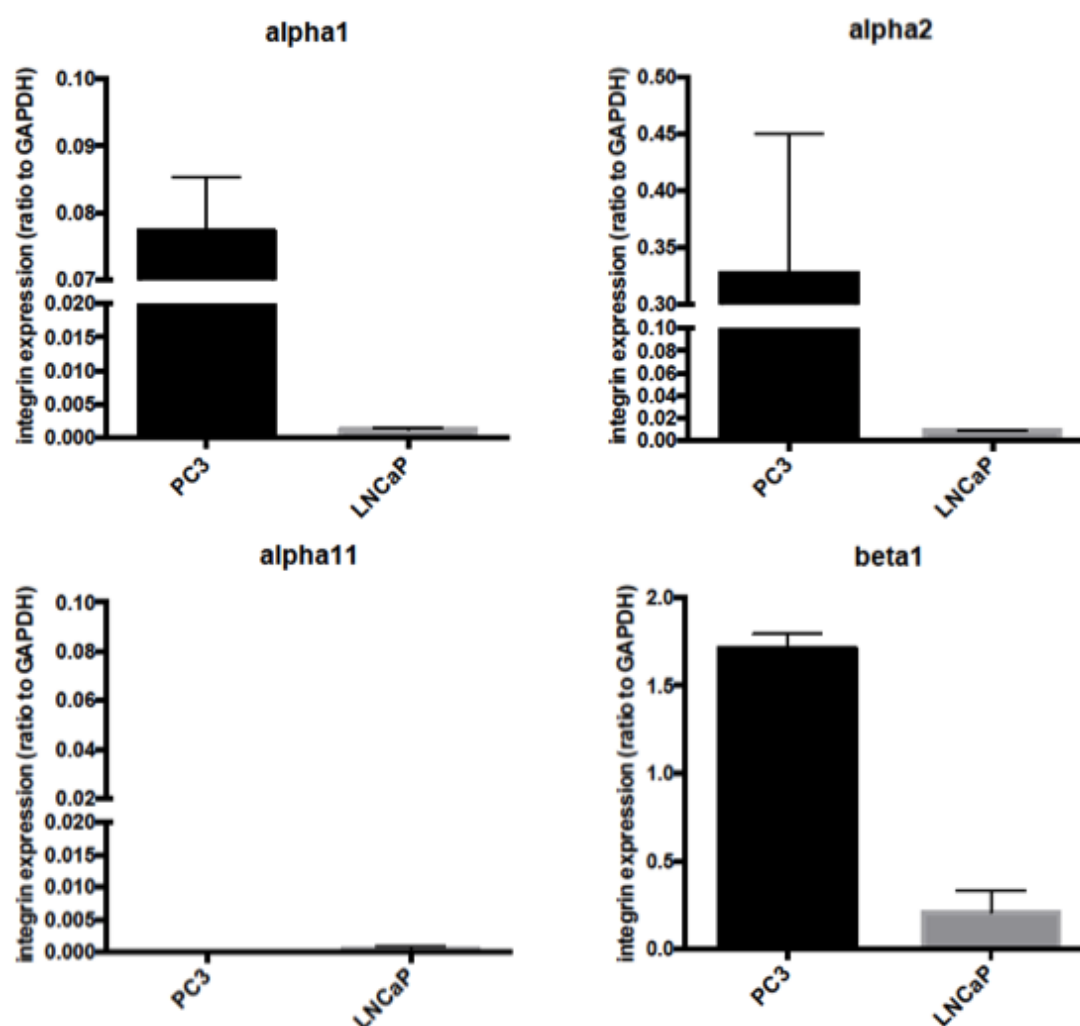


**Figure 22:** Quantitative RT-PCR analysis of Col-I-binding integrin expression in PC3 (black) and LNCaP (gray) cells correlated to the GAPDH expression level. Error bars correspond to standard error of the mean of two independent experiments.

#### 4.5. Col-I expression on SCP1 monolayers

To verify the expression of Col-I in our experimental system, we have applied primary antibody against Col-I molecules on the substrates in combination with secondary antibody, which emits green light at wavelength 488nm. The results were compared with the negative control experiments, which were missing primary antibody. We were able to detect the Col-I fibers on coated glass slides and extracellular secreted Col-I molecules on SCP1 monolayers (**Fig. 23** and **Fig. 24**). However, from confocal microscopy images of fluorescently labeled Col-I on SCP1 cells, the exact location of the collagen could not be unambiguously resolved as “on”, “in” or “below” the cell membrane. An image from the apical surface of the cell monolayer was given in **Fig. 24**. The collagen seems to be deposited in several layers of SCP1 monolayer; top, middle and as well as below the cells.

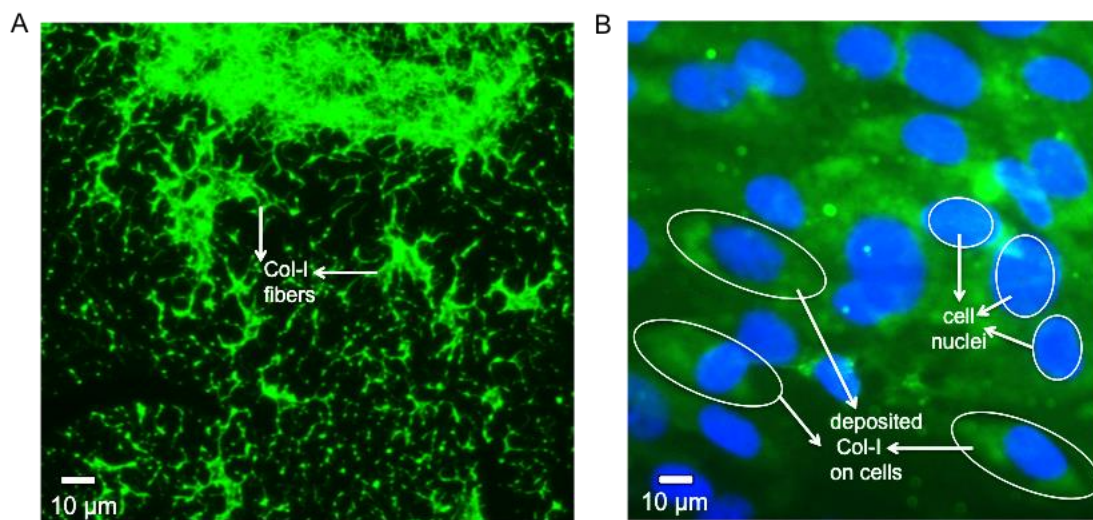


**Figure 23:** Immunofluorescence images of Col-I, labeled with AlexaFluor488 fluorescence dye appearing in green and cell nuclei stained with DAPI in blue. **(A)** On Col-I coated glass slide **(B)** SCP1 monolayer

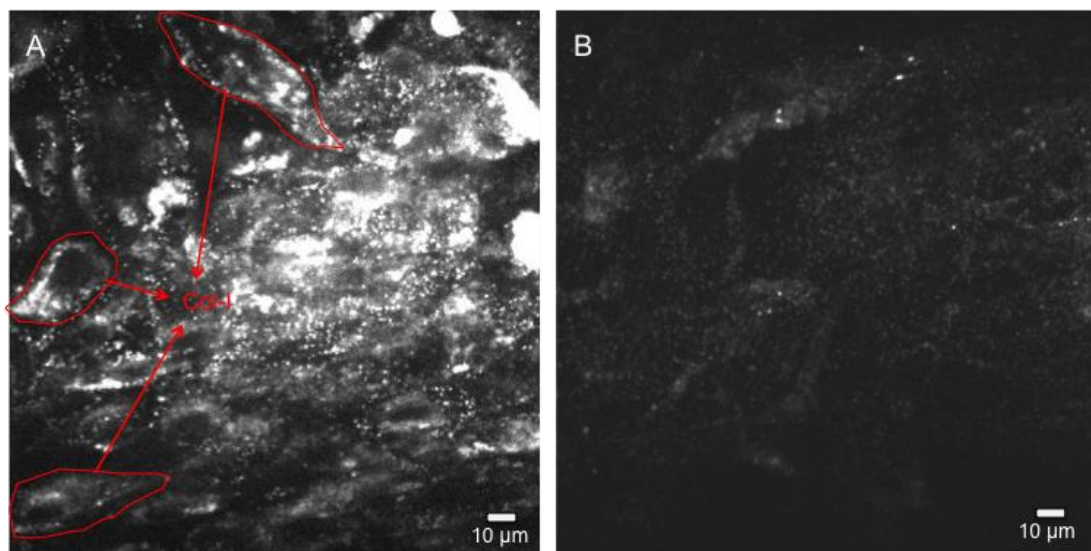


**Figure 24:** Detection of the Col-I molecules on the apical surface of SCP1 monolayer labeled with AlexaFluor488 fluorescence dye using confocal microscopy (A) Confocal microscopy image of the SCP1 monolayer apical surface (Col-I deposited on cells perimeters are marked by red lines) (B) Confocal microscopy negative control image of SCP1 monolayer without using primary Col-I binding antibody.

Consequently, our finding of extra cellularly expressed Col-I on the apical surface of the SCP1 cells may be one of the responsible partners for PC3 cell adhesion to this substrate.

#### **4.6. Long-term adhesion of PC3 cells with $\beta$ 1 integrin antibody blocking and collagenase treatment on Col-I coated surfaces**

In order to investigate the role of these Col-I binding cell surface receptors in PC3 adhesion to Col-I, we performed an optical density-based binding assay with untreated and anti- $\beta$ 1 integrin antibody treated PC3 cells on Col-I coated surfaces. In this assay, the relative number of adherent cells was determined after the cells were incubated for three different time periods. As negative control, we used untreated plastic surfaces and Col-I-coated surfaces, which were treated with collagenase, in order to proteolitically remove the accessible collagen. **Fig. 25** shows the affinity of untreated and of anti- $\beta$ 1 antibody-treated PC3 cells to Col-I coated surfaces, with or without collagenase treatment, which was evaluated by the optical adhesion assay. On Col-I, the adhesion rate of PC3 cells was approximately 40% after 30 min and over 90%

after 90 min. In contrast, after 30 min, PC3 cells incubated with  $\beta 1$  blocking antibody reached only 20%; however at 90 min, they could recover up to 80%. In contrast, PC3 cells on collagenase-treated and on bare plastic surfaces showed no pronounced differences as on both surfaces, we observed low cell adhesion, which even after 90 min reached only about 20%. These results show that collagenase treatment effectively deactivated the Col-I from the coated surfaces. Furthermore,  $\beta 1$  integrin blocking antibody could block the Col-I binding  $\beta 1$  integrins at least for short time periods (until 30 min, **Fig. 25B**) but cells could renew afterwards their integrin receptors.

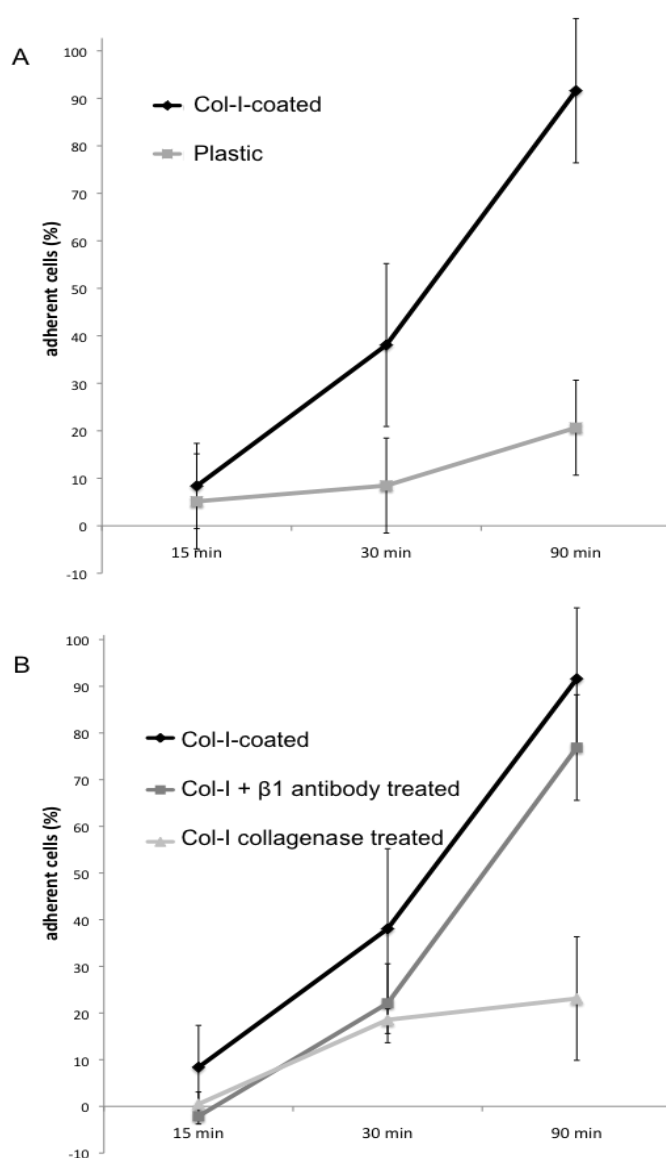


**Figure 25:** Optical density measurements of adherent cells at three different time points as a fraction of the amount of PC3 cells originally plated on four different surfaces. **(A)** Control measurements of PC3 on Col-I coated (black) and bare plastic surfaces (gray). **(B)** Lined up black to light gray respectively as: PC3 cells on Col-I coated surfaces,  $\beta 1$ -blocking antibody treated PC3 cells on Col-I coated surfaces, PC3 cells on Col-I coated and collagenase treated surfaces. Error bars correspond to standard deviations of 5 wells for each data point.

#### 4.7. Short-term adhesion of PC3 and LNCaP cells on Col-I and SCP1 surfaces with $\beta 1$ integrin antibody blocking and collagenase treatment

To quantify the binding strength of PC3 cells to Col-I and to the bone marrow-derived SCP1 cell line, AFM-based single cell force spectroscopy was performed: An untreated LNCaP cell, or an untreated or an  $\beta 1$  integrin blocking antibody-treated PC3 cell resting on a BSA coated surface was allowed to firmly adhere to a poly-l-lysine coated (tip-less) AFM force sensor. Next, the cell was brought into contact with an untreated or a collagenase treated Col-I surface, or with an untreated or a collagenase treated SCP1 monolayer, or a BSA coated control surface (**Fig. 26**). After a short contact of less than 0.3 seconds the force necessary to withdraw the cells from the addressed surface was determined.

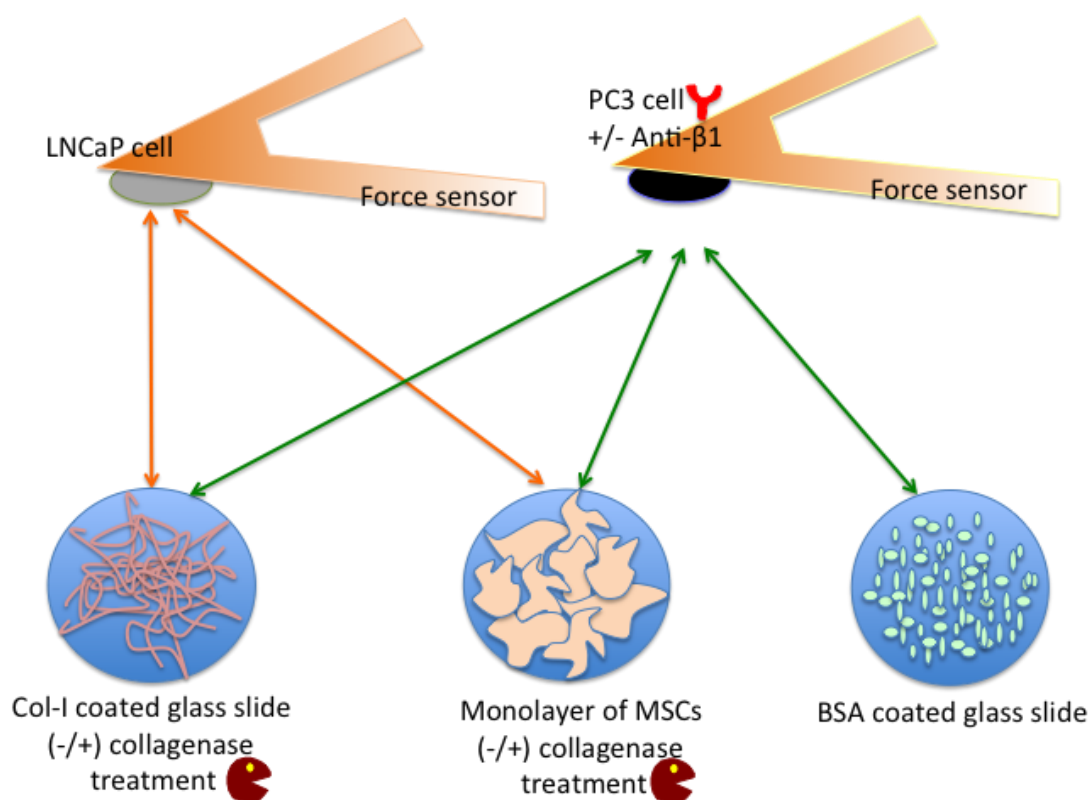


**Figure 26:** Experimental design for the AFM force spectroscopy characterizing the specific interaction of PC3 cells (expressing  $\alpha 1\beta 1$  and  $\alpha 2\beta 1$  integrins) with SCP1 cells or Col-1 surfaces. A single cell was immobilized to the force sensor. LNCaP cells lacking these integrins, antibody blocking of  $\beta 1$  integrins on PC3 cells, collagenase treatment of Col-I or SCP1 substrates or nonspecific BSA substrates served as control experiments.

The force measurements of PC3 on Col-I surfaces showed an overall adhesion rate (percentage of force traces with adhesive steps) of more than 60%, whereas the adhesion rates of LNCaP and PC3 cells blocked with  $\beta$ 1 antibody were lower than 40%, which is in the range of control measurements on the BSA coated surface. Adhesion rates of PC3 on collagenase treated Col-I substrates were a little higher than 40% but still significantly lower than adhesion rates on untreated Col-I. And also blocking of PC3 cells with the anti- $\beta$ 1 antibody, dropped the adhesion rate to about 30%, which is in the range of non-specific PC3 adhesion rates to BSA coated surfaces and LNCaP binding to Col-I (**Fig. 27A**).

A similar behavior was found for the number of de-adhesion force steps per force curve (**Fig. 27B**). With approximately 1.9 steps per curve, the average number of steps was highest for PC3 cells on Col-I, which is significantly higher than the rest of the data. For PC3 with anti- $\beta$ 1 blocking on Col-I, LNCaP on Col-I and PC3 on BSA, we observed no pronounced differences within these groups. In these cases, the average number of steps was lower than 1.4 (**Fig. 27B**). So these results tell us that blocking of PC3 cells with the anti- $\beta$ 1 antibody as well as collagenase treatment of Col-I coated surfaces effectively decrease the cell adhesion to Col-I surfaces.

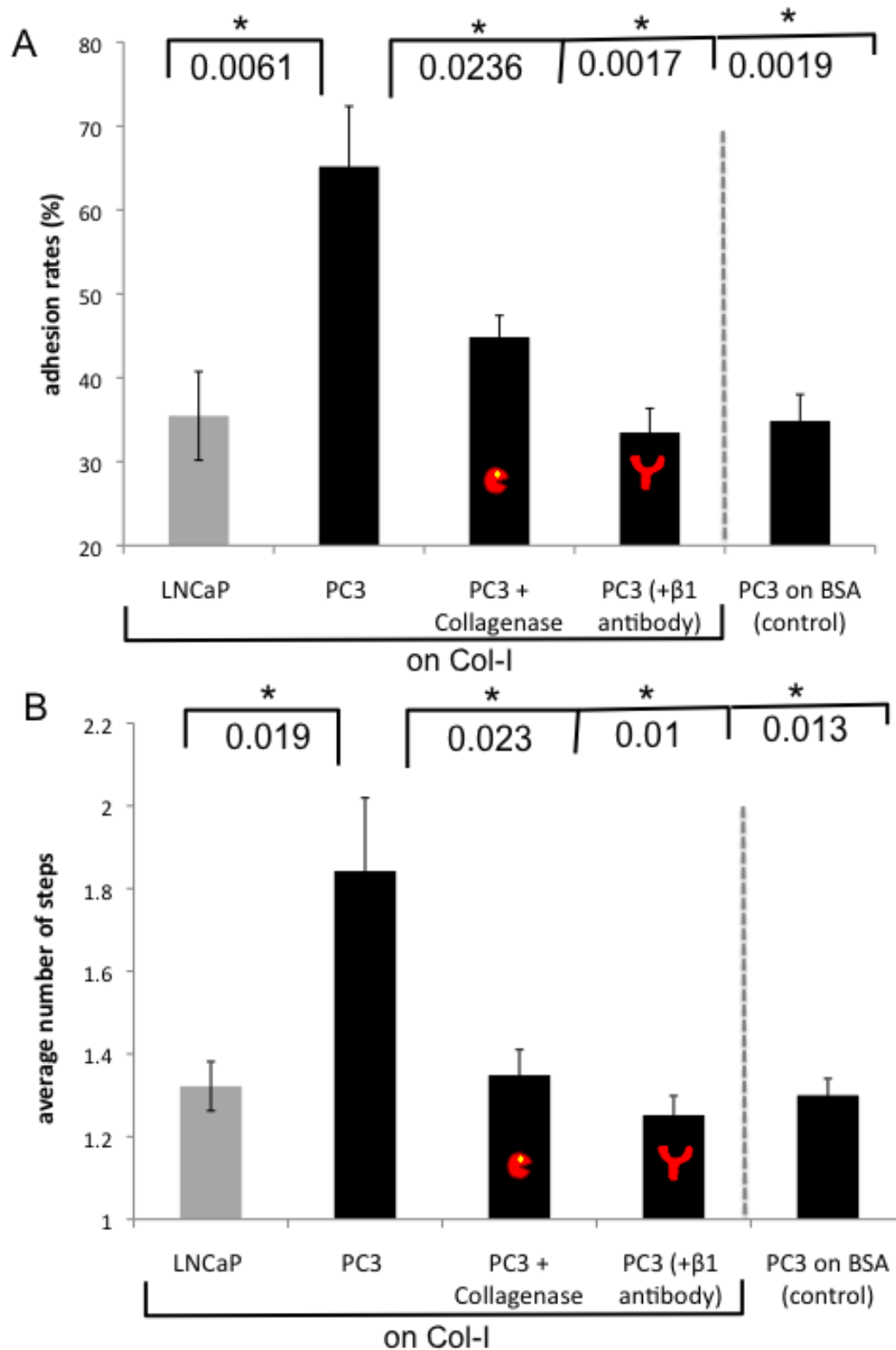


**Figure 27:** Adhesion rates and average number of steps in the force curves of PC3 and LNCaP cells on Col-I monolayer substrates. Mean values of at least 8 cell for **(A)** adhesion rates and **(B)** average number of steps of PC3 (+/- antibody) and LNCaP cells on Col-I (+/- collagenase) surfaces are given. Error bars shows the standard error of the means. P-values from an unpaired t-test of the “PC3 on Col-I” data versus the others are marked by  $^*(p < 0.05)$ .

Our findings are different for the measurements performed on the SCP1 surfaces. Treatment of SCP1 surfaces with collagenase solution did not result in significant difference for PC3 cells. PC3 cells showed adhesion rates higher than 55% and average number of steps higher than 1.5 steps per curve on SCP1 surfaces with or without collagenase treatment. For PC3 with anti- $\beta$ 1 blocking on SCP1, LNCaP on SCP1 and PC3 on BSA, the adhesion rates and average number of steps are significantly lower. We observed no pronounced differences within these groups. In these cases, the adhesion rates were 30-35% and the average number of steps was in the range of 1.3 steps per curve (**Fig. 28A** and **B**). Anti- $\beta$ 1 antibody also served as an adhesion blocking agent for PC3 cells on SCP1 surfaces, whereas collagenase treatment of SCP1 surfaces did not show the same result. This suggests that adhesion of PC3 cells with SCP1 cells is not mediated via the apical deposited Col-I matrix network, but goes through  $\beta$ 1 integrin receptors on PC3 cell and a ligand expressed on SCP1 itself, which for now remains unidentified.

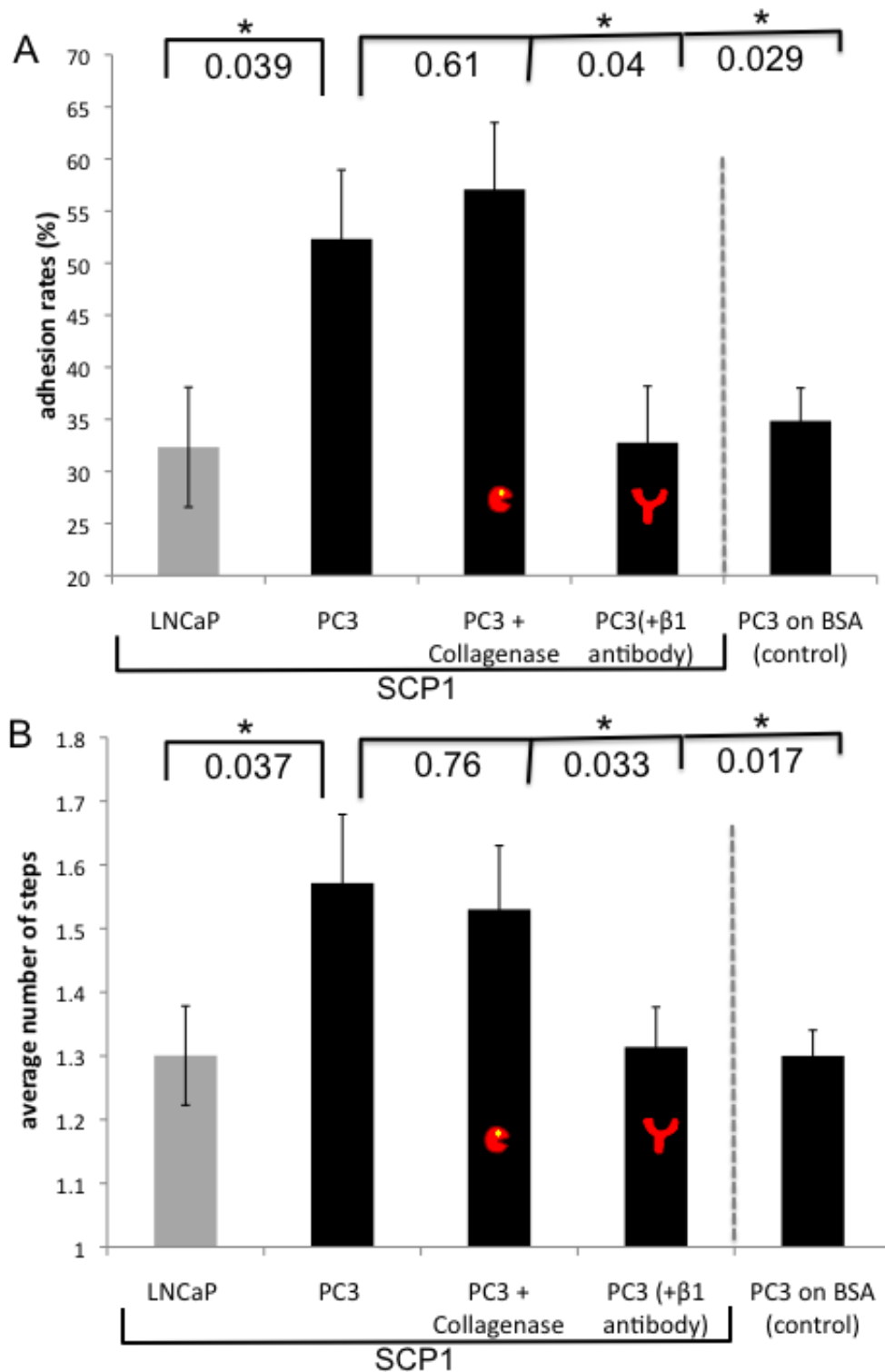


**Figure 28:** Adhesion rates and average number of steps in the force curves of PC3 and LNCaP cells on SCP1 monolayer substrates. Mean values of at least 8 cell for **(A)** adhesion rates and **(B)** average number of steps of PC3 (+/- antibody) and LNCaP cells on SCP1 (+/- collagenase) surfaces are given. Error bars show the standard error of the means. P-values from an unpaired t-test of the “PC3 on SCP1” data versus the others are marked by \*( $p < 0.05$ ).

Detachment forces are describing the highest measured adhesion (global maximum) per curve. We have measured 8 cells from each group and collected whole detachment forces data (from the force curves with at least one de-adhesion event) (**Fig. 29**). On Col-I surface without any treatment PC3 cells have the highest detachment force values and significantly different from the rest of the data. On the other hand, Col-I surfaces collagenase treatment reduced the detachment force to the BSA level, whereas on collagenase treatment of the SCP1 surface did not have a significant effect on detachment forces (**Fig. 29A and B**). In both of the surfaces, it is clearly seen that blocking of the PC3 cells with beta-1 antibodies dropped the detachment forces significantly to the level of unspecific adhesion of BSA surface. The detachment forces of LNCaP cells on both of the surfaces were significantly lower than PC3 (**Fig. 29A and B**). Here, we can also conclude that the PC3 cells use their  $\beta 1$  integrins to form these detachment forces when they adhere to SCP1 surfaces, and these integrins may have another ligand on SCP1 cells other than Col-I that is needed to identify.

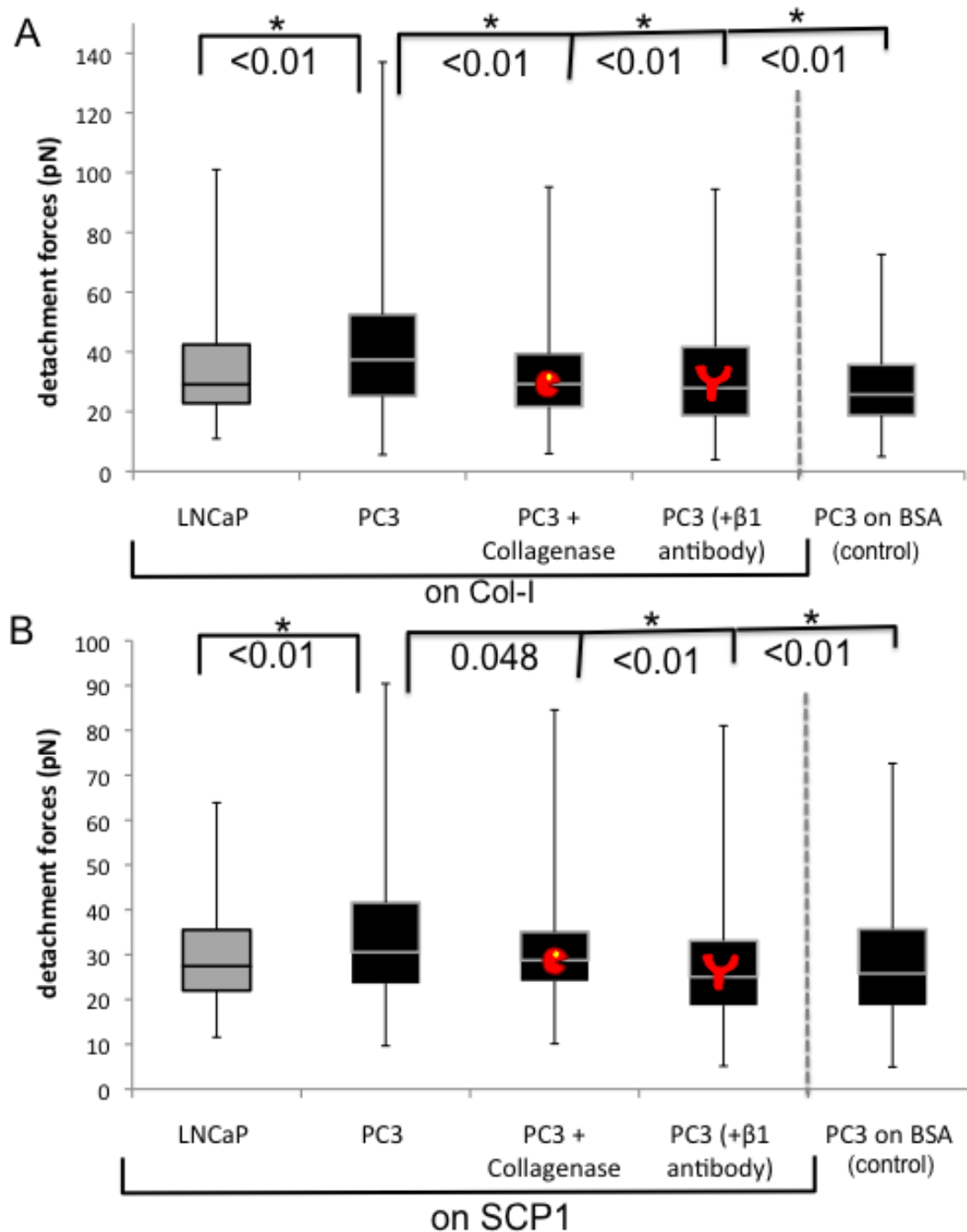


**Figure 29:** Detachment forces of PC3 and LNCaP cells on Col-I, SCP1 and BSA surfaces. Box-plots of detachment forces of PC3 (+/- antibody) and LNCaP cells **(A)** on Col-I (+/- collagenase) and BSA **(B)** on SCP1 (+/- collagenase) and BSA surfaces. Medians are indicated in the middle lines of boxes. Error bars cover the whole range of data in which a few extreme values are excluded. Box ranges covers the quartile values (+/- 25% of data from the median). Significant p-values from a nonparametric Mann-Whitney test of the “PC3 on Col-I” and “PC3 on SCP1” versus the others are marked by \*( $p < 0.01$ ).

#### 4.8. Membrane and cytoskeleton anchoring of cell surface receptors

Although there is a clear difference in four of the parameters (adhesion rate, the average number of steps and the detachment force) quantifying the interactions, no information about the type of interaction and in particular about the anchoring of the relevant receptors to their respective micro-environment can be obtained from these parameters. To gain more detailed insight into the type of interaction and the receptor anchoring to the cell membrane or cytoskeleton, we displayed the parameters position of steps [ $\mu\text{m}$ ] and slope prior to each step [ $\text{pN}/\mu\text{m}$ ] in two-dimensional (2D) probability density maps.

Receptor-ligand interactions of receptors linked to the cytoskeleton typically exhibit a clear rise in force, just before the unbinding event, just like the force curve displayed in **Fig. 30A** [107]. These kind of steps are characteristic of the rupturing of a transmembrane-receptor which is firmly connected to the cytoskeleton on its intracellular side [108]. On the other hand, long plateaus with slopes around zero, as displayed in **Fig. 30B**, are typical of tethers being pulled out of the cell membrane [106,109,110]. Here, the constant force prior to the unbinding event is caused by the constant tension of the plasma membrane.

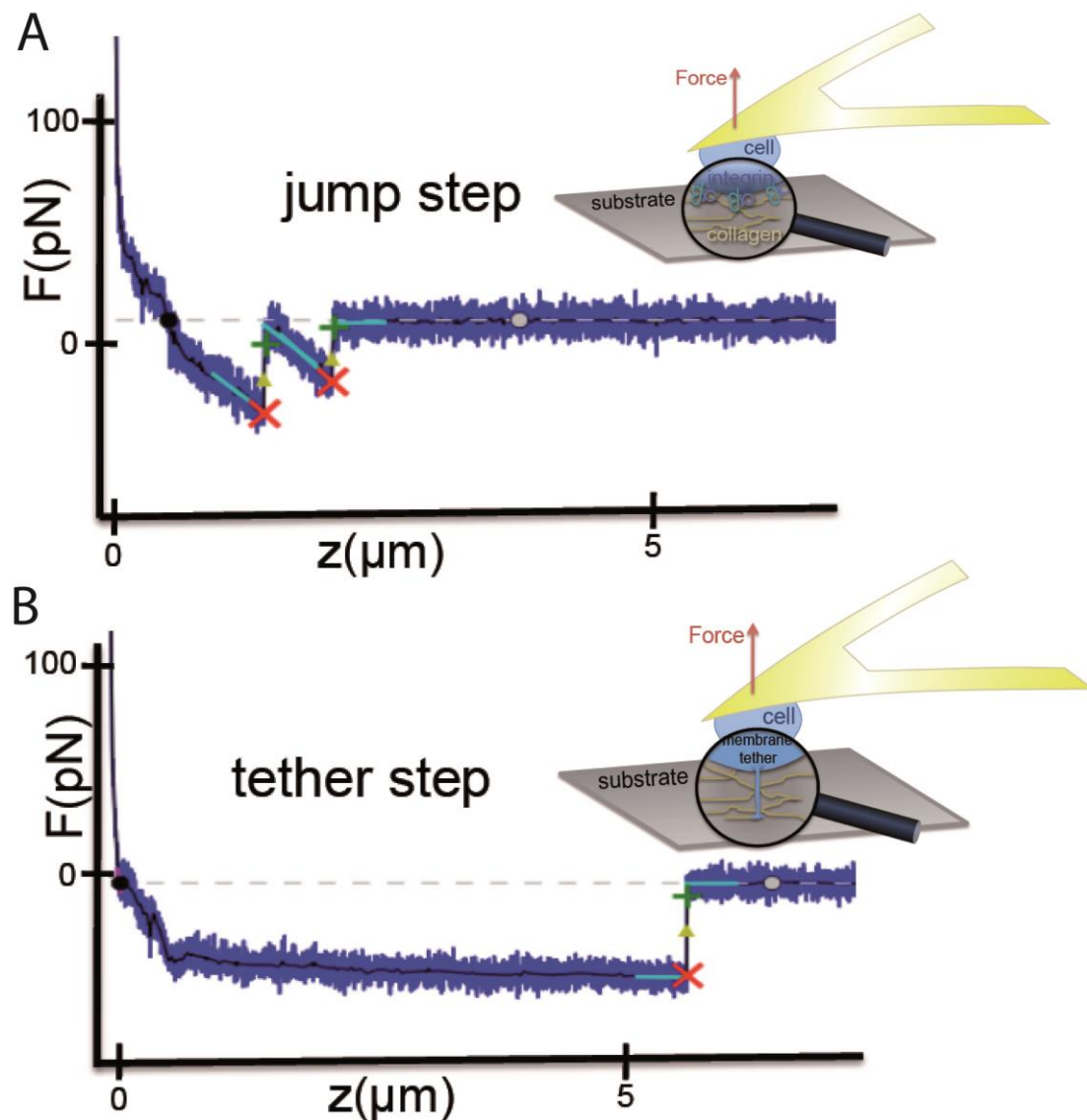


**Figure 30:** Two subsequent force traces (blue) from separating a PC-3 cell from a collagen substrate at a velocity of  $3 \mu\text{m/s}$  after contacts of  $0.3 \text{ s}$  at  $100 \text{ pN}$ . Red crosses mark steps; the black line is the smoothed force trace. A turquoise line-fit indicates the slope prior to a step. **(A)** Jump like steps appear at slopes below  $-10 \text{ pN}/\mu\text{m}$  (loading rates of  $-30 \text{ pN/s}$ ). **(B)** Tether like steps, caused by membrane tubes pulled from the cell by bonds not anchored to the cytoskeleton show typically slopes of  $0 \pm 10 \text{ pN}/\mu\text{m}$ .

The probability distribution of the force curve slope of each step versus the position of each step is visualized in density plots for the substrates SCP1 and Col-I in **Fig. 31A** and **B**. The step distribution observed for PC3 cells on SCP1 and Col-I displays one strong peak in the jump region, indicating mainly cell surface receptors, which are well connected to the cytoskeleton. On the SCP1 monolayer, the peak position is shifted by about 1  $\mu\text{m}$  (dashed circle at 1.6  $\mu\text{m}$ ), which can be explained by the fact that the SCP1 cells are much more compliant than the rigid Col-I substrate (dashed circle at 0.6  $\mu\text{m}$ ) [111]. On Col-I, a second, weaker peak can be observed in the tether region at about 2.8  $\mu\text{m}$ . -10  $\text{pN}/\mu\text{m}$  slope was picked as a border between tether and jump regions according to calculations made through histogram of tether steps identified by eye on PC3-Col-I data. The half width of the Gaussian distribution fitted to this tether distribution marks the -10 $\text{pN}/\mu\text{m}$  line chosen as a guide for the eye to separate between more tether like steps and more jump like steps.

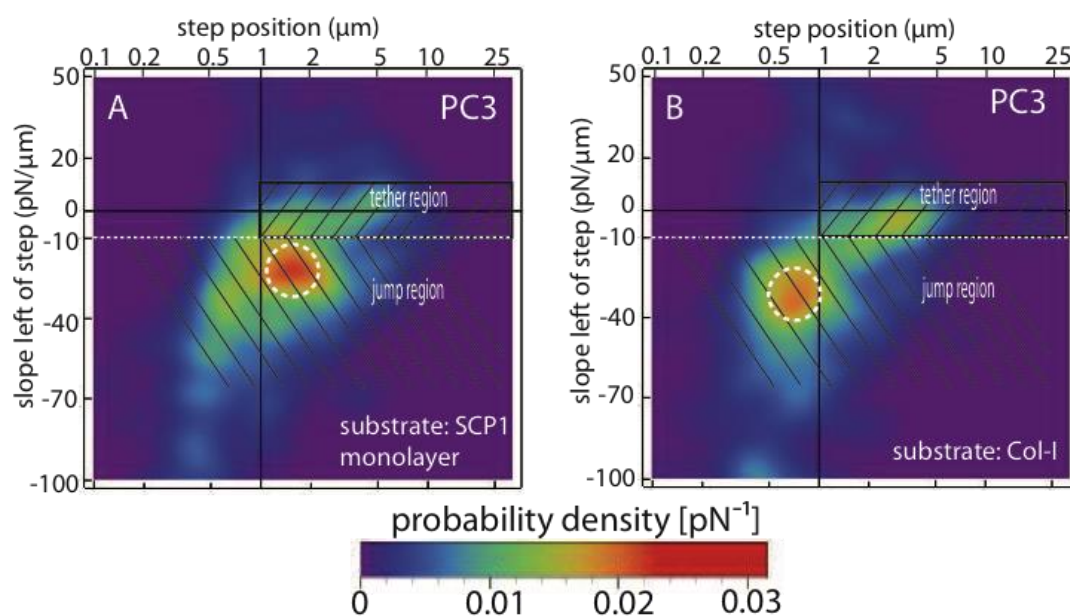


**Figure 31:** Probability density maps of force loading rates (slope of the force distance trace) prior to each step versus the step position. **(A)** PC3 cells on SCP1 monolayers **(B)** PC3 cells on Col-I coated glass slide. The y-axes (step position) in 2D maps are in logarithmic scale.

On SCP1 substrate, with collagenase treatment the jump peak is shifted further (out of the dashed circle) to around 2  $\mu\text{m}$  (**Fig. 32A**). These filopodia-

like steps (jumps) are mainly indicating cytoskeleton connected receptors in longer step positions. With collagenase treatment of the Col-I substrate, PC3 cells showed a broad peak between the tether and the jump region at positions around 2  $\mu\text{m}$  and a peak in the jump region is shifted to step positions around 1  $\mu\text{m}$  (**Fig. 32B**).

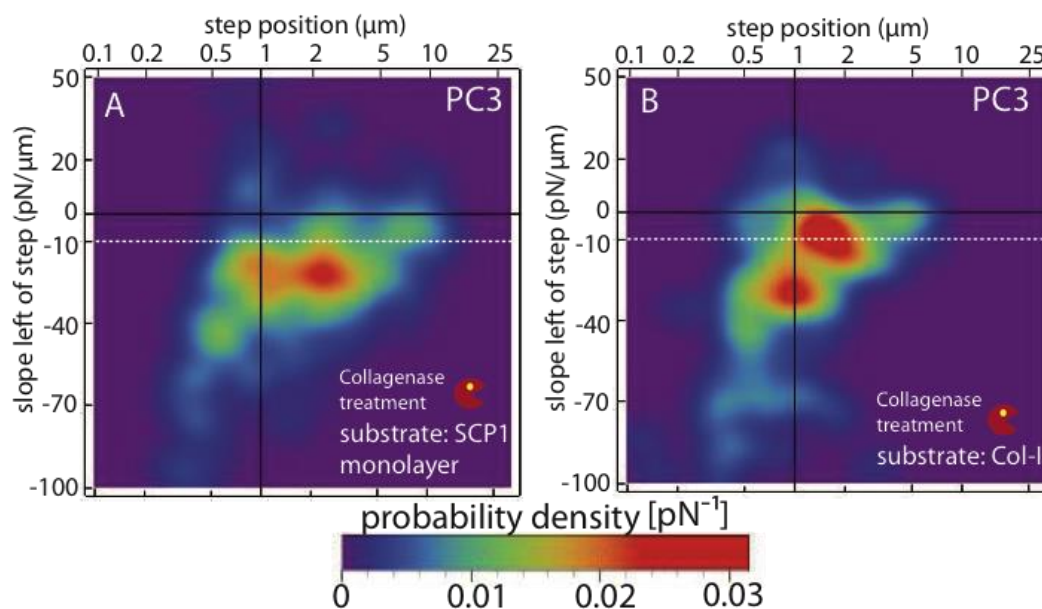


**Figure 32:** Probability density maps of force loading rates (slope of the force distance trace) prior to each step versus the step position. **(A)** PC3 cells on collagenase treated SCP1 monolayers **(B)** PC3 cells on collagenase treated Col-I coated glass slide. The y-axes (step position) in 2D maps are in logarithmic scale.

With the application of beta-1 blocking antibody to PC3 cells, the probability of occurring unspecific adhesions was increased. (Note that the density plots are normalized and the colors do not reflect the adhesion rate). And on SCP1 surface with the application of the  $\beta 1$  integrin blocking antibody, steps are concentrated at the same region but with a less intense peak (**Fig. 33A**). This suggests that in addition to  $\beta 1$  integrins, other receptor-ligand interactions might be involved in PC3-SCP1 interactions. With the blocking of  $\beta 1$  integrins, the filopodia-like jump steps seem to be replaced mostly by tethers forming two pronounced peaks there at about 1.4 and 3.5  $\mu\text{m}$  on Col-I substrate (**Fig. 33B**). This result showed that these specific filopodia like jump steps mostly replaced by unspecific membrane bounded tether steps on Col-I substrate.

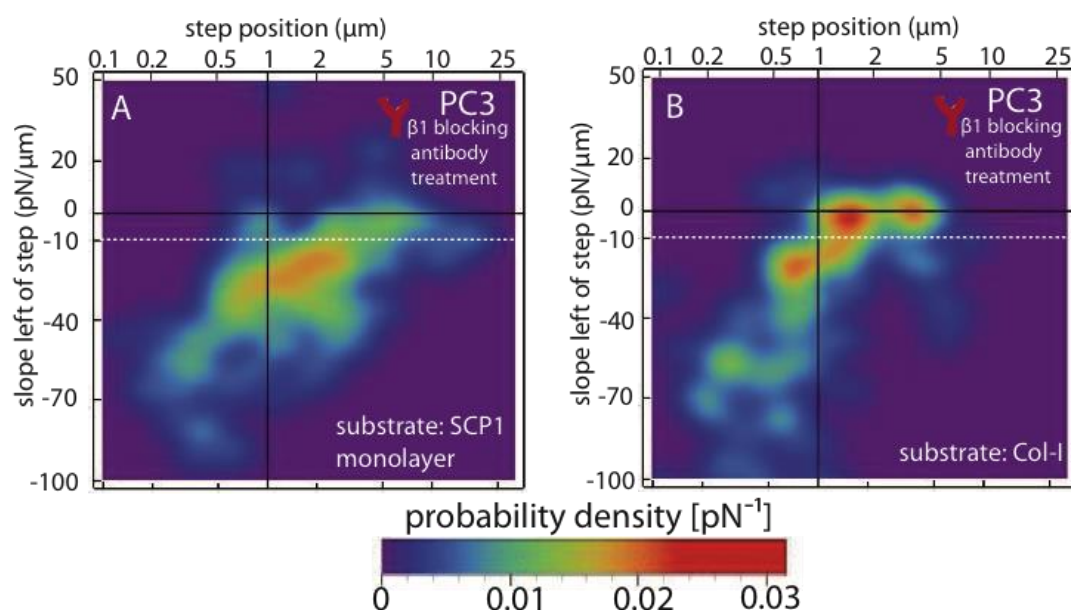


**Figure 33:** Probability density maps of force loading rates (slope of the force distance trace) prior to each step versus the step position. **(A)** PC3 cells treated with  $\beta 1$  integrin blocking antibody on SCP1 monolayer **(B)** PC3 cells treated with  $\beta 1$  integrin blocking antibody on Col-I coated glass slide. The y-axes (step position) in 2D maps are in logarithmic scale.

In case of tether signals on force curves, there may be differences on their set up. Additionally in the force curves of PC3 cells we have detected some special signatures of filopodia, which are steps rise with a negative slope (like a jump step), then continue with a constant force and then ruptures at some distant position like a common tether curve (**Fig. 34A**). We called these specific signatures as “filopodia-like tether curves”.

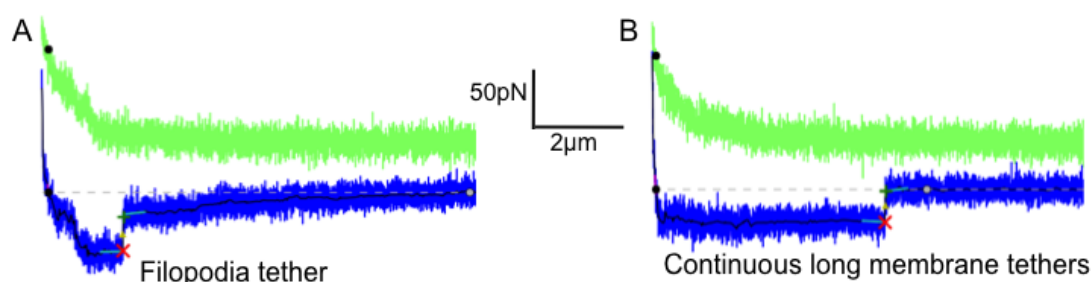


**Figure 34:** Specific signatures which were detected in tether steps of force curves. **(A)** Filopodia tethers result from actin-rich elongated membrane protrusions **(B)** Continuous long membrane tethers result from membrane attachments, which are not linked to cytoskeleton.

Last, we have performed additional control experiments to further validate that the obtained interactions of PC3 cells with Col-I and SCP1 were specific. Latrunculin-A was used to destroy actin cytoskeleton of the cells. This action of the drug was tested on PC3 cells and results of the latrunculin treatment can be seen on **Fig. 35**. Well established actin network of PC3 cells can be seen on **Fig. 35A**. Treatment of PC3 cells with latrunculin for 15 min cause them to lose their F-actin cytoskeleton, shrink and then form small round cells (**Fig. 35B**). Latrunculin-A is a drug which disrupts the actin cytoskeleton by binding and sequestering the g-actin [112].

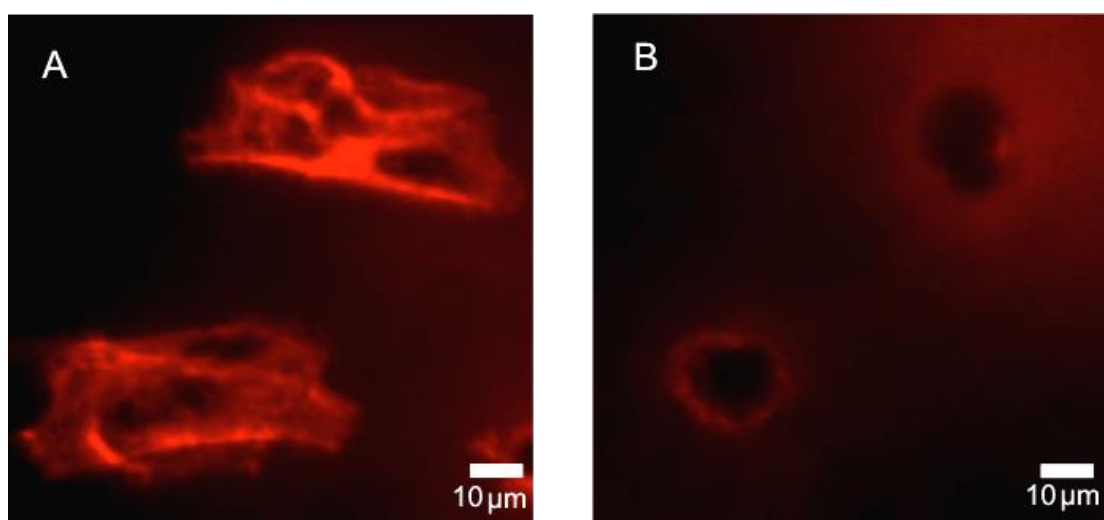


**Figure 35:** Fluorescent images of phalloidin labeled cells. (A) PC3 cells without treatment. Actin cytoskeleton of the cells is visible, cells were highly spreaded on the Col-I coated surface (B) PC3 cells after 15 min treatment of 0.2  $\mu$ M latrunculin-A. The F-actin fibers are destroyed leading to collapse of cell shape into sphere.

We have treated PC3 cells with Latrunculin-A to see the cells adhesion behaviors without direct participation of the actin cytoskeleton. PC3 cells without their intact actin network could not generate jump signals and also “filopodia-like tethers” on the force curves were absent which means that they lose their cytoskeleton connected membrane attachments to their substrates (**Fig. 36A**). On the BSA control surface (**Fig. 36B**), the density distribution resembles a characteristic way of unspecific binding; steps are accumulated in the center not obviously clustered in any of the jump and tether regions. Interestingly the control measurements with LNCaP cells on the Col-I (**Fig. 36C**) show a single peak in the tether region, whereas several peaks are

distributed along the density map in both tether and jump regions at different step positions for LNCaP cells on SCP1 monolayers (**Fig. 36D**).

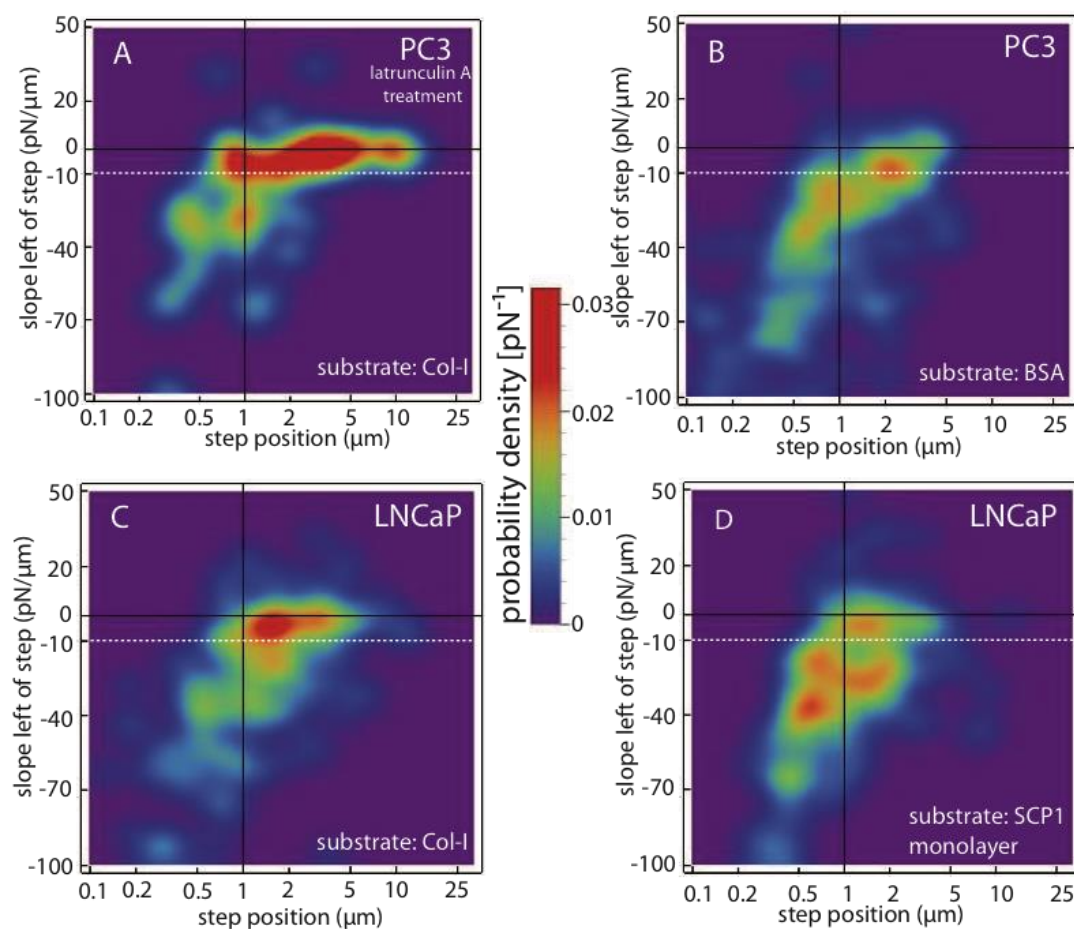


**Figure 36:** Probability density maps of force loading rates (slope of the force distance trace) prior to each step versus the step position. **(A)** Latrunculin-A treated PC3 cells on Col-I substrate. **(B)** PC3 cells on BSA substrate **(C)** LNCaP cells on BSA Col-I substrate **(D)** LNCaP cells on SCP1 monolayer. The y-axes (step position) in 2D maps are in logarithmic scale.

In the interaction of PC3 cells to Col-I and SCP1 substrates, we mainly detected jump and filopodia-like steps, which shows that these interactions were substrate specific. And when these interactions were blocked with anti  $\beta 1$  integrin antibody and when the cells actin cytoskeleton was disrupted with latrunculin-A on Col-I substrates, these specific signals were changed mainly to membrane tethers. Taken together, these results suggest that PC3 cells are using cytoskeleton connected integrin adhesion complexes and their filopodia like structures in these interactions.

## 5. Discussion

Prostate cancer (PC) is one of the leading cancer type among men and cause of death in Europe [113]. The ability of prostate cancer cells to metastase into bone tissue is very often event in these cases. Therefore, in the main focus of this study was to investigate in great detail the interaction forces of prostate cancer cells with the bone marrow-derived substrates namely, Collagen-I (Col-I) protein and mesenchymal stem cells (SCP1 cell line)

### **Relevance of the methods used in the study to investigate PC cell interactions with the bone marrow substrates**

We used two types of PC cells, which are PC3 and LNCaP cell lines. PC3 is a bone metastasis-originated cell line that is highly differentiated type [114]. LNCaP is a lymph node metastasis-derived cell line that is moderately differentiated type [115]. We have used as substrates two different kind of surfaces, namely the bone extracellular matrix protein Col-I and the bone marrow residing mesenchymal stem cells (MSC, SCP1 cell line). We have investigated the expressionof collagen-binding integrins ( $\alpha 1$ ,  $\alpha 2$ ,  $\alpha 11$  and  $\beta 1$ ) in the two PC cell types by isolating total cell RNA, then synthesing cDNA, and finally performing semi-quantitative and quantitative PCR. Cell adhesion and proliferation assays were used to see long-term adhesion of cells and theirpropagaton abilities on these surfaces. AFM-based single cell force spectroscopy (SCFS) was implicated to study short-term adhesion events as well as single cell adhesion forces. SCFC is a method that uses a whole vital cell as a probe and which allows viewing of single molecule interactions. Hence, SCFS represents an additional important tool to look deeper into the adhesion mechanisms.

As mentioned above we investigated the binding efficiency of PC3 to Col-I and bone marrow-derived SCP1 cells by long-term adhesion assays (optical density-based and fluorescence-based) and by AFM-based single cell force spectroscopy. Both approaches highlight different aspects of the cellular interactions between prostate cancer cells and mesenchymal stem cells. The optical density- and fluorescence-based adhesion assays provide insights into

the time evolution of the cell-substrate interactions on a whole cell population level, while force spectroscopy experiments focus on interactions immediately after the cells have been brought into contact with their respective binding partners on a single cell level. Hence combining both types of methods result in a more fundamental understanding of cancer cell interactions with their metastatic environment from initial formation of adhesion and the forces involved to long-term interaction between cells.

### **PC3 cells differed from LNCaP cells in means of adhesion, spreading and proliferation onto bone marrow components**

Previous studies using optical microscopy as well as AFM imaging already showed that PC3 cells adhere and proliferate much better than LNCaP cells on Col-I, and that PC3 adhesion, proliferation, and cell stiffness was significantly enhanced on Col-I, compared to other ECM proteins, such as fibronectin [57].

Time-lapse microscopy observations allowed us to have a detailed look on the behavior of the PC cells when they were cultured on MSC monolayers (SCP1 cell line). We have tried to answer the following questions: 1) how cells adhere to this substrate; 2) how was their cell shape affected; and 3) how effectively they could proliferate on SCP1. From the first hours of co-cultivation up to several days in culture, prostate cancer cells derived from bone metastasis (PC3) proliferated and spreaded well on SCP1. In contrast the control group, which was derived from lymph metastasis (LNCaP), were rounder in shape and could not spread on SCP1, not only showed much fewer adherent cells during the initial hours of co-cultivation, but the number of cells further decreased after five days in culture. These results clearly demonstrated that PC3 cells are much adapted to survive on bone marrow cells.

### **The attachment forces involved in cell-to-cell and cell-to-matrix interactions were higher for PC3 cells than LNCaP cells**

To obtain a deeper insight into the nature of the observed cell-cell and the previously described cell-matrix interactions, we quantified the interaction forces on the single cell level using AFM based force spectroscopy. With the AFM, interaction forces of a much smaller number of cells can be determined quantitatively on the single cell level. This approach concentrates on forces arising during the initial cellular contact, since the cell was not allowed to develop the cell contact for more than 0.3 seconds before it was retracted and forced to unbind. Although, as mentioned above, AFM only probes the initial cellular contacts, the results we obtained were in agreement with our optical microscopy data, as well as with previous findings [57]. On both Col-I and on the SCP1 monolayer, the percentage of cellular interactions (adhesion rate), the number of interactions per successful force experiment (number of steps), the step position, the force of a single interaction event (step height), the detachment force, and the total work of detachment were larger for PC3 than for LNCaP. Our findings clearly reported that PC3 cells are very distinct from LNCaP cells in regards to their adhesive behavior. In particular, PC3 cells showed significantly stronger adhesion on both substrates (Col-I and SCP1), when compared to LNCaP. Due to their smaller Youngs` modulus (**Fig. 11**), LNCaP cells had a larger contact area during adhesion experiments with the AFM force spectroscopy. The same finding was also true for when these cells spreaded on cell matrix proteins such as Col-I and fibronectin. When they spreaded on cell matrix protein- coated surfaces, they could build up their cytoskeleton network and become stiffer than when they were attached on PDL-coated AFM cantilever. One of the other possible reason of having stiffer cells when they were spreaded on surfaces is that underlying glass was sensed during measurements. In this case, they had Youngs` Moduli at kPa range. PC3 cells were more than 2-fold stiffer in comparison to LNCaP cells [57]. In any case PC3 cells seem to be well adapted for invasion of bone substituents with their high capability of forming strong adhesion to these substrates.

### **Extracellularly secreted Col-I participation in the interactions between PC3 cells and SCP1 cells**

Cells could form their own extracellular matrix network. SCP1 cells did the same when they are cultured and build up a meshwork of extracellular materials. Furthermore, within each individual cell line, PC3 or LNCaP, both cell lines showed similar results in the parameter values extracted from the AFM measurements on Col-I and on SCP1 (**Fig. 14** to **Fig. 19**). The only difference was that the step position was shorter on Col-I and larger on SCP-1 monolayers due to the fact that the cells of the monolayer contributed their compliance and membrane tethers and hence led to enlargement of the interaction distances. These findings indicated that the adhesion of the prostate cancer cells to SCP1 cells could be mediated mainly by their interaction with Col-I, which was found by us and others to be expressed extracellularly by MSCs also on their apical side [101,116,117]. This observation was confirmed by immunofluorescence staining of Col-I in SCP1 cells and on the Col-I-coated microscope slides, which both showed a strong fluorescence signal (**Fig. 23** and **Fig. 24**). With this result, we concluded that in the interaction of PC3 cells to SCP1 cells, contributing effect of Col-I to the adhesion should be taken into account which is subject for further experiments.

### **Col-I-binding integrin expression levels were higher in PC3 cells compared to LNCaP cells**

Integrins are cell surface receptors responsible for adhesion of cells to e.g. extracellular matrix proteins. We have investigated the role of the Col-I binding integrin receptors  $\alpha 1\beta 1$ ,  $\alpha 2\beta 1$  and  $\alpha 11\beta 1$ , in the interaction of prostate cancer cells with the extracellular matrix protein Col\_I and human MSC. Quantitative PCR of these Col-I binding integrin receptor subunits revealed that  $\alpha 1$ ,  $\alpha 2$  and  $\beta 1$  integrins are expressed in PC3 cells, and that  $\alpha 2\beta 1$  is the most abundant of these receptors in the PC3 cell line. On the contrary LNCaP cells showed only very low expression level of  $\beta 1$  integrins (**Fig. 22**). In this study, the partner  $\alpha$  subunit in LNCaP cells was not determined. Consistent with previous literature reports showing that PC3 cells express a number of

Col-I- binding integrin receptors [55,97], while LNCaP cells lack some of these integrins [56], we showed that  $\alpha 1\beta 1$  and  $\alpha 2\beta 1$  integrins are potential candidates to mediate the detected force patterns. Moreover, our PCR results suggest that among the two receptor combinations  $\alpha 2\beta 1$  is the dominant one in PC3 cells.

### **Collagenase treatment effectively degrades Col-I from coated surfaces and caused a reduction in cell adhesion**

Next, we blocked these interactions by either incubating the PC3 cells with an antibody against  $\beta 1$  integrin or by treating the Col-I substrate with collagenase. The optical density-based adhesion assay showed that the PC3 cells adhered well to Col-I-coated surfaces, which is in agreement with our previous studies [57]. Moreover, in the present study we also applied collagenase treatment as a control to inhibit the interactions of PC3 with the Col-I-coated surfaces and found strong reduction of PC3 adhesion to this substrate: the percentage of adherent cells dropped to the levels observed on the control uncoated plastic surface (**Fig. 25**). This result proved that the collagenase treatment effectively hydrolyzed accessible Col-I molecules and reduced the number of binding events on the substrate to the level of the untreated control surface.

### **Blocking of $\beta 1$ integrin reduced the PC3 binding to Col-I**

When PC3 cells were blocked with the anti- $\beta 1$  antibody, the fraction of adherent cells initially decreased on Col-I-coated substrates, however, after an incubation time of 90 min, the cells started to recover from the blocking effect. Nevertheless, the number of adherent cells still remained lower than the one observed for PC3 cells without antibody treatment (**Fig. 25B**). This observed recovery of PC3 affinity to Col-I could be the result of integrin turnover which provides fresh  $\beta 1$  subunits for the formation of new functional integrin receptors on the cell surface. Yuan et al analyzed the dynamics of the integrin adhesion complexes in long-term cell-ECM adhesion and found that these complexes undergo integrin turnover by assembling and disassembling their units in time scales of 2-7 minutes [118].

### **PC3 to MSC interactions were mainly mediated via $\beta$ 1 integrin receptors**

Force spectroscopy results showed that the antibody blocking clearly inhibited the interactions on both Col-I and on the SCP1 monolayer. Adhesion rate, number of interactions steps and detachment force were lower for the antibody-treated PC3 cells in comparison to untreated PC3 cells on both substrates (**Fig. 27, Fig. 28, Fig. 29**). These results clearly revealed that cell-to-cell interactions between PC3 and SCP1 are mediated also via  $\beta$ 1 integrins. However, we did not observe a difference between the adhesion of PC3 cells on SCP1 monolayers with and without collagenase treatment (**Fig. 28**). The adhesion rate and number of steps were not significantly different between measurements of PC3 cells on SCP1 substrates with or without collagenase. Furthermore there was only a small difference (not significant) between detachment forces (**Fig. 29B**). Despite the fact that SCP1 cells express Col-I on their apical side (**Fig. 24**), we hypothesized that upon removal of Col-I from the apical surface, the adhesion of PC3 cells to SCP1 monolayer should reduce. However it remained constant, collagenase treatment did not make any significant difference. This may be because the SCP1 monolayers were cultured for only two days, whereas deposition of an entire extracellular Col-I matrix in 2D monolayer cultures requires up to 3 weeks according to Koellmer et al [117]. On the other hand, our observation also indicated that with the removal of Col-I from the apical side of the SCP1 cells, additional adhesion molecules expressed by the SCP1 cells were exposed and could contribute to the interaction between PC3 and SCP1 cells. Another possibility to explain our data is that the treatment with the collagenase enzyme might not have effectively removed Col-I from the apical side of the SCP1 cells due to the protective effect of polysaccharides in the glycocalix of the SCP1 cells. Michigami et al. reported that cell-to-cell contact between bone marrow stromal and myeloma cells can also be established via VCAM-1 binding to  $\alpha$ 4 $\beta$ 1-integrin [119]. Another study showed that co-cultured PC3 and bone marrow stromal cells regulate their cell adhesion via  $\alpha$ 1, and  $\alpha$ 2 integrin subunits and VCAM-1 [68]. Furthermore, both VCAM-1 and  $\alpha$ 4 integrin subunits are highly expressed in bone marrow derived MSCs and PC3, respectively [119,120]. Therefore, we propose that in addition to Col-I,

VCAM-1 might be an important partner for mediating the adhesive interactions between prostate cancer cells and bone marrow MSCs. However, to further rule out the involvement of VCAM-1 follow up studies have to be carried out.

### **Cytoskeleton anchored membrane receptors were involved in the interactions of PC3 cells to Col-I and MSCs**

In addition to the adhesion, rate the average number of steps and the detachment force, we have also analyzed the force loading rates (slope of the force distance trace) prior to each step as a function of the step position: A horizontal plateau preceding a force step, is characteristic for a tether being pulled out of the cell membrane [106,109,110]. Here, the constant force prior to the unbinding event is caused by the constant tension of the plasma membrane [121]. However an increasing force just before the step (denoted as jump) is characteristic for the rupturing of a transmembrane-receptor, which is firmly connected to the cytoskeleton on its intracellular side [107,108].

As shown in **Fig. 20**, we have counted the numbers of jump steps (F-step) and tethers (T-steps) and compare between PC3 and LNCaP. The results showed that in the case of PC3 cells, more than 50% of all detected steps exhibited filopodia and less than 40% exhibited the typical signature of tethers. For LNCaP cells, on the other hand, less than 40% of the steps appeared as filopodia steps and about 45% as tether-like steps. Important to note, this type of calculation has limits, since we had to remove steps and also slopes of positions shorter than 1  $\mu\text{m}$ , and which we were not able to clearly distinguish too close at the border line (at slope = -10 pN/ $\mu\text{m}$ ). Therefore, we added the parameter of step positions to the plots to make a clear distinction and drew 2D maps of the data (step positions vs slope). Hence, we could use the whole data sets without removing any shorter position steps or the steps close to the border line. The density distribution images of the force loading rate (slope) versus the step position shown in figures 31, 32, 33 and 34 revealed differences in the degree of cytoskeleton connection beneath the cell surface receptors involved in cell-cell and cell-substrate interaction. For PC3 cells on Col-I substrate, after collagenase or

antibody treatment, the receptors were less connected to the cytoskeleton than in the case of untreated PC3 cells and Col-I substrates (**Fig. 31B, 32B and 33B**). For PC3 cells on SCP1 substrates, collagenase treatment did not change much the distribution of steps but moved the peak to higher step positions (**Fig. 32A**). This we concluded may be the effect by the removal of the tiny Col-I layer from SCP1 monolayers; thus, the cells could form easier and longer cell - cell attachment sites with their exposed membrane protrusions than in the previous case. Application of  $\beta 1$  blocking antibody to PC3 cells decreased the number of interactions between two cell types (**Fig. 28**), but the distribution of steps was not much affected, and showed only broadened peak at the same position (**Fig. 33A**). However, these observations for PC3 - SCP1 interactions also suggested that different surface receptors can be involved depending on whether  $\beta 1$  integrins were blocked by an antibody or accessible Col-I was removed by collagenase treatment. This may also reflect the fact that, depending on their state, the involved integrin receptors can form or dissolve bonds to the actin cytoskeleton [105,122]. On Col-I substrate application of  $\beta 1$  blocking antibody to PC3 cells cause appearance of two tether peaks (**Fig. 33B**). This showed effective blocking of interactions between  $\beta 1$  integrins and Col-I.

Taken together with the establishment of this new presentation method of the single cell force spectroscopy data, dynamics of the cell adhesion could be tested and for the first time the plots thus visualize details of the anchoring of bonds to the cell and provide a better understanding of the specificity of the receptor-ligand interactions.

### **Cell membrane protrusions, such as filopodia actively took part in the interactions of PC cells to bone marrow constituents**

Cell migration is essential not only for tissue infiltration and the formation of metastases, but also for non-pathological processes, such as angiogenesis and leukocyte extravasation. In order to migrate, a cell has to pass through a sequence of distinct processes. Migration is initiated by cell polarization and the formation of membrane protrusions at the leading edge. Integrins fix cellular protrusions to the ECM, interact with the actin cytoskeleton, and

trigger the association of many different signaling molecules at the so-called focal contacts [123]. Filopodia are thin, actin-rich plasma-membrane protrusions that function as antennae for cells to probe their environment. Consequently, filopodia have an important role in cell migration. The initiation and elongation of filopodia depend on the precisely regulated polymerization, convergence and crosslinking of actin filaments [124]. Our observation that PC3 cells exhibited much more jump and filopodia steps which are formed by cytoskeleton-connected membrane proteins at the extended positions than LNCaP cells (**Fig. 16**, **Fig. 17** and density plots in **Fig. 31** to **Fig. 36**) may reflect the fact that PC3 cells tend to actively extrude filopodia when they come into contact with Col-I or SCP1 cells, while LNCaP cells form membrane tethers as they are not connected to the cytoskeleton. This novel observation is consistent with high resolution AFM and fluorescence microscopy studies [57], which showed that on Col-I-coated substrates, PC3 cells exhibit a large number of well pronounced filopodia, while LNCaP cells on Col-I coated substrates remain smooth and show almost no filopodia. Taken together, these findings suggest a role for filopodias in promoting cell adhesion to ECM proteins and to surrounding neighbor cells in PC metastasis and this adhesion may have a major role in migration of PC cells in bone tissue.

## 6. Conclusions and outlook

PC metastasis into bone tissue is still a major problem that should be deeply investigated to define the mechanism of invasion. Several aspects of PC metastasis into bone have been enlightened, but there are still some gaps in our understanding of this process. Col-I and MSCs are important components of the bone marrow environment and seem to play distinct roles in the PC invasion of bone. However, the exact interaction mechanisms of PC cells with these bone marrow components still needs to be elucidated and the responsible cell adhesion molecules to be identified. This necessity led us to investigate in a great detail the PC cell adhesion mechanism to Col-I and mesenchymal stem cells (MSCs). Following our extensive analyses we concluded:

1. When co-cultured with the SCP1 cells, PC3 cells showed enhanced adhesion, spreading and proliferation rate. Furthermore, we have found that prostate cancer cells derived from bone metastasis (PC3) have a higher affinity to MSCs (SCP1 cell line) as well as to the extra cellular bone matrix protein collagen type I (Col-I), than lymph-derived prostate cancer cells (LNCaP).
2. Col-I-binding integrins  $\alpha1\beta1$  and  $\alpha2\beta1$  integrins were expressed at higher levels on PC3 cells than LNCaP cells. Among the two different combinations  $\alpha2\beta1$  receptor was the dominant one in PC3. PC3 cell adhesion to Col-I substrates was mediated via this integrin.
3. On Col-I substrate and on SCP1 monolayer, PC3 cells formed significantly more frequent interactions and stronger adhesion forces than LNCaP cells.
4. Blocking of  $\beta1$  integrin caused a clear reduction in the adhesion of PC3 cells to Col-I and SCP1. Cell-to-cell interactions between PC3 cells and SCP1 cells appeared to be also mediated by  $\beta1$  integrins. On the other hand proteolytic degradation of the extracellularly expressed Col-I on SCP1 monolayers did not change the adhesion regime of PC3 cells. These results suggest that in addition to Col-I, other potent ligands for  $\beta1$

integrins are expressed by MSCs and may play a role in facilitating PC3-MSC interactions.

5. We have shown that deriving and generating slope-position density-plots from force spectroscopy data is a very novel and useful method to visualize the embedding and anchorage of adhesion molecules in the cell. These plots reflect the substrate-dependent complex adhesion behavior of the cells. With the results of these analyses, we concluded that PC3 cells use cytoskeleton-connected membrane receptors to generate specific de-adhesion forces during interaction with bone marrow-derived substrates (Col-I and MSCs). Moreover, our new data may reflect the fact that PC3 cells tend to actively extrude filopodia when they come into contact with Col-I or SCP1 cells, while LNCaP cells form membrane tethers as they are not connected to cytoskeleton. These findings, to our knowledge, are for the first time reported.

Biophysical characterization of PC cell interaction to bone marrow components will help researchers tremendously in understanding the nature of PC bone metastasis. Our study has demonstrated remarkable effect of  $\beta 1$  integrins in the adhesion of PC3 cells to MSCs. In addition, we have found that extracellularly secreted Col-I is not the only partner for these integrins in PC3-MSC interaction. Next, we have defined a novel method to discriminate the adhesion steps in force spectroscopy of cells, which is based on the anchorage of membrane receptors to cytoskeleton elements. With the help of these analyses we concluded that PC3 cells could use cytoskeleton-connected membrane-anchored receptors and seem to utilize their filopodia to establish these adhesive bonds. Together with the present study, follow up investigations could help to shed more light on the membrane molecular partner of  $\beta 1$  that is expressed on the MSCs and governs PC3-MSC interaction. Cumulatively, we believe that reaching a complete understanding of the mechanism of action of prostate cancer cells could be used to design and generate very specific therapeutic agents or strategies that powerfully block the metastatic behavior of certain prostate cancer cells towards bone tissue.

The results presented in the sections 4.1 to 4.5 are already published in the research article entitled “Probing the Interaction Forces of Prostate Cancer Cells with Collagen I and Bone Marrow-Derived Stem Cells on the Single Cell Level” by Sariisik et al., Plos One, in 2013 [101].

Some of the results presented in sections 4.7 and 4.8 are also used in the research article entitled “Decoding Cytoskeleton-Anchored and Non-Anchored Receptors from Single-Cell Adhesion Force Data”, by Sariisik et al., Biophysical Journal, in 2015 [125].

## 7. Summary

Prostate cancer is one of the most commonly diagnosed cancer in males. At the early stages of cancer surgical and hormonal therapies can be useful applied. The principal problem arising from prostate cancer is its predisposition to metastasize. After some point they form hormone independent cells, which can also be highly invasive. This tendency arises from specific molecular mechanisms and interactions that together lead to metastatic invasion into bone.

In order to investigate in detail on this topic, typical components of bone tissue were presented as substrates for two species of prostate carcinoma cell lines (PC3 and LNCaP). This study was conducted with a variety of complementary techniques to investigate cell adhesion. While PC3 cells turned out to instantly interact strongly with bone tissue, LNCaP cells interacted weak and in contrast to PC3 even refused proliferating in this environment. By quantitative PCR and real time PCR,  $\beta$ 1-integrins were identified as key players for the interaction between PC3 cells and bone tissue. Therefore, a prostate cell immobilized to the force sensor was mechanically brought in a controlled short contact to a collagen type-I (Col-I) substrate or to a monolayer of a bone marrow derived mesenchymal stem cell line (SCP1). Then the cell was retracted while recording interaction forces. An antibody specifically blocking  $\beta$ 1-integrins corroborated the hypothesis that  $\beta$ 1-integrins play a major role in this interaction, but also showed that due to a high integrin turnover rate antibody treatment might not be the ultimate strategy to interfere with prostate carcinoma metastasis into the bone marrow. Similar findings characterized a treatment of SCP1 monolayers with collagenase.

Even though all measured parameters resulting from the force measurements revealed an almost identical behavior of the PC3 cells probed on both surfaces Col-I and SCP1, the treatment with collagenase suggested the possibility of PC3 cells involving different mechanisms for the interaction to Col-I or to SCP1 respectively.

Long-term assays up to days for PC3 and LNCaP adhesion, proliferation and spreading in co-culture with SCP1 uncovered a very similar picture for the cell interactions as the force measurements.

AFM, furthermore, provided a direct measure of the cell elasticity (Young's modulus) and showed PC3 cells to be mechanically three times stiffer than LNCaP cells.

Last during this project, a new evaluation method for force measurements was developed, that allowed to conclude on the connection of the adhesion molecules (integrins) to the intracellular cytoskeleton. From loading-rate vs. position probability density plots the anchorage of each individual detected unbinding event could be classified as rather membrane bound (tether) or cytoskeleton bound (jump). This method was clearly verified by treating the cells with Latrunculin-A a destructor of the actin filaments. For the interaction of prostate cell lines with bone tissue this evaluation method revealed not only that PC3 cells rather utilize cytoskeleton-supported receptors (filopodia) in contrast to LNCaP cells utilizing membrane bound receptors (tether) but also how blocking antibody treatment removed cytoskeleton-anchored receptors from participating in adhesion.

Taken together, these findings might open a window for new applications to interfere with prostate carcinoma metastasis at the intracellular side of adhesion receptors by preventing cytoskeleton anchorage.

## 8. Zusammenfassung

Zu den am häufigsten in männlichen Patienten diagnostizierten Krebsarten gehört Prostatakrebs. Im Anfangsstadium können Resektion und Hormontherapie mit Erfolg eingesetzt werden. Aus seiner Neigung zur Metastasierung erwächst allerdings ein grundlegendes Problem, denn ab einem bestimmten Stadium werden die Zellen hormonresistent und können dann auch sehr invasiv werden. Diese Eigenschaft rührt von bestimmten molekularen Mechanismen und Wechselwirkungen, die in Kombination zu metastatischem Eindringen in das Knochengewebe führen.

Um diese Zusammenhänge genauer zu verstehen wurden zwei Arten von Prostatakrebszelllinien (PC3 und LNCap) typische Bestandteile des Knochengewebes präsentiert. In dieser Studie kamen unterschiedliche komplementäre Techniken zur Untersuchung der Zelladhäsion zum Einsatz. Dabei wechselwirkten PC3 Zellen sofort und sehr stark mit Knochengewebe, während die LNCaP Zellen schwach wechselwirkten und im Gegensatz zu PC3 Zellen sich in diesem Milieu nicht teilten. Mittels Quantitativer PCR und Echtzeit PCR wurden die  $\beta$ 1-Integrine als die Hauptverantwortlichen für die Wechselwirkung zwischen PC3 Zellen und dem Knochengewebe identifiziert. Mittels Kraftmikroskopie (AFM) wurden die Kräfte zwischen den Prostata Zelllinien und dem Knochengewebe direkt gemessen. Hierfür wurde eine am Kraftsensor immobilisierte Prostata Krebszelle kontrolliert für einen kurzen Moment mechanisch in Kontakt mit einem Kollagen Typ-I (Col-I) Substrat oder mit einem Zellmonolayer einer mesenchymen Stammzelllinie aus dem Knochenmark (SCP1) gebracht. Die Wechselwirkungskräfte wurden aufgezeichnet, während die Zelle wieder vom Substrat getrennt wurde. Ein  $\beta$ 1-Integrin blockender Antikörper bestätigte noch einmal die Hypothese, dass  $\beta$ 1-Integrine für diese Wechselwirkung die wesentliche Rolle spielen. Aber es zeigte sich auch, dass eine Behandlung gegen Metastasierung von Prostata Karzinomen in das Knochenmark mit diesem Antikörper wegen des hohen Integrin Durchsatzes nicht die beste Strategie sein kann. Ähnliche Ergebnisse erzielte die Behandlung mit von SCP1 Monolayern mit Kollagenase.

Obwohl alle Parameter aus den Kraftmessungen darauf hin deuteten, dass die PC3 Zellen sich nahezu identisch sowohl auf Col-I als auch auf SCP1 verhielten, legte der Einsatz von Kollagenase nahe, dass PC3 Zellen möglicherweise verschiedene Mechanismen für die Wechselwirkung mit Col-I oder SCP1 verwenden.

Langzeit Testreihen von bis zu einigen Tagen zur Adhäsion, zur Zellteilung und zur Ausbreitung von PC3 und LNCaP Zellen in Mischkultur mit SCP1 Zellen zeichneten ein sehr ähnliches Bild der zellulären Wechselwirkungen wie die Kraftmessungen.

Zusätzlich bietet das AFM die direkte Bestimmung der Zellelastizität (Youngs' Modul) und es zeigte sich, dass PC3 Zellen mechanisch dreimal steifer sind als die LNCaP Zellen.

Insbesondere wurde im Rahmen dieses Projektes eine neue Auswertungsmethode entwickelt, die Rückschlüsse über die Verankerung der Adhäsionsmoleküle (Integrine) mit dem intrazellulären Zytoskelett erlaubt. Durch Auftragung der Wahrscheinlichkeitsdichte der Ladungsrate gegen die Position konnte die Verankerung jedes einzelnen detektierten Bindungsereignisses in eher membrangebunden (Tether) oder Zytoskelettverbunden (Jump) unterteilt werden. Durch die Behandlung der Zellen mit dem Aktinfilament zersetzenden Latrunkulin-A konnte diese Methode eindeutig bestätigt werden. In Bezug auf die Wechselwirkung der Prostata Zelllinien mit Knochengewebe konnte diese Auswertungsmethode nicht nur zeigen, dass PC3 Zellen eher zytoskelettgebundene Rezeptoren (Filpodien) verwenden, während LNCaP Zellen eher membrangebundene Rezeptoren (Tether) verwenden, sondern sie zeigte auch, dass der Einsatz des blockierenden Antikörpers zytoskelettgebundene Rezeptoren daran hinderte an der Adhäsion mit zu wirken.

Diese Ergebnisse könnten eine Tür zu neuen Anwendungen gegen Metastasierung von Prostata Krebs an der Intrazellulären Seite der Rezeptoren öffnen wobei deren Verankerung mit dem Zytoskelett unterbunden wird.

## 9. Literature

1. Greene DR, Fitzpatrick JM, Scardino PT. Anatomy of the prostate and distribution of early prostate cancer. *Semin Surg Oncol*. 1995;11: 9–22. doi:10.1002/ssu.2980110104
2. Cheng L, Zincke H, Blute ML, Bergstralh EJ, Scherer B, Bostwick DG. Risk of prostate carcinoma death in patients with lymph node metastasis. *Cancer*. 2001;91: 66–73. doi:10.1002/1097-0142(20010101)91:1<66::AID-CNCR9>3.0.CO;2-P
3. Keller ET, Brown J. Prostate cancer bone metastases promote both osteolytic and osteoblastic activity. *J Cell Biochem*. 2004;91: 718–729. doi:10.1002/jcb.10662
4. Chaffer CL, Weinberg RA. A Perspective on Cancer Cell Metastasis. *Science*. 2011;331: 1559–1564. doi:10.1126/science.1203543
5. Clarke NW, Hart CA, Brown MD. Molecular mechanisms of metastasis in prostate cancer. *Asian J Androl*. 2009;11: 57–67. doi:10.1038/aja.2008.29
6. van Zijl F, Krupitza G, Mikulits W. Initial steps of metastasis: Cell invasion and endothelial transmigration. *Mutat Res Mutat Res*. 2011;728: 23–34. doi:10.1016/j.mrrev.2011.05.002
7. Logothetis CJ, Lin S-H. Osteoblasts in prostate cancer metastasis to bone. *Nat Rev Cancer*. 2005;5: 21–28. doi:10.1038/nrc1528
8. Galasko C. Skeletal Metastases. *Clin Orthop*. 1986; 18–30.
9. Clarke NW, Hart CA, Brown MD. Molecular mechanisms of metastasis in prostate cancer. *Asian J Androl*. 2009;11: 57–67. doi:10.1038/aja.2008.29
10. Nishida N, Yano H, Nishida T, Kamura T, Kojiro M. Angiogenesis in Cancer. *Vasc Health Risk Manag*. 2006;2: 213–219.
11. Stewart DA, Cooper CR, Sikes RA. Changes in extracellular matrix (ECM) and ECM-associated proteins in the metastatic progression of prostate cancer. *Reprod Biol Endocrinol RBE*. 2004;2: 2. doi:10.1186/1477-7827-2-2
12. Liotta LA. Tumor Invasion and Metastases—Role of the Extracellular Matrix: Rhoads Memorial Award Lecture. *Cancer Res*. 1986;46: 1–7.
13. Thiery JP, Sleeman JP. Complex networks orchestrate epithelial–mesenchymal transitions. *Nat Rev Mol Cell Biol*. 2006;7: 131–142. doi:10.1038/nrm1835

14. Charafe-Jauffret E, Ginestier C, Birnbaum D. Breast cancer stem cells: tools and models to rely on. *BMC Cancer*. 2009;9: 202. doi:10.1186/1471-2407-9-202
15. Thiery JP. Epithelial–mesenchymal transitions in tumour progression. *Nat Rev Cancer*. 2002;2: 442–454. doi:10.1038/nrc822
16. Yang J, Weinberg RA. Epithelial-Mesenchymal Transition: At the Crossroads of Development and Tumor Metastasis. *Dev Cell*. 2008;14: 818–829. doi:10.1016/j.devcel.2008.05.009
17. Mani SA, Guo W, Liao M-J, Eaton EN, Ayyanan A, Zhou AY, et al. The Epithelial-Mesenchymal Transition Generates Cells with Properties of Stem Cells. *Cell*. 2008;133: 704–715. doi:10.1016/j.cell.2008.03.027
18. Gal A, Sjöblom T, Fedorova L, Imreh S, Beug H, Moustakas A. Sustained TGF $\beta$  exposure suppresses Smad and non-Smad signalling in mammary epithelial cells, leading to EMT and inhibition of growth arrest and apoptosis. *Oncogene*. 2007;27: 1218–1230. doi:10.1038/sj.onc.1210741
19. Birchmeier W, Behrens J. Cadherin expression in carcinomas: role in the formation of cell junctions and the prevention of invasiveness. *Biochim Biophys Acta BBA - Rev Cancer*. 1994;1198: 11–26. doi:10.1016/0304-419X(94)90003-5
20. Frixen UH, Behrens J, Sachs M, Eberle G, Voss B, Warda A, et al. E-cadherin-mediated cell-cell adhesion prevents invasiveness of human carcinoma cells. *J Cell Biol*. 1991;113: 173–185. doi:10.1083/jcb.113.1.173
21. Cheng L, Nagabhushan M, Pretlow TP, Amini SB, Pretlow TG. Expression of E-cadherin in primary and metastatic prostate cancer. *Am J Pathol*. 1996;148: 1375–1380.
22. Yu M, Stott S, Toner M, Maheswaran S, Haber DA. Circulating tumor cells: approaches to isolation and characterization. *J Cell Biol*. 2011;192: 373–382. doi:10.1083/jcb.201010021
23. Honn KV, Tang DG. Adhesion molecules and tumor cell interaction with endothelium and subendothelial matrix. *Cancer Metastasis Rev*. 1992;11: 353–375. doi:10.1007/BF01307187
24. Orr FW, Sanchez-Sweatman OH, Kostenuik P, Singh G. Tumor-Bone Interactions in Skeletal Metastasis. *Clin Orthop*. 1995;312. Available: [http://journals.lww.com/corr/Fulltext/1995/03000/Tumor\\_Bone\\_Interactions\\_in\\_Skeletal\\_Metastasis\\_.4.aspx](http://journals.lww.com/corr/Fulltext/1995/03000/Tumor_Bone_Interactions_in_Skeletal_Metastasis_.4.aspx)
25. Lehr JE, Pienta KJ. Preferential Adhesion of Prostate Cancer Cells to a Human Bone Marrow Endothelial Cell Line. *J Natl Cancer Inst*. 1998;90: 118–123. doi:10.1093/jnci/90.2.118

26. Morrissey C, Vessella RL. The role of tumor microenvironment in prostate cancer bone metastasis. *J Cell Biochem.* 2007;101: 873–886. doi:10.1002/jcb.21214
27. Kopp H-G, Avecilla ST, Hooper AT, Rafii S. The Bone Marrow Vascular Niche: Home of HSC Differentiation and Mobilization. *Physiology.* 2005;20: 349–356. doi:10.1152/physiol.00025.2005
28. Alix-Panabières C, Riethdorf S, Pantel K. Circulating Tumor Cells and Bone Marrow Micrometastasis. *Clin Cancer Res.* 2008;14: 5013–5021. doi:10.1158/1078-0432.CCR-07-5125
29. Hood JD, Cheresh DA. Role of integrins in cell invasion and migration. *Nat Rev Cancer.* 2002;2: 91–100. doi:10.1038/nrc727
30. Mp S, D F, Cg G, D C. Cell migration as a five-step cycle. *Biochem Soc Symp.* 1998;65: 233–243.
31. Kim J, Wong CW, Goldsmith JD, Song C, Fu W, Allion M-B, et al. Rapid apoptosis in the pulmonary vasculature distinguishes non-metastatic from metastatic melanoma cells. *Cancer Lett.* 2004;213: 203–212. doi:10.1016/j.canlet.2004.03.042
32. Aguirre-Ghiso JA. Models, mechanisms and clinical evidence for cancer dormancy. *Nat Rev Cancer.* 2007;7: 834–846. doi:10.1038/nrc2256
33. Yao D, Dai C, Peng S. Mechanism of the mesenchymal-epithelial transition and its relationship with metastatic tumor formation. *Mol Cancer Res MCR.* 2011;9: 1608–1620. doi:10.1158/1541-7786.MCR-10-0568
34. Hugo H, Ackland ML, Blick T, Lawrence MG, Clements JA, Williams ED, et al. Epithelial—mesenchymal and mesenchymal—epithelial transitions in carcinoma progression. *J Cell Physiol.* 2007;213: 374–383. doi:10.1002/jcp.21223
35. Chaffer CL, Dopheide B, Savagner P, Thompson EW, Williams ED. Aberrant fibroblast growth factor receptor signaling in bladder and other cancers. *Differentiation.* 2007;75: 831–842. doi:10.1111/j.1432-0436.2007.00210.x
36. Matsubara A, Kan M, Feng S, McKeenan WL. Inhibition of Growth of Malignant Rat Prostate Tumor Cells by Restoration of Fibroblast Growth Factor Receptor 2. *Cancer Res.* 1998;58: 1509–1514.
37. Yates C, Wells A, Turner T. Luteinising hormone-releasing hormone analogue reverses the cell adhesion profile of EGFR overexpressing DU-145 human prostate carcinoma subline. *Br J Cancer.* 2005;92: 366–375. doi:10.1038/sj.bjc.6602350

38. Yates CC, Shepard CR, Stolz DB, Wells A. Co-culturing human prostate carcinoma cells with hepatocytes leads to increased expression of E-cadherin. *Br J Cancer*. 2007;96: 1246–1252. doi:10.1038/sj.bjc.6603700
39. Bf B, De H, Kr W, L X, A D. Recent advances in bone biology provide insight into the pathogenesis of bone diseases. *Lab Investig J Tech Methods Pathol*. 1999;79: 83–94.
40. Autzen P, Robson CN, Bjartell A, Malcolm AJ, Johnson MI, Neal DE, et al. Bone morphogenetic protein 6 in skeletal metastases from prostate cancer and other common human malignancies. *Br J Cancer*. 1998;78: 1219–1223.
41. Guise TA, Yin JJ, Mohammad KS. Role of endothelin-1 in osteoblastic bone metastases. *Cancer*. 2003;97: 779–784. doi:10.1002/cncr.11129
42. Hall CL, Kang S, MacDougald OA, Keller ET. Role of wnts in prostate cancer bone metastases. *J Cell Biochem*. 2006;97: 661–672. doi:10.1002/jcb.20735
43. Logothetis CJ, Lin S-H. Osteoblasts in prostate cancer metastasis to bone. *Nat Rev Cancer*. 2005;5: 21–28. doi:10.1038/nrc1528
44. Shariat SF, Shalev M, Menesses-Diaz A, Kim IY, Kattan MW, Wheeler TM, et al. Preoperative Plasma Levels of Transforming Growth Factor Beta1 (TGF- $\beta$ 1) Strongly Predict Progression in Patients Undergoing Radical Prostatectomy. *J Clin Oncol*. 2001;19: 2856–2864.
45. Dai J, Kitagawa Y, Zhang J, Yao Z, Mizokami A, Cheng S, et al. Vascular Endothelial Growth Factor Contributes to the Prostate Cancer-Induced Osteoblast Differentiation Mediated by Bone Morphogenetic Protein. *Cancer Res*. 2004;64: 994–999. doi:10.1158/0008-5472.CAN-03-1382
46. Fudge K, Wang CY, Stearns ME. Immunohistochemistry analysis of platelet-derived growth factor A and B chains and platelet-derived growth factor alpha and beta receptor expression in benign prostatic hyperplasias and Gleason-graded human prostate adenocarcinomas. *Mod Pathol Off J U S Can Acad Pathol Inc*. 1994;7: 549–554.
47. Charhon SA, Chapuy MC, Delvin EE, Valentin-Opran A, Edouard CM, Meunier PJ. Histomorphometric analysis of sclerotic bone metastases from prostatic carcinoma with special reference to osteomalacia. *Cancer*. 1983;51: 918–924. doi:10.1002/1097-0142(19830301)51:5<918::AID-CNCR2820510526>3.0.CO;2-J
48. Clarke NW, McClure J, George NJ. Osteoblast function and osteomalacia in metastatic prostate cancer. *Eur Urol*. 1993;24: 286–290.
49. Clarke NW, McClure J, George NJ. Morphometric evidence for bone resorption and replacement in prostate cancer. *Br J Urol*. 1991;68: 74–80.

50. Chung LWK, Baseman A, Assikis V, Zhou HE. Molecular insights into prostate cancer progression: The missing link of tumor microenvironment. *J Urol.* 2005;173: 10–20. doi:10.1097/01.ju.0000141582.15218.10
51. Shoulders MD, Raines RT. COLLAGEN STRUCTURE AND STABILITY. *Annu Rev Biochem.* 2009;78: 929–958. doi:10.1146/annurev.biochem.77.032207.120833
52. Velleman SG. The Role of the Extracellular Matrix in Skeletal Development. *Poult Sci.* 2000;79: 985–989. doi:10.1093/ps/79.7.985
53. Tong W, Glimcher MJ, Katz JL, Kuhn L, Eppell SJ. Size and Shape of Mineralites in Young Bovine Bone Measured by Atomic Force Microscopy. *Calcif Tissue Int.* 2003;72: 592–598. doi:10.1007/s00223-002-1077-7
54. Voet D, Voet JG. *Biochemistry.* John Wiley & Sons; 2004.
55. Kiefer JA, Farach-Carson MC. Type I collagen-mediated proliferation of PC3 prostate carcinoma cell line: implications for enhanced growth in the bone microenvironment. *Matrix Biol.* 2001;20: 429–437. doi:10.1016/S0945-053X(01)00159-7
56. Hall CL, Dai J, van Golen KL, Keller ET, Long MW. Type I Collagen Receptor ( $\alpha 2\beta 1$ ) Signaling Promotes the Growth of Human Prostate Cancer Cells within the Bone. *Cancer Res.* 2006;66: 8648–8654. doi:10.1158/0008-5472.CAN-06-1544
57. Docheva D, Padula D, Schieker M, Clausen-Schaumann H. Effect of collagen I and fibronectin on the adhesion, elasticity and cytoskeletal organization of prostate cancer cells. *Biochem Biophys Res Commun.* 2010;402: 361–366. doi:10.1016/j.bbrc.2010.10.034
58. Langholz O, Röckel D, Mauch C, Kozłowska E, Bank I, Krieg T, et al. Collagen and collagenase gene expression in three-dimensional collagen lattices are differentially regulated by alpha 1 beta 1 and alpha 2 beta 1 integrins. *J Cell Biol.* 1995;131: 1903–1915. doi:10.1083/jcb.131.6.1903
59. Nabha SM, dos Santos EB, Yamamoto HA, Belizi A, Dong Z, Meng H, et al. Bone marrow stromal cells enhance prostate cancer cell invasion through type I collagen in an MMP - 12 dependent manner. *Int J Cancer.* 2008;122: 2482–2490. doi:10.1002/ijc.23431
60. Kadler KE, Holmes DF, Trotter JA, Chapman JA. Collagen fibril formation. *Biochem J.* 1996;316 ( Pt 1): 1–11.
61. Docheva D, Popov C, Mutschler W, Schieker M. Human mesenchymal stem cells in contact with their environment: surface characteristics and the integrin system. *J Cell Mol Med.* 2007;11: 21–38. doi:10.1111/j.1582-4934.2007.00001.x

62. Studeny M, Marini FC, Dembinski JL, Zompetta C, Cabreira-Hansen M, Bekele BN, et al. Mesenchymal Stem Cells: Potential Precursors for Tumor Stroma and Targeted-Delivery Vehicles for Anticancer Agents. *J Natl Cancer Inst.* 2004;96: 1593–1603. doi:10.1093/jnci/djh299
63. Fritz V, Brondello J m., Gordeladze J o., Reseland J e., Bony C, Yssel H, et al. Bone-metastatic prostate carcinoma favors mesenchymal stem cell differentiation toward osteoblasts and reduces their osteoclastogenic potential. *J Cell Biochem.* 2011;112: 3234–3245. doi:10.1002/jcb.23258
64. Chanda D, Isayeva T, Kumar S, Hensel JA, Sawant A, Ramaswamy G, et al. Therapeutic Potential of Adult Bone Marrow–Derived Mesenchymal Stem Cells in Prostate Cancer Bone Metastasis. *Clin Cancer Res.* 2009;15: 7175–7185. doi:10.1158/1078-0432.CCR-09-1938
65. Cross N, Papageorgiou M, Eaton C. Bone marrow stromal cells promote growth and survival of prostate cancer cells. *Biochem Soc Trans.* 2007;35: 698.
66. Eaton CL, Coleman RE. Pathophysiology of bone metastases from prostate cancer and the role of bisphosphonates in treatment. *Cancer Treat Rev.* 2003;29: 189–198. doi:10.1016/S0305-7372(03)00071-9
67. Nyambo R, Cross N, Lippitt J, Holen I, Bryden G, Hamdy FC, et al. Human Bone Marrow Stromal Cells Protect Prostate Cancer Cells From TRAIL-Induced Apoptosis. *J Bone Miner Res.* 2004;19: 1712–1721. doi:10.1359/JBMR.040703
68. J W, AS L, Jr SR. Identification of a unique set of genes altered during cell-cell contact in an in vitro model of prostate cancer bone metastasis. *Int J Mol Med.* 17: 849.
69. Knight CG, Morton LF, Peachey AR, Tuckwell DS, Farndale RW, Barnes MJ. The Collagen-binding A-domains of Integrins  $\alpha 1\beta 1$  and  $\alpha 2\beta 1$  Recognize the Same Specific Amino Acid Sequence, GFOGER, in Native (Triple-helical) Collagens. *J Biol Chem.* 2000;275: 35–40. doi:10.1074/jbc.275.1.35
70. Cabodi S, Stefano PD, Leal M del PC, Tinnirello A, Bisaro B, Morello V, et al. Integrins and Signal Transduction. In: Becchetti A, MD AA, editors. *Integrins and Ion Channels.* Springer New York; 2010. pp. 43–54. Available: [http://link.springer.com/chapter/10.1007/978-1-4419-6066-5\\_5](http://link.springer.com/chapter/10.1007/978-1-4419-6066-5_5)
71. Brakebusch C, Fässler R. New EMBO Member`s review: The integrin-actin connection, an eternal love affair. *EMBO J.* 2003;22: 2324–2333. doi:10.1093/emboj/cdg245
72. Cabodi S, Stefano PD, Leal M del PC, Tinnirello A, Bisaro B, Morello V, et al. Integrins and Signal Transduction. In: Becchetti A, MD AA, editors. *Integrins and Ion Channels.* Springer New York; 2010. pp. 43–54. Available: [http://link.springer.com/chapter/10.1007/978-1-4419-6066-5\\_5](http://link.springer.com/chapter/10.1007/978-1-4419-6066-5_5)

73. Dike LE, Farmer SR. Cell adhesion induces expression of growth-associated genes in suspension-arrested fibroblasts. *Proc Natl Acad Sci.* 1988;85: 6792–6796.
74. Sastry SK, Burridge K. Focal Adhesions: A Nexus for Intracellular Signaling and Cytoskeletal Dynamics. *Exp Cell Res.* 2000;261: 25–36. doi:10.1006/excr.2000.5043
75. Lock JG, Wehrle-Haller B, Strömblad S. Cell–matrix adhesion complexes: Master control machinery of cell migration. *Semin Cancer Biol.* 2008;18: 65–76. doi:10.1016/j.semcancer.2007.10.001
76. Geiger B, Bershadsky A, Pankov R, Yamada KM. Transmembrane crosstalk between the extracellular matrix and the cytoskeleton. *Nat Rev Mol Cell Biol.* 2001;2: 793–805. doi:10.1038/35099066
77. Evans EA, Calderwood DA. Forces and Bond Dynamics in Cell Adhesion. *Science.* 2007;316: 1148–1153. doi:10.1126/science.1137592
78. Giancotti FG, Tarone G. Positional Control of Cell Fate Through Joint Integrin/Receptor Protein Kinase Signaling. *Annu Rev Cell Dev Biol.* 2003;19: 173–206. doi:10.1146/annurev.cellbio.19.031103.133334
79. Miranti CK, Brugge JS. Sensing the environment: a historical perspective on integrin signal transduction. *Nat Cell Biol.* 2002;4: E83–E90. doi:10.1038/ncb0402-e83
80. Webb DJ, Donais K, Whitmore LA, Thomas SM, Turner CE, Parsons JT, et al. FAK–Src signalling through paxillin, ERK and MLCK regulates adhesion disassembly. *Nat Cell Biol.* 2004;6: 154–161. doi:10.1038/ncb1094
81. Defilippi P, Di Stefano P, Cabodi S. p130Cas: a versatile scaffold in signaling networks. *Trends Cell Biol.* 2006;16: 257–263. doi:10.1016/j.tcb.2006.03.003
82. Danen EH, Sonnenberg A. Erratum: Integrins in regulation of tissue development and function. *J Pathol;* 200: 471–480. *J Pathol.* 2003;201: 632–641. doi:10.1002/path.1472
83. Cress AE, Rabinovitz I, Zhu W, Nagle RB. The  $\alpha 6\beta 1$  and  $\alpha 6\beta 4$  integrins in human prostate cancer progression. *Cancer Metastasis Rev.* 1995;14: 219–228. doi:10.1007/BF00690293
84. Goel HL, Fornaro M, Moro L, Teider N, Rhim JS, King M, et al. Selective modulation of type 1 insulin-like growth factor receptor signaling and functions by beta(1) integrins (vol 166, pg 407, 2004). *J Cell Biol.* 2004;167: 565–565. doi:10.1083/jcb.200403003102504c
85. Hall CL, Dubyk CW, Riesenberger TA, Shein D, Keller ET, van Golen KL. Type I Collagen Receptor ( $\alpha 2\beta 1$ ) Signaling Promotes Prostate Cancer Invasion through RhoC GTPase. *Neoplasia N Y N.* 2008;10: 797–803.

86. Mizejewski GJ. Role of Integrins in Cancer: Survey of Expression Patterns. *Exp Biol Med.* 1999;222: 124–138.
87. Brooks PC, Clark RA, Cheresh DA. Requirement of vascular integrin alpha v beta 3 for angiogenesis. *Science.* 1994;264: 569–571. doi:10.1126/science.7512751
88. Felding-Habermann B, Mueller BM, Romerdahl CA, Cheresh DA. Involvement of integrin alpha V gene expression in human melanoma tumorigenicity. *J Clin Invest.* 1992;89: 2018–2022.
89. Filardo E, Brooks P, Deming S, Damsky C, Cheresh D. Requirement of the Npxy Motif in the Integrin Beta-3 Subunit Cytoplasmic Tail for Melanoma Cell-Migration in-Vitro and in-Vivo. *J Cell Biol.* 1995;130: 441–450. doi:10.1083/jcb.130.2.441
90. Serini G, Trusolino L, Saggiorato E, Cremona O, DeRossi M, Angeli A, et al. Changes in integrin and E-cadherin expression in neoplastic versus normal thyroid tissue. *J Natl Cancer Inst.* 1996;88: 442–449. doi:10.1093/jnci/88.7.442
91. Scott LJ, Clarke NW, George NJR, Shanks JH, Testa NG, Lang SH. Interactions of human prostatic epithelial cells with bone marrow endothelium: binding and invasion. *Br J Cancer.* 2001;84: 1417–1423. doi:10.1054/bjoc.2001.1804
92. Benoit M, Gabriel D, Gerisch G, Gaub HE. Discrete interactions in cell adhesion measured by single-molecule force spectroscopy. *Nat Cell Biol.* 2000;2: 313–317.
93. Helenius J, Heisenberg C-P, Gaub HE, Muller DJ. Single-Cell Force Spectroscopy. *J Cell Sci.* 2008;121: 1785–1791. doi:10.1242/jcs.030999
94. Rodríguez JP, Montecinos L, Ríos S, Reyes P, Martínez J. Mesenchymal Stem Cells from Osteoporotic Patients Produce a Type I Collagen-Deficient Extracellular Matrix Favoring Adipogenic Differentiation. 2000; Available: <http://www.captura.uchile.cl/handle/2250/132617>
95. Böker W, Yin Z, Drosse I, Haasters F, Rossmann O, Wierer M, et al. Introducing a single-cell-derived human mesenchymal stem cell line expressing hTERT after lentiviral gene transfer. *J Cell Mol Med.* 2008;12: 1347–1359. doi:10.1111/j.1582-4934.2008.00299.x
96. Schmitz J, Benoit M, Gottschalk K-E. The Viscoelasticity of Membrane Tethers and Its Importance for Cell Adhesion. *Biophys J.* 2008;95: 1448–1459. doi:10.1529/biophysj.107.124289
97. Taubenberger A, Cisneros DA, Friedrichs J, Puech P-H, Muller DJ, Franz CM. Revealing Early Steps of  $\alpha 2\beta 1$  Integrin-mediated Adhesion to Collagen Type I by Using Single-Cell Force Spectroscopy. *Mol Biol Cell.* 2007;18: 1634–1644. doi:10.1091/mbc.E06-09-0777

98. Kohler J, Popov C, Klotz B, Alberton P, Prall WC, Haasters F, et al. Uncovering the cellular and molecular changes in tendon stem/progenitor cells attributed to tendon aging and degeneration. *Aging Cell*. 2013;12: 988–999. doi:10.1111/ace1.12124
99. Docheva D, Padula D, Popov C, Mutschler W, Clausen-Schaumann H, Schieker M. Researching into the cellular shape, volume and elasticity of mesenchymal stem cells, osteoblasts and osteosarcoma cells by atomic force microscopy. *J Cell Mol Med*. 2008;12: 537–552. doi:10.1111/j.1582-4934.2007.00138.x
100. Popov C, Radic T, Haasters F, Prall WC, Aszodi A, Gullberg D, et al. Integrins  $\alpha 2\beta 1$  and  $\alpha 11\beta 1$  regulate the survival of mesenchymal stem cells on collagen I. *Cell Death Dis*. 2011;2: e186. doi:10.1038/cddis.2011.71
101. Sariisik E, Docheva D, Padula D, Popov C, Opfer J, Schieker M, et al. Probing the Interaction Forces of Prostate Cancer Cells with Collagen I and Bone Marrow Derived Stem Cells on the Single Cell Level. *PLoS ONE*. 2013;8: e57706. doi:10.1371/journal.pone.0057706
102. Opfer J, Gottschalk K-E. Identifying Discrete States of a Biological System Using a Novel Step Detection Algorithm. *PLoS ONE*. 2012;7: e45896. doi:10.1371/journal.pone.0045896
103. Huang GT-J, Shagramanova K, Chan SW. Formation of Odontoblast-Like Cells from Cultured Human Dental Pulp Cells on Dentin In Vitro. *J Endod*. 2006;32: 1066–1073. doi:10.1016/j.joen.2006.05.009
104. Zhang X, Wojcikiewicz E, Moy VT. Force Spectroscopy of the Leukocyte Function-Associated Antigen-1/Intercellular Adhesion Molecule-1 Interaction. *Biophys J*. 2002;83: 2270–2279. doi:10.1016/S0006-3495(02)73987-8
105. Sheetz MP. Cell control by membrane–cytoskeleton adhesion. *Nat Rev Mol Cell Biol*. 2001;2: 392–396. doi:10.1038/35073095
106. Benoit M, Selhuber-Unkel C. Measuring Cell Adhesion Forces: Theory and Principles. In: Braga PC, Ricci D, Walker JM, editors. *Atomic Force Microscopy in Biomedical Research*. Humana Press; 2011. pp. 355–377. Available: <http://www.springerlink.com/content/l565781826621241/abstract/>
107. Friedrichs J, Legate KR, Schubert R, Bharadwaj M, Werner C, Müller DJ, et al. A practical guide to quantify cell adhesion using single-cell force spectroscopy. *Methods*. 2013;60: 169–178. doi:10.1016/j.ymeth.2013.01.006
108. Friedrichs J, Helenius J, Muller DJ. Quantifying cellular adhesion to extracellular matrix components by single-cell force spectroscopy. *Nat Protoc*. 2010;5: 1353–1361. doi:10.1038/nprot.2010.89

109. Sattler KD. Handbook of Nanophysics: Nanomedicine and Nanorobotics. CRC Press; 2010.
110. Sun M, Graham JS, Hegedüs B, Marga F, Zhang Y, Forgacs G, et al. Multiple Membrane Tethers Probed by Atomic Force Microscopy. *Biophys J*. 2005;89: 4320–4329. doi:10.1529/biophysj.104.058180
111. Puech P-H, Poole K, Knebel D, Muller DJ. A new technical approach to quantify cell–cell adhesion forces by AFM. *Ultramicroscopy*. 2006;106: 637–644. doi:10.1016/j.ultramic.2005.08.003
112. Coué M, Brenner SL, Spector I, Korn ED. Inhibition of actin polymerization by latrunculin A. *FEBS Lett*. 1987;213: 316–318. doi:10.1016/0014-5793(87)81513-2
113. Ferlay J, Parkin DM, Steliarova-Foucher E. Estimates of cancer incidence and mortality in Europe in 2008. *Eur J Cancer*. 2010;46: 765–781. doi:10.1016/j.ejca.2009.12.014
114. Nemeth JA, Yousif R, Herzog M, Che M, Upadhyay J, Shekarriz B, et al. Matrix Metalloproteinase Activity, Bone Matrix Turnover, and Tumor Cell Proliferation in Prostate Cancer Bone Metastasis. *J Natl Cancer Inst*. 2002;94: 17–25. doi:10.1093/jnci/94.1.17
115. Jeet V, Tevz G, Lehman M, Hollier B, Nelson C. Elevated YKL40 is associated with advanced prostate cancer (PCa) and positively regulates invasion and migration of PCa cells. *Endocr Relat Cancer*. 2014;21: 723–737. doi:10.1530/ERC-14-0267
116. Alberton P, Popov C, Prägert M, Kohler J, Shukunami C, Schieker M, et al. Conversion of Human Bone Marrow-Derived Mesenchymal Stem Cells into Tendon Progenitor Cells by Ectopic Expression of Scleraxis. *Stem Cells Dev*. 2012;21: 846–858. doi:10.1089/scd.2011.0150
117. Koellmer M, Keskar V, Hauk TG, Collins JM, Russell B, Gemeinhart RA. Stem Cell-Derived Extracellular Matrix Enables Survival and Multi lineage Differentiation within Superporous Hydrogels. *Biomacromolecules*. 2012;13: 963–973. doi:10.1021/bm300332w
118. Yuan L, Fairchild MJ, Perkins AD, Tanentzapf G. Analysis of integrin turnover in fly myotendinous junctions. *J Cell Sci*. 2010;123: 939–946. doi:10.1242/jcs.063040
119. Michigami T, Shimizu N, Williams PJ, Niewolna M, Dallas SL, Mundy GR, et al. Cell–cell Contact Between Marrow Stromal Cells and Myeloma Cells Via VCAM-1 and A4 $\beta$ 1-Integrin Enhances Production of Osteoclast-Stimulating Activity. *Blood*. 2000;96: 1953–1960.
120. Jones EA, English A, Kinsey SE, Straszynski L, Emery P, Ponchel F, et al. Optimization of a flow cytometry-based protocol for detection and phenotypic characterization of multipotent mesenchymal stromal cells

- from human bone marrow. *Cytometry B Clin Cytom.* 2006;70B: 391–399. doi:10.1002/cyto.b.20118
121. Benoit M. Force Spectroscopy on Cells. In: Sattler KD, editor. *Handbook of Nanophysics: Nanomedicine and Nanorobotics.* CRC Press; 2010. pp. 9:1–29.
122. Tulla M, Helenius J, Jokinen J, Taubenberger A, Müller DJ, Heino J. TPA primes  $\alpha 2\beta 1$  integrins for cell adhesion. *FEBS Lett.* 2008;582: 3520–3524. doi:10.1016/j.febslet.2008.09.022
123. Brakebusch C, Bouvard D, Stanchi F, Sakai T, Fässler R. Integrins in invasive growth. *J Clin Invest.* 2002;109: 999–1006. doi:10.1172/JCI15468
124. Mattila PK, Lappalainen P. Filopodia: molecular architecture and cellular functions. *Nat Rev Mol Cell Biol.* 2008;9: 446–454. doi:10.1038/nrm2406
125. Sariisik E, Popov C, Müller JP, Docheva D, Clausen-Schaumann H, Benoit M. Decoding Cytoskeleton-Anchored and Non-Anchored Receptors from Single-Cell Adhesion Force Data. *Biophys J.* 2015;109: 1330–1333. doi:10.1016/j.bpj.2015.07.048

**10. List of abbreviations**

AFM	Atomic force microscopy
BMP	Bone morphogenic protein
BMSC	Bone marrow stromal cells
BSA	Bovine serum albumin
cdc42	Cell division control protein 42 homolog protein
CAM	Cell adhesion molecule
CFDA	Carboxyfluorescein diacetate
Col-I	Collagen type-I
CTC	Circulating tumor cell
DAPI	4',6-diamidino-2-phenylindole
ECM	Extra cellular matrix
EDTA	Ethylenediaminetetraacetic acid
EGFR	Epidermal growth factor receptor
ET-1	Endothelin-1
FBS	Fetal bovine serum
FGF	Fibroblast growth factor
GAPDH	Glyceraldehyde 3-phosphate dehydrogenase
GTP	Guanosine-5'-triphosphate
ICAM-1	Intercellular adhesion molecule - 1
LNCaP	Prostate cancer cell line derived from lymph-nodes
MSCs	Mesenchymal stem cells
MMP-12	Matrix metalloproteinase-12
PBS	Phosphate buffer solution
PC	Prostate cancer
PC3	Prostate cancer cell line derived from bone metastasis
PDGF	Platelet derived growth factor
PDL	Poly-D-Lysine
PDT	Population doubling time
PECAM-1	Platelet endothelial cell adhesion molecule - 1
RANKL	Receptor activator of nuclear factor kappa-B ligand
RT-PCR	Reverse transcriptase polymerase chain reaction
SCP1	Single cell-derived and immortalized mesenchymal stem cell line

SCFC	Single cell force spectroscopy
TGF $\beta$	Transforming growth factor beta
VCAM-1	Vascular cell adhesion molecule -1
VEGF	Vascular endothelial growth factor

## 11. Curriculum vitae (CV)

<b>Name:</b>	EDİZ SARIİŞİK
<b>Tel:</b>	+491778450036 +905558308273
<b>Email:</b>	ediz.sariisik@gmail.com
<b>Adress:</b>	Amalienstr. 54, 80799, München-Deutschland
<b>Birth date:</b>	30.11.1984
<b>Birth place:</b>	Ankara/Turkey
<b>Nationality:</b>	Turkey
<b>Education:</b>	
2008 – 2010	<b>MSc.-Major:</b> Middle East Technical University, Dept. of Biology, Molecular Biophysics Lab. Ankara, Turkey CPGA:3.50/4.00
2003 – 2008	<b>BSc.-Major:</b> Middle East Technical University, Molecular Biology&Genetics. Ankara, Turkey CGPA: 3.06 / 4.0
1996 – 2003	<b>High School:</b> Kalaba Anadolu Lisesi, Ankara, Turkey CGPA: 4.92/5.00
<b>Research work:</b>	
01.04.2010 – ongoing	<b>Ph.D project:</b> Interdisciplinary project of “Investigation of the molecular and biophysical mechanisms of prostate cancer cell interactions with bone marrow-derived proteins and stem cells.” Experimed (LMU) & Biophysics (LMU), Munich, Germany <b>Side Ph.D project:</b> “Characterization of the interactions of prostate and breast cancer cell lines with mineralized and demineralized bone-like surfaces.” CANTER (University of applied sciences), Munich, Germany
01.07.2008 – 31.12.2009	<b>Master thesis:</b> “Investigation of interactions between cholesterol reducing agent simvastatin and charged model membranes” in Molecular Biophysics Lab. of Prof. Feride Severcan, Department of Biology, METU, Ankara, Turkey

01.08.2007 – 20.02.2008 **Special project** of “Effects of radiation and radioprotectants on rat membrane tissues” in Molecular Biophysics Lab. of Prof. Feride Severcan, Department of Biology, METU, Ankara

16.01.2007 – 30.02.2007 **Internship** project “Study on genotype analysis on human gene polymorphisms related to some important human diseases” at Hacettepe Teknokent, Genar Molecular Genetics Laboratory, Ankara, Turkey

### **Publications:**

○ **Sariisik, E.**, Docheva D, Padula D, Popov C, Opfer J, Schieker M, Clausen-Schaumann H, Benoit M, “Probing the Interaction Forces of Prostate Cancer Cells with Collagen I and Bone Marrow Derived Stem Cells on the Single Cell Level”, PLoS ONE, 2013;8: e57706.

doi:10.1371/journal.pone.0057706

○ **Sariisik E.**, Popov C, Müller J, Docheva D, Clausen-Schaumann H, Benoit M, “Decoding Cytoskeleton-Anchored and Non-Anchored Receptors from Single-Cell Adhesion Force Data”, Biophysical Journal, 2015;109: 1330-1333.

doi:10.1016/j.bpj.2015.07.048

### **Expertises:**

- AFM imaging
- Single cell force spectroscopy
- Elasticity measurements
- Immuno-fluorescence imaging
- Cell culture of human cells
- RNA isolation, cDNA synthesis, RT-PCR, PCR
- Immuno-Fluorescence imaging of cells
- FTIR spectroscopy
- Differential Scanning Calorimetry
- Maldi-Toff Mass spectroscopy
- DNA sequencing procedures
- Plasmid and human genomic DNA isolation, Agarose Gel Electrophoresis
- Bacterial, yeast transformation with plasmid DNA
- Restriction enzyme digestion and Southern transfer
- 2D-SDS-Page separation of proteins

**Scientific meetings**

- **Sariisik E.**, Zistl D., Docheva D., Benoit M., Clausen-Schaumann H. Linz Winter Workshop, 2015, Poster presentation: Interaction Forces of Prostate Cancer Cells with Bone Marrow Derived Stem Cells, Collagen, as well as Mineralized and Demineralized Bone-Like Surfaces.
- **Sariisik E.**, Zistl D., Docheva D., Benoit M., Clausen-Schaumann H. Hochschule-München-Forschungsforum / 4. PhD-Symposium for Applied Sciences, 2014, Poster presentation: Probing the Interaction Forces of Prostate Cancer Cells with Bone Marrow Derived Stem Cells, Collagen, as well as Mineralized and Demineralized Bone-Like Surfaces
- **Sariisik E.**, Docheva D., Benoit M., Clausen-Schaumann H. CeNS Workshop Venice, 2011, Poster Presentation: Integrin generated forces in prostate cancer bone metastasis.

**Languages:**

- Turkish (Native)
- English (Fluent) TOEFL (IBT) SCORE: 93 (Date: 17.11.2007)
- German (Intermediate)

## 12. Acknowledgements

I would like to express my sincere gratitude to the following people who contributed to this thesis and my research experience.

Prof. Dr. Mathias Schieker, Head of Experimental Surgery and Regenerative Medicine (Experimed, LMU) and Prof. Hermann Gaub, Head of the Biophysics (LMU) for giving me the opportunity to perform my thesis in their laboratories.

Priv. Doz. Dr. Denitsa Docheva, my direct supervisor in Experimed, I would like to give my gratitude for supervising my biology experiments, guidance during thesis design and writing as well as time she spent for this project.

Dr. Martin Benoit, my supervisor in Biophysics, for his continuous interest in my research, guidance for all AFM experiments, encouragement and helps that he gave me throughout my PhD years.

Prof. Hauke Clausen-Schaumann (University of Applied Sciences, CANTER Laboratory, Munich) for his helpful advices, guidance and long discussions which helped me to accomplish the research publications.

My colleagues Dr. Cvetan Popov (ExperiMed), Jochen Müller (Biophysics), Dr. Stefanie Sudhop (CANTER) for their advices and contributions for the experiments I performed. Angelika Kardinal, Thomas Nicolaus (Biophysics) and Martina Burggraff (Experimed) for their help in cell culture and laboratory organization. Seçkin Eroğlu for his friendship and suggestions. Samet Kocabey for being a good fellow and for all of the help he offered to me.

Lastly, to my lovely family, my mother, father, sister and all my friends for their whole support throughout my life experience.

## Eidesstattliche Versicherung

SARIISIK, Ediz

Name, Vorname

Ich erkläre hiermit an Eides statt,  
dass ich die vorliegende Dissertation mit dem Thema

**“Investigation of the molecular and biophysical mechanisms of prostate  
cancer cell interactions with bone marrow-derived proteins and stem  
cells”**

selbständig verfasst, mich außer der angegebenen keiner weiteren Hilfsmittel bedient und alle Erkenntnisse, die aus dem Schrifttum ganz oder annähernd übernommen sind, als solche kenntlich gemacht und nach ihrer Herkunft unter Bezeichnung der Fundstelle einzeln nachgewiesen habe.

Ich erkläre des Weiteren, dass die hier vorgelegte Dissertation nicht in gleicher oder in ähnlicher Form bei einer anderen Stelle zur Erlangung eines akademischen Grades eingereicht wurde.

Ort, Datum

München,  
14.06.2016